STUDY ON PERFORMANCE CHARACTERISTICS OF DIAGONAL TYPE NONEQUILIBRIUM PLASMA MHD GENERATOR(Dissertation_全文)

AUTHOR(S):

Ishikawa, Motoo

STUDY ON PERFORMANCE CHARACTERISTICS OF DIAGONAL TYPE NONEQUILIBRIUM PLASMA MHD GENERATOR

BY

MOTOO ISHIKAWA

FEBRUARY 1978

INSTITUTE OF ATOMIC ENERGY

KYOTO UNIVERSITY

JAPAN

STUDY ON PERFORMANCE CHARACTERISTICS OF DIAGONAL TYPE NONEQUILIBRIUM PLASMA MHD GENERATOR

BY

MOTOO ISHIKAWA

FEBRUARY 1978

INSTITUTE OF ATOMIC ENERGY

KYOTO UNIVERSITY

JAPAN

PREFACE

The electrical energy used not only in Japan but also in the whole world shows a remarkable yearly increase. However, the overall thermal efficiency of a present large scale steam power plant remains at about 40 percent and that of an atomic power plant is about 30 percent. Large thermal pollution with air contamination and efficient usage of fuels will be supposed to become serious problems unless the efficiency is improved. Thus, it is a pressing need to develop a method of energy conversion with high efficiency and low pollution.

An MHD (magnetohydrodynamic) -steam binary power plant is expected to have a potential to increase its overall thermal efficiency as large as to 50 or 60 percent. Moreover, the MHD generation will have the largest capacity among various methods giving high conversion efficiency.

In Japan, experimental researches of several open-cycle MHD power generators with an alkali-metal seeded combustion gas of fossil fuel have been made in the Electrotechnical Laboratory as a National Project since 1966 [1.1]. In foreign contries, experimental investigations of the open-cycle MHD generator have been made by Dicks et al. of UTSI, Petty et al. of AVCO [1.3] in USA, and by Sheindlin and Biturin et al. of High Temperature Institute in USSR [1.4]. In addition, numerous theoretical studies have been performed by Hurwitz [1.5], Dzung [1.6], Celinski [1.7], Oliver [1.8], Argyropoulos [1.9], et al. With these research and development, it is now expected that the open-cycle MHD-steam power plant will be operated commercially in the latter half of the 1980's.

On the other hand, for closed-cycle MHD power generation, in which nonequilibrium plasma of an alkali-metal seeded rare gas is

utilized as the working fluid, there have been made fundamental experiments and theoretical analyses, and such as a fossil fuel fired heat exchanger [1.10], a future nuclear fusion reactor, and a solar furnace are thought as heat sources. A low temperature working gas can be used in the closed-cycle MHD which will provide higher energy conversion efficiency and power density compared with those of the open-cycle MHD generator.

Theoretical studies on the closed-cycle MHD generator have been done by Velikhov [1.11], Solbes [1.12], Yoshikawa [1.13], Tanaka [1.14], and many other workers, and experimental studies by Bertolini [1.15], Brederlow [1.16], Zauderer [1.17], Nakamura [1.18], Rietjens [1.19], Shioda [1.20], et al. They have shown that the closed-cycle MHD power generation has potentiality of increasing the conversion efficiency, but the effective Hall parameter will be difficult to exceed 2 or 3 under the existence of ionization instabilities unless fully ionization of seed atoms is fulfilled.

As a working gas for the closed-cycle MHD power generation, alkali-metal seeded argon or helium is usually utilized. In this thesis, cesium-seeded helium is chosen as a working fluid.

So long as linear generator types are concerned, three types have been proposed so far. Although a Faraday type generator will reveal the best generator performance, it requires many DC-AC inverters corresponding to each output electrode pairs. Hence, the plant system containing a Faraday type generator will be complicated due to many number of inverters.

By contrast, a Hall type generator can be operated with only a single load in principle, but needs high Hall parameter to give good performance [1.21]. It will hence show fairly poor performance characteristics if the ionization instability is not suppressed.

As an intermediate of the above two types, a diagonal type generator is thought to be possessed of good characteristics even

for low Hall parameters [1.21], and it can be operated with a single load or a few, and hence requires a few DC-AC inverters. A plant system containing the diagonal type generator will be more simplified with respect to operational control than that containing a Faraday type generator. In addition, its performance characteristics are expected to be as close as to those of a Faraday type generator.

Consequently, diagonal type generators with nonequilibrium plasma will be promising for commercial scale generators, nevertheless they have not been investigated so far, although diagonal type combustion gas MHD generators have been well studies by Dicks [1.2], Petty [1.3], Dishchikov [1.22], et al.

The purpose of this thesis is to investigate theoretically the performance characteristics of a diagonal type MHD generator with a nonequilibrium plasma of cesium-seeded helium, and the thesis consists of two parts.

In part I, an optimization of a large scale diagonal type MHD generator is investigated. This part consists of the following three chapters.

In Chapter 1, studies of optimizations of MHD generators made until now are briefly introduced. Also, the purpose and significance of the investigation are stated.

In Chapter 2, quasi one-dimensional basic equations for the working gas flow are introduced in a diagonal and a Faraday type generators, in which the friction and heat losses, electrode voltage drops, and finite segmentation effects of electrodes are considered, and it is assumed that the end effects can be neglected. In addition, the relaxation of ionization is neglected, because it affects only electrical characteristics in the generator inlet region [1.15]. As an estimation function for the optimization of the generators, total thermal efficiency is adopted. Beside, the isentropic efficiency, output power density, etc. of the generator,

some constraints for the optimization, and expressions of the electrical conductivity and Hall parameter of the working gas are derived.

In Chapter 3, by the optimization theory derived in the preceding chapter, numerical calculation is made for the typical closed-cycle diagonal type MHD-steam power plant with about 2000 MW of thermal input. Influences of the Mach number, inclination parameter, duct length, inlet pressure and temperature of a diagonal type generator on the total thermal efficiency of the plant are investigated in detail. As the results the optimum duct with optimum Mach number, inclination parameter, and duct length giving the maximum efficiency is found out. In the similar way, the optimization of a Faraday type generator is further studied, and a comparative study of the generator performances of both types is made.

In part II, the electrical characteristics of a diagonal type nonequilibrium plasma MHD generator are investigated by two-dimensional analyses. Part II consists of the following six chapters.

In Chapter 1, two- or three-dimensional analyses of a Faraday, Hall, and diagonal type MHD generators carried out until now are introduced briefly.

In Chapter 2, basic equations, which are to be used in the analyses, are introduced. By use of the stream and potential functions, two-dimensional partial differential equations are derived from the basic equations together with boundary and subsidiary conditions required for a diagonal type generator. Expressions of the electrical efficiency and the specific Hall voltage are shown.

In Chapter 3, basic electrical characteristics of a generator duct are investigated by two-dimensional analyses for spatially constant and variable electrical conductivity and Hall parameters. Influences of the load factor, the Hall parameter, and the inclination parameter of sidebars on the current and potential distributions and the electrical efficiency are then investigated.

In Chapter 4, effects of a resistive electrode and of a distribution of the applied magnetic flux on the electrical characteristics of a generator are studied by two-dimensional analyses. Influences of the conductivity and configuration of wedge-shaped resistive electrodes on the current concentration at the electrode, electrical efficiency, etc. are studied. And also the electrical characteristics of a generator with the spatially attenuating magnetic flux in the region near the duct wall are compared with those of the generator with the spatially constant magnetic flux.

In Chapter 5, end effects are investigated by two-dimensional analyses. Influences of the attenuation of the magnetic flux, and position of the output electrodes of various types on the current distribution and the internal resistance are studied in detail for two cases, i.e., spatially constant and spatially variable electrical conductivity and electron mobility.

In Chapter 6, effects of internal or external connection of electrodes in a diagonal type generator are investigated by two-dimensional analyses in the plane perpendicular to the plasma flow. Current and potential distributions for two cases are then compared from view point of electrical efficiency for various parameters of the load factor, duct wall temperature, and inclination parameter.

ACKNOWLEDGMENTS

This doctoral thesis has been studied under the guidance of Professor Dr. Juro Umoto of Kyoto University. The author wishes to express his highest gratitude for his guidance and continuous encouragements enabling the author to complete the work. Professor J. Umoto also strictly read the manuscript of the thesis and gave accurate comments which were sincerely appreciated.

The author would like to thank Professor Yoshio Hattori of the Institute of Atomic Energy, Kyoto University for valuable discussions.

The author also wishes to express his thanks to Associate Professor Takehisa Hara and Assistant Masaharu Yoshida of Professor J. Umoto's Laboratory, and Associate Professor Kiyoshi Yoshikawa, Mr. Daijiro Tanaka, and Mr. Hisayuki Toku of the Institute of Atomic Energy for discussions. Mr. Jun Shimada, Mr. Masayuki Saito, and Mr. Ryutaro Himeno helped with the calculations.

Preparation of this thesis has been helped by Miss Etsuko Morisaki in typewriting. Lastly, the author wishes to thank to Mrs. Machiko Ishikawa for her encouragement.

CONTENTS

NOMENCLATURE

Latin symbols

A	cross-section of duct (Part I)
A	square matrix (APPENDIX III)
A_0, A_1	cross-section of duct inlet and outlet, respectively
a	inclination parameter of electrodes
a_{opt}	optimum value of a
$\boldsymbol{B}$	applied magnetic induction vector
B	z-component of $\boldsymbol{B}$
B_w	magnetic flux density at duct wall
B_0	magnetic flux density at center of duct
$\boldsymbol{b}$	known column vector
C_p	specific heat at constant gas pressure
c	electrode width
c_f	friction factor
c_ξ, c_ζ	coefficient defined by Eqs.(1.42) to (1.44)
D	hydraulic dimeter of generator duct (Part I)
D	diagonal matrix (APPENDIX III)
$\boldsymbol{E}$	electric field intensity vector
$\boldsymbol{E}'$	electric field intensity vector in resistive electrode
E	lower triangular matrix
E_x, E_y, E_z	x, y, and z component of $\boldsymbol{E}$
E'_x, E'_y	x and y component of $\boldsymbol{E}'$
$(E_x)_{open}$	x component of $\boldsymbol{E}$ for open circuit condition
e	electric charge of electron
F	upper triangular matrix
f	friction loss on duct wall
g	gradient of B in end region
h	duct height
h'	Planck's constant
I	load current of generator
I'	current defined by Eq.(2.94)

I_i	current defined by Eq.(2.69)
I_x	x-component of I
I_y	y-component of I
I'_y	current flowing into anode
$I_y^{(n)}$	current flowing into anode A_n
i	mesh number in the x direction
i_z	ratio of the current flowing into one conducting sidewall to I'
$\boldsymbol{J}$	current density vector
$\boldsymbol{J}'$	current density vector in resistive electrode
J_n	current density perpendicular to cross-section C'A' in Fig.2.1
J_{peak}	maximum current density on electrodes (Part II, Chapter 4)
J_x, J_y, J_z	x, y, and z component of $\boldsymbol{J}$
J'_x, J'_y	x and y component of $\boldsymbol{J}'$
$\langle J \rangle_{el}$	average current density on electrodes (Part II, Chapter 4) or on output electrodes (Part II, Chapter 5)
j	mesh number in the y direction (Part II, Eq.2.44) or electrode number where B begins decreasing in end region (Part II, Chapter 5)
k	Boltzmann's constant
k_s	equivalent sand roughness
L	generator duct length
L_{opt}	optimum value of L
M_{opt}	optimum value of M_0
M_0	Mach number of the working fluid
m, m'	constant in Eqs.(2.8) and (2.9)
m_e	electron mass
m_i	mass of ion
m_s	mass of seed atom
m_0	mass flow rate (Part I)
m_0	mass of parent gas atom (Part II)

n, n'	constant in Eqs.(2.86) and (2.87)
n_e	number density of electron
n'_e	normalized electron density
n_{es}	electron density obtained from Saha's equation
n_s	number density of seed atom
n_{s0}	original number density of seed atom befor ionization
n_0	number density of parent gas atom
P_{com}	driving power of compressor
P_{MHD}	DC output of MHD generator
P_{st}	AC output of steam generator
P_t	total AC output of MHD-steam plant
P_w	power density of generator
p	static gas pressure
p_{com}	pressure at compressor entrance
p_e	partial pressure of electron
p_r	Prandtl number
p_s	stagnation pressure
p_{s0}, p_{s1}	stagnation pressure at duct inlet and outlet
p_1	static gas pressure at duct outlet
Q_{ei}	collision cross-section between electrons and ions
Q_H	specific Hall voltage
Q_{in}	thermal input to MHD-steam plant
Q_{is}	collision cross-section between ions and seed atoms
Q_{i0}	collision cross-section between ions and parent gas atoms
Q_{loss}	heat loss of the generator
Q_s	collision cross section between electrons and seed atoms
Q_{st-in}	thermal input to steam cycle
Q_0	collision cross-section between electrons and parent gas atoms
q	heat loss on duct wall
R	gas constant of working fluid
R_b	ballast resistance

R_{b0}	R_b for g=0
R_i	internal resistance of end region
R_{i0}	R_i for g=0
R'_i	resistance between A_i and C_i in Fig.2.34
r	recovery factor
S_i	arbitary surface crossing the insulating wall surfaces A'_i and C'_i in Fig.2.34
s	electrode pitch
T	static gas temperature
T_{com}	temperature at compressor entrance
T_e	electron temperature
T'_e	normalized electron temperature
T_{eopt}	optimum value of T_e
T_{e0}, T_{el}	electron temperature at duct inlet and outlet
T_s	stagnation temperature
T_{s0}, T_{sl}	stagnation temperature at duct inlet and outlet
T_w	duct wall temperature
T_0	gas temperature at the center of duct
T_6	temperature given in Fig.1.2(a)
T_8	temperature at exit of compressor
U	unit matrix
$\boldsymbol{u}$	gas velocity vector
u	x component of gas velocity
u_0	gas velocity at the center of duct
V	duct volume (Part I)
V	potential difference between output electrode pair and n-th electrode in Fig.2.34 (Part II)
V_H	potential difference per one electrode pitch
V_i	potential difference between A_i and C_i in Fig.2.34
V'_i	ionized voltage of seed atom
V_{ideal}	ideal potential difference per one electrode pitch
V'_{sc}	quantity approximately proportional to the required quantity of the super-conducting wire
V'_x	potential difference per one electrode pitch

V_y	potential difference between anode and cathode
V_0	no-load potential difference between the output electrode pair and n-th electrode in Fig.2.34
v	volume of hexahedron
v_D	ratio of electrode voltage drop to V_y
w	width of the duct in the z direction
X	$(\gamma-1)M_0^2/2$
x	unknown column vector
x_i	defined by Eq.(2.44)
x_1	x co-ordinate of the right edge of the insulating wall C_n' in Fig.2.34
y_j	defined by Eq.(2.44)
Z	stage number of compressors
x,y,z	space co-ordinates

Greek symbols

α	$\gamma/(\gamma-1)$ (Part I)
α	angle between J and the direction normal to the boundary surface in Fig.2.21 (Part II)
α'	angle between J' and the boundary surface in Fig.2.21
β	local Hall parameter for electrons
β_{crit}	critical Hall parameter
β_{eff}	effective Hall parameter
β_i	local Hall parameter for ions
γ	specific heat ratio
Δ	dimensionless voltage drop (Part I)
Δ	width of mesh in difference scheme (Part II)
δ	collision loss factor
δ_B	shown in Fig.2.28
ε	$1 + \beta\beta_i$
ε_s	seed fraction
ε_0	permittivity of free space
ζ	new variable derived from T_s (Part I)

	or from y (Part II)
η	total thermal efficiency of MHD-steam plant
η_b	boiler efficiency
η_{com}	compressor efficiency
η_{DA}	conversion efficiency of a DC-AC inverter
η_d	diffuser efficiency
η_e	electrical efficiency
η_h	heat exchanger efficiency
η_i	isentropic efficiency of generator duct
η_{MHD}	enthalpy extraction from generator duct
η_{re}	recovery efficiency of heat loss of duct
η_{st}	efficiency of steam cycle
θ	angle of inclination to the y axis of straight lines joining equipotential electrodes
θ'	angle between a total average current density J and x-axis
κ	load factor of diagonal type generator
κ_f	load factor of Faraday type generator
Λ	given by Eq.(2.13)
λ	parameter of finite segmentation effect of electrodes
μ	viscosity of working gas
μ_e	electron mobility
ν_e	average electron momentum-transfer collision frequency
$\nu_{es}, \nu_{e0}, \nu_{ei}$	coefficient defined by Eq.(2.6)
ν_r	coefficient defined by Eq.(2.2)
ξ	new variable derived from p_s (Part I) or from x (Part II)
ρ	mass density of working fluid
σ	local electrical conductivity
σ_e	electrical conductivity of resistive electrode
σ_{eff}	effective electrical conductivity of gas
σ', σ''	given by Eq.(2.19)
$\langle\sigma\rangle_i$	average electrical conductivity of plasma between A_i and C_i in Fig.2.34

Φ	potential function
Ψ	stream function
ψ	normalized stream function
ψ_{ij}	value of ψ at the point (x_i, y_j)
Ω	relaxation parameter matrix
$\omega, \omega^*, \omega_0$	relaxation parameter
ω', ω''	constants on relaxation parameter
$< >$	shows average value per one electrode pitch

PART I

OPTIMIZATION OF DIAGONAL TYPE NONEQUILIBRIUM PLASMA MHD GENERATOR

CHAPTER 1
INTRODUCTION

In designing an MHD generator duct, it is necessary that the generator duct is constructed in an optimum form. Hitherto, optimizations of the open-cycle diagonal type generator, in which an alkali-metal seeded combustion gas of fossil fuel is used, have been studied theoretically by Takano [1.23], Convey [1.24], Bobbio [1.25], Gorb [1.26], Yoshida [1.27], et al., and that of the closed-cycle Faraday type generator, in which alkali-metal seeded rare gas in nonequilibrium ionization is utilized, by Zauderer [1.28], Shioda [1.29], et al. On the other hand, optimization of the closed-cycle diagonal type generator has not been studied by anyone except the author [1.30]-[1.35].

In this part, an optimization of a large scale diagonal type MHD generator with nonequilibrium plasma of cesium-seeded rare gas is investigated. The generator is optimized so as to maximize the total thermal efficiency of an MHD-steam power plant by varying separately some parameters such as the Mach number, diagonal angle, duct length, inlet stagnation pressure or temperature, etc.

For grasping exactly performance characteristics of an MHD generator, a two- or three-dimensional analysis is required. However, by the usual two- or three-dimensional analysis, we can analyze only a local characteristics of the large scale generator. In this part, since the whole performance of the generator is studied the working fluid is assumed to be a quasi one-dimensional gas.

In Chapter 2, there are introduced quasi one-dimensional basic equations for the working gas flow in the diagonal and Faraday type generators, in which the friction and heat losses along the duct, the electrode voltage drop, the finite segmentation effect of electrodes, etc. are considered and it is assumed that the end effects of a generator and the relaxation of ionization can be neglected.

Next, as an estimation function for the optimization of the

generators, the total thermal efficiency is adopted. The isentropic efficiency, output power density, etc. of the generator, some constraints for the optimization, etc. are derived.

In Chapter 3, by the optimization theory derived in Chapter 2, numerical calculation is made for an example of the closed-cycle diagonal type MHD-steam power plant of the thermal input of about 2000 MW. Influences of the Mach number, inclination parameter, duct length, inlet pressure and temperature, etc. of the diagonal type generator on the total thermal efficiency of the plant are investigated in detail. As the results, an optimum duct of optimum Mach number, inclination parameter, duct length, etc., which maximize the efficiency, is found out. Next, in the similar way, the optimization of the Faraday type generator is studied, and a comparative study of the performances of both type generators is made.

CHAPTER 2
OPTIMIZATION THEORY

2.1 Introduction

In this chapter, first, there are introduced quasi one-dimensional basic equations for the working gas flow in the diagonal and Faraday type generators, in which friction and heat losses along the generator duct, the electrode voltage drop, the finite segmentation effect of electrode, etc. are considered. Next, as an estimation function for the optimization of the generators, the total thermal efficiency is adopted. Besides, the isentropic efficiency, output power density, etc. of the generator, some constraints for the optimization are derived. The expressions of the electrical conductivity and the Hall parameter are derived, where ionization instabilities are considered.

Finally, for the constant Mach number type generators, the numerically solvable differential equations for the stagnation pressure and temperature are derived from the above basic equations.

2.2 Basic Equations in MHD Generator Duct

The MHD flow in a diagonal type generator duct [see Fig.1.1] is described by the following set of quasi one-dimensional basic equations, namely the continuity equation

$$\rho u A = m_0, \tag{1.1}$$

the momentum equation

$$\rho u \frac{du}{dx} + \frac{dp}{dx} = J_y B - f, \tag{1.2}$$

the energy equation

$$\rho u \frac{d}{dx}\left(C_p T + \frac{u^2}{2}\right) = E_x J_x + E_y E_y - q, \tag{1.3}$$

the state equation

$$p = \rho R T, \tag{1.4}$$

the current continuity equation

$$(J_x + aJ_y)A = I, \quad a = \tan\theta, \tag{1.5}$$**

and the generalized Ohm's law

$$\left.\begin{aligned} J_x &= \frac{\sigma_{eff}}{1+\beta_{eff}^2}[E_x + \beta_{eff}\{uB(1-\Delta) - E_y\}] \\ J_y &= \frac{\sigma_{eff}}{1+\beta_{eff}^2}[\{E_y - uB(1-\Delta)\} + \beta_{eff}E_x] \end{aligned}\right\}, \tag{1.6}$$

where

$$E_y = aE_x. \tag{1.7}$$**

In these equations and Fig.1.1, A is the duct cross section, a the electrode inclination parameter*, B the applied magnetic flux density*, $C_p=\alpha R$ the specific heat* at constant pressure, E_x and E_y the x- and y-components of the electric field intensity, respectively, f the friction loss on the duct wall, I the load current*, J_x and J_y the x- and y-components of the current density, respectively, m_0 the mass flow rate*, p the gas pressure, q the heat transfer loss on the duct wall, R the gas constant*, T the gas temperature, u the gas velocity, $\alpha = \gamma/(\gamma-1)$*, β_{eff} the effective Hall parameter, γ the specific heat ratio*, σ_{eff} the effective electrical conductivity, Δ the dimensionless voltage drop*, and θ the angle* of inclination to the y axis of the straight lines joining the equipotential electrodes. The duct cross section is treated as square.

2.3 Estimation Function and Constraints for Optimization

2.3.1 Estimation function

A total thermal efficiency η of an MHD-steam plant is adopted

---

* Quantities which are assumed constant when the basic equations are solved.

** See Appendix I.

as an estimation function of the generator performance. For comparison between the diagonal and Faraday type generators, the quantity V'_{sc} is evaluated, which is approximately proportional to a required volume of the super-conducting wire [1.36]. In addition, the isentropic efficiency η_i and the output power density P_w of the generator and the enthalpy extraction η_{MHD} from the generator are also calculated.

Figures 1.2(a) and (b) show the block diagram and rough T-S diagram, respectively, of the MHD-steam plant for the analysis in this thesis.

In the plant, η, η_i, η_{MHD}, P_w, and V'_{sc} are given by

$$\left.\begin{aligned} \eta &= P_t/Q_{in}, \\ P_t &= \eta_{DA}P_{MHD} + P_{st} - P_{com}, \\ Q_{in} &= m_0 C_p (T_{s0} - T_8), \end{aligned}\right\}, \tag{1.8}$$

$$\eta_i = P_{MHD}/[m_0 C_p T_{s0}\{1 - (p_{s1}/p_{s0})^{1/\alpha}\}], \tag{1.9}$$

$$\eta_{MHD} = P_{MHD}/m_0 C_p T_{s0}, \tag{1.10}$$

$$P_w = P_{MHD}/V, \tag{1.11}$$

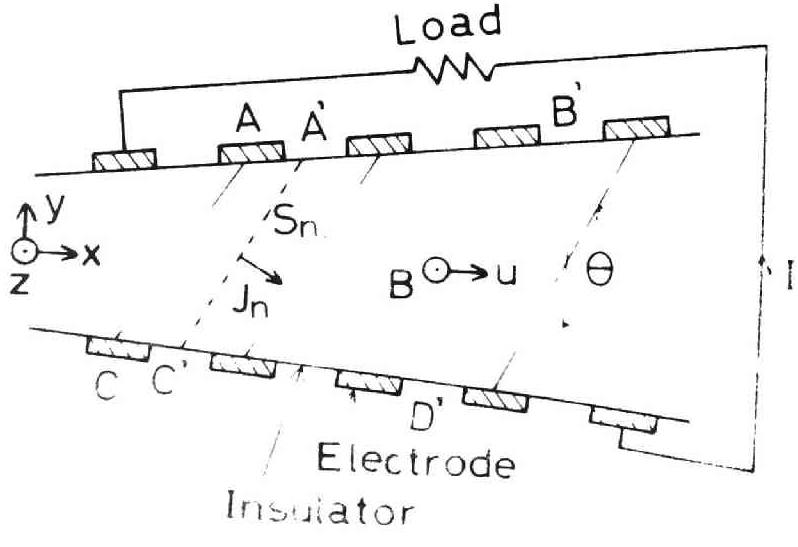

Fig. 1.1. Schema of a diagonal type MHD generator duct.

$$V'_{sc} = \sqrt{A_1}(1.8\sqrt{A_1} + L), \tag{1.12}$$

respectively, where P_t is the total AC output, P_{com} the driving power of the compressor, P_{MHD} the DC output of the MHD generator, P_{st} the output of the steam generator, Q_{in} the thermal input, V the duct volume, p_{s0} and p_{s1} the stagnation pressure at the duct inlet

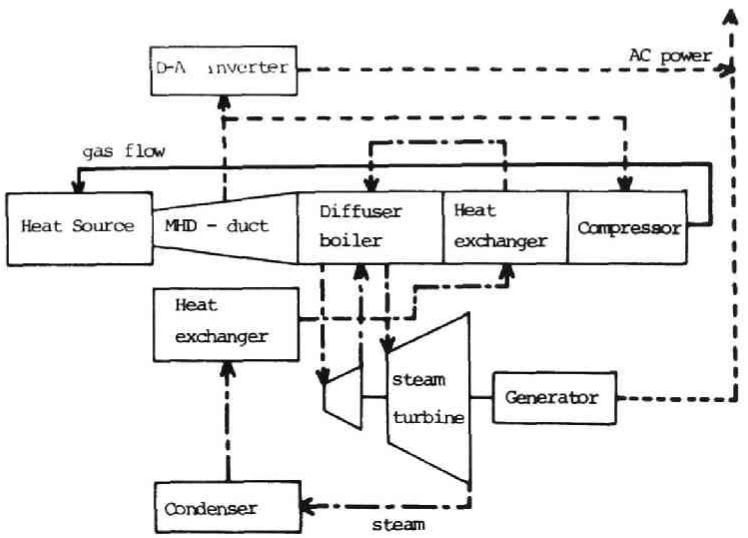

(a)

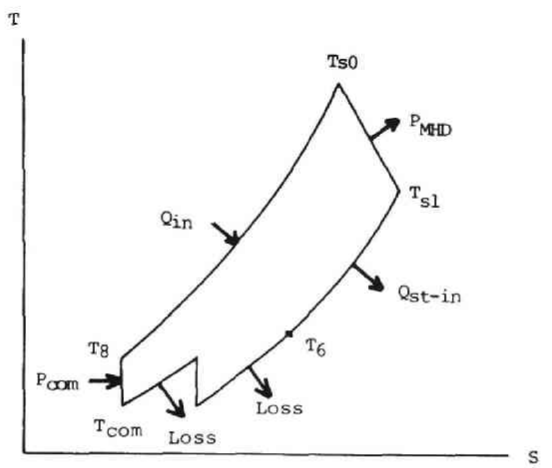

(b)

Fig. 1.2. (a) Block diagram of MHD-steam plant.
(b) T-S diagram.

and exit, respectively, T_{s0} the stagnation temperature at the duct inlet, T_8 the temperature at the compressor exit, A_1 the cross section of the duct exit, L the duct length and η_{DA} the inversion efficiency of DC-AC inverters.

Next, since it has been ascertained that Eq.(1.12) is available for $4T \leq B \leq 7T$ [1.36], let us assume that it is approximately valid for B=8 to 10 T, too. And P_{MHD}, P_{st}, P_{com}, T_8, and V are given by

$$P_{MHD} = -\int_0^L (E_x J_x + E_y J_y) A dx$$

$$= \frac{IB(1-\Delta)}{1+a^2} \int_0^L \kappa u (\beta_{eff} - a) dx, \tag{1.13}$$

$$P_{st} = Q_{st\text{-}in} \eta_{st}, \tag{1.14}$$

$$P_{com} = Z m_0 C_p T_{com} \{ (p_{s0}/p_{com})^{1/Z\alpha} - 1 \} / \eta_{com}, \tag{1.15}$$

$$T_8 = T_{com} (p_{s0}/p_{com})^{1/Z\alpha}, \tag{1.16}$$

$$V = \int_0^L A dx, \tag{1.17}$$

where $Q_{st\text{-}in}$ is the thermal input to the steam cycle, T_{com} and p_{com} the temperature and the pressure at compressor inlet, Z the stage number of compressors, κ the load factor defined by Eq.(1.41) and η_{com} and η_{st} the efficiencies of the compressor and the steam cycle, respectively. Here, $Q_{st\text{-}in}$ and p_{com} are given by

$$Q_{st\text{-}in} = Q_{loss} \eta_{re} + m_0 C_p (T_d - T_b) \eta_b$$

$$+ m_0 C_p (T_b - T_6) \eta_h, \tag{1.18}$$

$$p_{com} = p_1 + (p_{s1} - p_1) \eta_d, \tag{1.19}$$

where $Q_{loss} = \int_0^L Q A dx$ is the heat loss of the generator, T_b, T_d and, T_6 the temperatures at the boiler, the diffuser, and the heat-exchanger exits, respectively, p_1 and p_{s1} the static and stagnation pressures at the duct exit, and η_b, η_d, η_h, and η_{re} the efficiencies of the boiler, the diffuser, the heat exchanger, and the recovery of Q_{loss}, respectively. In addition, η_{st} varies usually

with the value of Q_{st-in} [1.37].

2.3.2 Constraints

In this article, let us introduce some constraints to be considered when the estimation function is evaluated.

First, in order that the end effects and the boundary layers may not become too large, it is assumed that the ratio of the duct length L to the width $\sqrt{A}$ is limited by

$$4 < L/\sqrt{A} < 18 \tag{1.20}$$

on reference to [1.28], [1.38], and [1.39].

Next, since too much enthalpy extraction causes the gas dynamic instabilities such as choking of the gas flow and the separation of the boundary layer, the following constraint

$$\eta_{MHD} < 45\ \% \tag{1.21}$$

is adopted on reference to [1.28] and [1.40].

2.4 Electrical Conductivity, Hall Parameter, and Fluid Losses

2.4.1 Electrical conductivity and Hall parameter

In this part, the effects of the relaxation of ionization is not considered as already described. It is assumed that the ionization instability occurs in the gas plasma, the electrons obtain their energies only by the Joule heating and lose those only by collisions, and the fluctuation of the electron temperature can be neglected [1.15]. On these assumptions, the electron temperature T_e, the effective electrical conductivity σ_{eff} and the effective Hall parameter β_{eff} are obtained as

for $\beta < \beta_{crit}$:

$$T_e/T = 1 + 2\gamma M_0^2\, \beta^2(1-\Delta)^2/\{3\delta(1+a^2)(1+\beta_{eff}^2)\}$$
$$\times \{(1+a^2) + \kappa(\beta_{eff}^2 - a^2)$$
$$-(\beta_{eff}-a)^2(1-\kappa)\kappa\}, \tag{1.22}$$

$$\sigma_{eff} = \lambda\sigma, \quad \beta_{eff} = \lambda\beta, \tag{1.23}$$

for $\beta > \beta_{crit}$:

$$T_e/T = 1 + 2\gamma M_0^2 \beta\beta_{crit}(1-\Delta)^2/\{3\delta(1+a^2)(1+\beta_{eff}^2)\}$$
$$\times \{(1+a^2) + \kappa(\beta_{eff}^2 - a^2)$$
$$- (\beta_{eff} - a)^2(1-\kappa)\kappa\}, \qquad (1.24)$$

$$\sigma_{eff}/\sigma = \beta_{eff}/\beta, \qquad \beta_{eff} = \lambda\beta_{crit}, \qquad (1.25)$$

where σ is the local scalar electrical conductivity, β and β_{crit} the local and critical Hall parameters for electrons, respectively, λ the parameter of the finite segmentation effect of the electrode, δ the collision loss factor, and M_0 the Mach number, in which λ is assumed constant [1.5], and moreover the grade of reduction of β_{eff} is assumed equal to that of σ_{eff} by reference to [1.21].

The local electrical conductivity σ and the Hall parameter β are given by

$$\sigma = n_e e^2/m_e\nu_e, \qquad (1.26)$$

$$\beta = eB/m_e\nu_e, \qquad (1.27)$$

where e, m_e and n_e are electron charge, mass, and number density, respectively, and ν_e the average momentum transfer collision frequency.

If the relaxation of ionization can be neglected, n_e is evaluated by Saha's equation, namely

$$n_e^2 = n_s(2\pi m_e kT_e/h'^2)^{3/2} exp(-eV_i'/kT_e),$$
$$n_s = n_{s0} - n_e, \qquad (1.28)$$

where h' is Planck's constant, k Boltzmann's constant, n_s the number density of seed atom, n_{s0} the original number density of seed atom before ionization, and V_i' the ionization potential of seed atom.

Next, ν_e is given by

$$\nu_e = (8kT_e/\pi m_e)^{1/2}(n_s Q_s + n_0 Q_0 + n_e Q_{ei}), \tag{1.29}$$

where n_0 is the number density of parent gas atom, and Q_0, Q_{ei}, or Q_s are the collision cross-sections between electron and parent gas atom, ion, or seed atom, respectively.

If T_e does not rise much, n_e becomes much smaller than n_s. Then, we have

$$n_s = \varepsilon_s p/kT, \tag{1.30}$$

where ε_s is the seed fraction, and $n_e Q_{ei}$ becomes negligible in comparison with $n_s Q_s$ and $n_0 Q_0$.

Consequently, substitution of Eqs.(1.28) to (1.30) into Eqs. (1.26) and (1.27) yields

$$\sigma = (2\pi m_e k/h'^2)^{3/4}(\pi\varepsilon_s/8m_e)^{1/2}e^2$$
$$\times p^{-1/2}T^{1/2}T_e^{1/4}/\{(1-\varepsilon_s)Q_0 + \varepsilon_s Q_s\}$$
$$\times exp(-eV_i'/2kT_e), \tag{1.31}$$

$$\beta = (k\pi/8m_e)^{1/2}eBp^{-1}TT_e^{-1/2}$$
$$/\{(1-\varepsilon_s)Q_0 + \varepsilon_s Q_s\}. \tag{1.32}$$

2.4.2 Friction and heat losses

It is assumed that the friction loss f and the heat loss q are given by

$$f = 2\rho u^2 c_f/D, \tag{1.33}$$

$$q = 4\rho u C_p/D \cdot c_f/2 \cdot (T_s - T_w)$$
$$/(1 + \sqrt{c_f/2}\beta_N), \tag{1.34}$$

respectively, where

$$\left.\begin{aligned} c_f &= \{2.87 + 1.58\log(x/k_s)\}^{-2.5} \\ &\quad /\{1 + r(\gamma-1)M_0^2/2\}, \\ r &= \sqrt{p_r}, \quad D = \sqrt{A}, \\ \beta_N &= 0.52(\rho u\sqrt{c_f/2}k_s/\mu)^{0.45} p_r^{0.8} \end{aligned}\right\}, \tag{1.35}$$

where c_f is the friction factor, D the hydraulic diameter, k_s the equivalent sand roughness which represents the roughness level of a plate surface, p_r the Prandtl number, r the recovery factor, T_s the local stagnation temperature in the main stream, T_w the wall temperature, and μ the viscosity of the gas [1.41]. Equations (1.33) to (1.35) are those which Schlichting has obtained for a compressible turbulent boundary layer on a rough plate [1.41].

2.5 Transformation of Basic Equations for Constant Mach Number Generator

2.5.1 Diagonal type generator

The basic flow equations (1.2) and (1.3) can be rewritten by the new variables defined by

$$\left.\begin{aligned} \xi &= \log(p_{s0}/p_s), \\ \zeta &= \log(T_{s0}/T_s), \end{aligned}\right\}, \tag{1.36}$$

and the adiabatic law

$$\log(p_s/p) = \alpha\log(T_s/T) = \alpha\log(1 + X), \tag{1.37}$$

where

$$X = (\gamma-1)M_0^2/2, \tag{1.38}$$

as follows:

$$d\xi/dx = \sigma_{eff} uB^2(1-\Delta)\{1 + (\beta_{eff}^2 - a^2)\kappa/(1+a^2)\}$$

$$/\{(1 + \beta_{eff}^2)p\} - \alpha X d\zeta/dx - f/p, \tag{1.39}$$

$$d\zeta/dx = I(\beta_{eff} - a)B\kappa(1-\kappa)/\{\alpha(1+X)pA(1+a^2)\}$$

$$+ q/\{\alpha(1+X)up\}, \tag{1.40}$$

where

$$\left.\begin{aligned} I &= (1-\kappa)\sigma_{eff}uBA(1-\Delta)(\beta_{eff}-a)/(1 + \beta_{eff}^2), \\ \kappa &= E_x/(E_x)_{I=0} \\ &= -(1 + a^2)E_x/\{(\beta_{eff} - a)uB(1-\Delta)\}. \end{aligned}\right\}, \tag{1.41}$$

Next, using Eqs.(1.22) or (1.24), (1.23) or (1.25), (1.31), (1.32), and (1.41), we can obtain the following equation

$$dT_e/dx = c_\xi d\xi/dx + c_\zeta d\zeta/dx, \tag{1.42}$$

where for $\beta < \beta_{crit}$:

$$\left.\begin{aligned} c_\xi &= T(f_1 f_{2p} + f_2 f_{1p})/\{1 - T(f_1 f_{2e} + f_2 f_{1e})\}, \\ c_\zeta &= T(-T_e/T + f_1 f_{2T} + f_2 f_{1T}) \\ &\quad /\{1 - T(f_1 f_{2e} + f_2 f_{1e})\}, \\ f_1 &= 2\gamma M_0^2 \beta^2 (1-\Delta)^2/\{3\delta(1+a^2)(1+\beta_{eff}^2)\}, \\ f_2 &= 1+a^2 + \kappa(\beta_{eff}^2 - a^2) - (\beta_{eff} - a)^2(1-\kappa)\kappa, \\ f_{1p} &= -f_{1T} = 2f_1/(1 +\beta_{eff}^2), \\ f_{1e} &= -f_1/\{T_e(1 + \beta_{eff}^2)\}, \\ c_{11} &= 2a + \kappa(\beta_{eff} - a), \\ c_{12} &= \beta_{eff}\{2\kappa(\beta_{eff} - a)\beta_{eff} + (\beta_{eff}^2 - 2a\beta_{eff} - 1)\} \\ &\quad /(1 + \beta_{eff}^2), \end{aligned}\right\}, \tag{1.43}$$

$$
\left.
\begin{aligned}
f_{2p} &= c_{11}\{1/2 + (1-\kappa)(\beta_{eff} - a) + c_{12}\}, \\
f_{2T} &= c_{11}\{-1/2 + (1-\kappa)(\beta_{eff} - a) + c_{12}\}, \\
f_{2e} &= c_{11}\{1/4 + T_i/T_e - c_{12}\}/T_e,
\end{aligned}
\right\}
$$

and for $\beta > \beta_{crit}$:

$$
\left.
\begin{aligned}
c_\xi &= (T_e - T + c_e)/c_0, \\
c_\zeta &= -(2T_e - T + c_e)/c_0, \\
c_0 &= 1 - \{c_e(2T_i/T_e + 3/2) - (T_e - T)/2\}/T_e, \\
c_e &= 2\gamma M_0^2 \beta\beta_{crit}(1-\Delta)^2 T(\beta_{eff} - a)(1-\kappa) \\
&\quad \times\{a + (\beta_{eff} - a)\kappa\}/\{3\delta(1+a^2)(1 + \beta_{eff}^2)\}.
\end{aligned}
\right\}, \quad (1.44)
$$

Now, for obtaining the values of p, T, etc. in the diagonal type generator we have to assume beforehand one value of M_0, u, A, etc. or one relation among them. We assume that M_0 is constant by reference to the previous investigation of the Faraday type generator [1.42]. Then, Eqs.(1.39),(1.40), and (1.42) can be numerically solved with the assumed values of m_0, p_{s0}, T_{s0}, M_0, I, and L. Thus, the optimum generator duct can be obtained which makes maximum under the constraints (1.20) and (1.21).

2.5.2 Faraday type generator

The momentum and energy equations for the Faraday type generator, which correspond to Eqs.(1.2) and (1.3), respectively, in the case of $J_x=0$, are transformed to the following equations

$$
d\xi/dx = \sigma_{eff} uB^2(1-\Delta)(1 - \kappa_f)/p - \alpha X d\zeta/dx + f/p, \quad (1.45)
$$

$$
\begin{aligned}
d\zeta/dx &= \sigma_{eff} uB^2(1-\Delta)^2\kappa_f(1 - \kappa_f)/\{\alpha(1+X)p\} \\
&\quad + q/\{\alpha(1+X)up\},
\end{aligned} \quad (1.46)
$$

similar to Eqs.(1.39) and (1.40), respectively, for the diagonal type, where κ_f is the load factor of the Faraday type generator defined by

$$\kappa_f = E_y/\{uB(1 - \Delta)\}. \tag{1.47}$$

In addition, since two conditions are necessary to analyze the performances of the Faraday type generator, by reference to [1.42], it is assumed that the Mach number $M = M_0$ and the electron temperature $T_e = T_{e0}$ are constant. Then, κ_f is written as

$$\kappa_f = 1 - \{3\beta\delta(T_{e0} - T)/(2\beta_{crit}\gamma T)\}^{1/2} /\{M_0(1-\Delta)\beta\}, \tag{1.48}$$

2.6 Concluding Remarks

In this chapter, an optimization theory of the MHD generator has been described. The main conclusions are as follows.

(1) The numerically solvable differential equations for the stagnation pressure, temperature, and electron temperature were derived from the basic MHD equations for the constant Mach number generator. For these equations, the electrode voltage drop, effect of finite segmentation, friction and heat losses at the duct wall, and ionization instabilities were considered.

(2) As the estimation function of the generators the total thermal efficiency of an MHD-steam power plant for the optimization was derived, where the efficiencies of diffuser, heat exchanger, and compressor, etc. were considered, and some constraints required for the estimation function were introduced.

CHAPTER 3
NUMERICAL INVESTIGATION

3.1 Introduction

In this chapter, using the optimization theory derived in the preceding chapter, numerical calculation is made for a closed cycle diagonal type MHD-steam power plant with about 2000 MW of the thermal input. Influences of the Mach number, inclination parameter, duct length, inlet pressure and temperature, etc. of the diagonal type generator on the total thermal efficiency of the plant are investigated in detail. As the results, an optimum duct of optimum Mach number, inclination parameter, duct length, etc. is found out, which maximizes the efficiency. Then, the distributions of physical quantities in the optimum duct are discussed.

Next, in the similar way, the optimization of the Faraday type generator is discussed, and the optimum Mach number, duct length, etc. are obtained. Finally, a comparative study of the performances of both type generators is made.

3.2 Numerical Conditions

A numerical analysis is carried out for the cesium-seeded helium in nonequilibrium ionization. We assume that the thermal input Q_{in} = 2000 MW as previously mentioned. Also the magnetic flux density B = 6 to 10 T, the inlet stagnation pressure p_{s0} = 5 to 15 atm, and the inlet stagnation temperature T_{s0} = 1600 to 2200 K are used. We adopt the seed fraction ε_s = 0.3 % and the compressor stage number Z = 2, which maximize the total thermal efficiency η under the conditions that L = 10 m, p_{s0} = 10 atm, and T_{s0} = 2000 K. Also η_{st} is given by

$$\eta_{st} = \left\{ \begin{array}{ll} 38.25 & \text{for } Q_{st\text{-}in} < 380 \text{ MW}, \\ 41.04 & \text{for } 380 \leq Q_{st\text{-}in} < 1000 \text{ MW}, \\ 41.76 & \text{for } 1000 \leq Q_{st\text{-}in} < 1500 \text{ MW}, \end{array} \right\} , \quad (1.49) \qquad [1.37$$

$$42.30 \quad \text{for} \quad 1500 < Q_{st\text{-}in}. \qquad \Big)$$

Moreover, the case of η_{st} = 42.0 % is considered, too, in which it is assumed that some MHD generators and a steam turbine generator are operated together.

In Table 1.1, the above mentioned and the other assumed conditions are listed.

Table 1.1 Values of quantities used in numerical calculations

B	(T)	6 - 10	α		2.52
C_p	(J/Kg deg)	5.30×10^{3}	β_{crit}		2.0
k_s	(m)	4.0×10^{-4}	γ		1.67
m_0	(Kg/sec)	2.8×10^{3}	Δ		0.01
p_r		0.664	δ		2
p_{s0}	(atm)	5 - 15	ε_s	(%)	0.3
Q_0	(m^2)	5.4×10^{-20}	η_{com}	(%)	90.0
Q_s	(m^2)	300×10^{-20}	η_{DA}	(%)	98.0
T_{com}	(K)	300	η_b	(%)	99.0
T_6	(K)	350	η_d	(%)	90.0
T_w	(K)	1000	η_h	(%)	99.0
T_{s0}	(K)	1600 2200	η_{re}	(%)	98.0
V_i	(eV)	3.87	λ		0.9

3.3 Optimization of Diagonal Type Generator

3.3.1 Influence of Mach number and inclination parameter

In Fig.1.3 the variations of η by M_0 and a are shown in the case of p_{s0} = 10 atm, T_{s0} = 2000 K, and L = 10 m. From the figure, it is seen that there exists an optimum Mach number M_{opt} which maximizes η, M_{opt} becomes larger with $|a|$, M_{opt} = 1.38 at a = -2.2, and the maximum value of η varies little for $-1.8 < a < -2.6$.

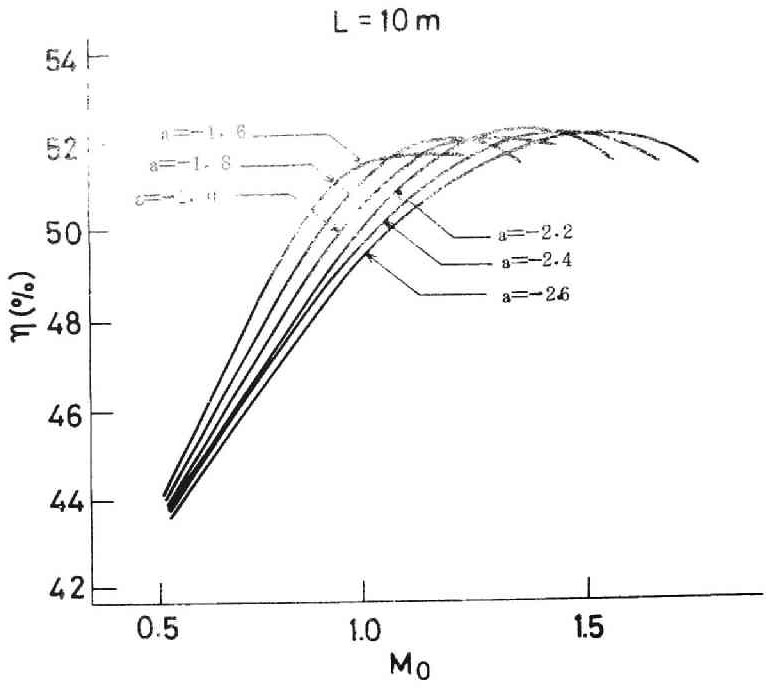

Fig. 1.3. Influence of M_0 and a on η.

3.3.2 Influence of duct length

Figure 1.4 illustrates the influences of L and a on the maximum value of η corresponding to $M_0 = M_{opt}$ in the case of p_{s0} = 10 atm and T_{s0} = 2000 K. The figure presents that there exists an optimum inclination parameter a_{opt} which makes η maximum and that the variation of η by L is fairly small except the case of L = 8 m where the constraint (1.20) prevents η from increasing because of a short duct length. Then, η has the maximum value 52.1 % at a = -2.2 and L = 10 m. Next, Fig.1.5 shows the variations of η by M_0 when η_{st} has the constant value 42.0 % and the variable values given by Eq.(1.45) under the same conditions as in Fig.4. It indicates that the value of η is heightened about 0.2 % by combining some MHD generators and one steam cycle.

3.3.3 Influence of inlet stagnation pressure

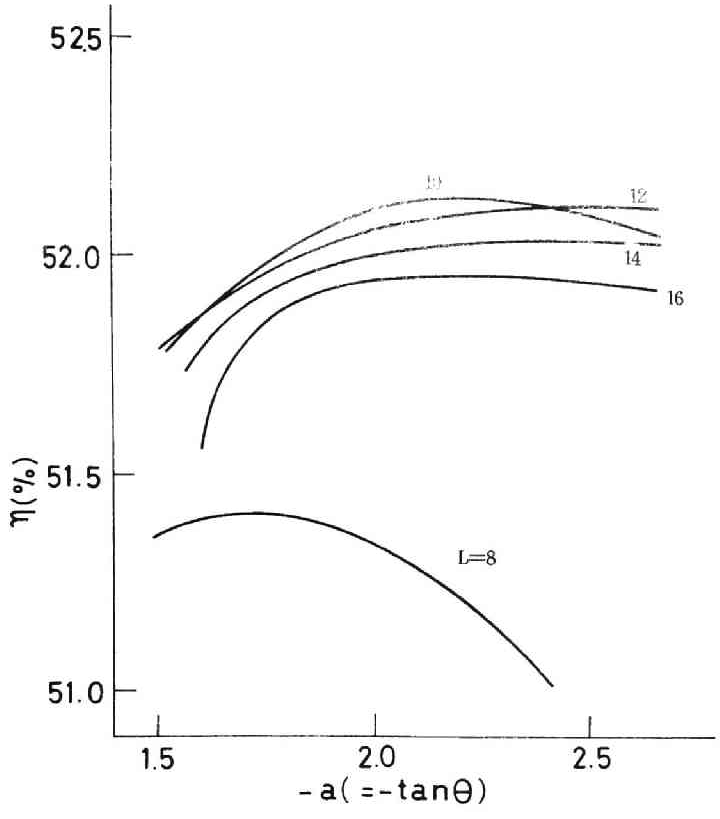

Fig. 1.4. Influence of L and a on η.

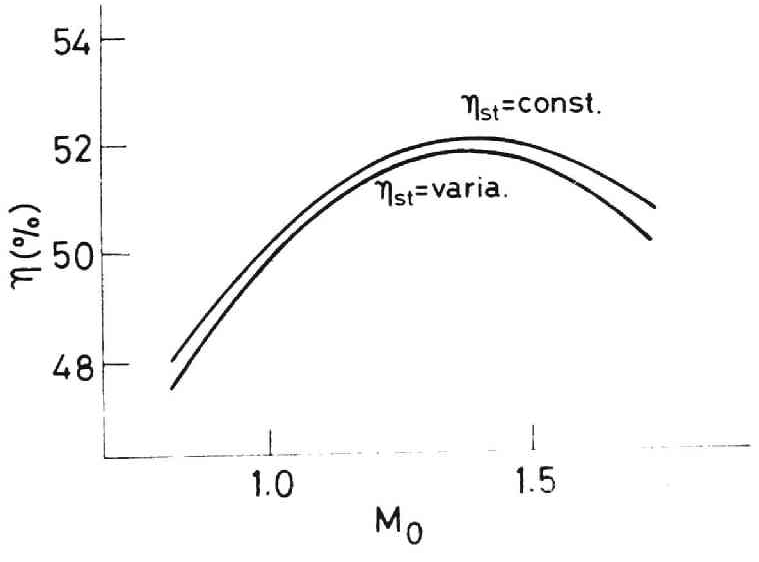

Fig.1.5. η vs. M_0 when η_{st} is assumed constant or variable.

Figure 1.6 denotes the variation of η by p_{s0} and a in the case of T_{s0} = 2000 K and L = 10 m. It is shown that the smaller p_{s0} is, the larger η and a_{opt} are, and for example, the maximum values of η reach 53.4 and 53.1 % for p_{s0} = 5 and 7.5 atm, respectively.

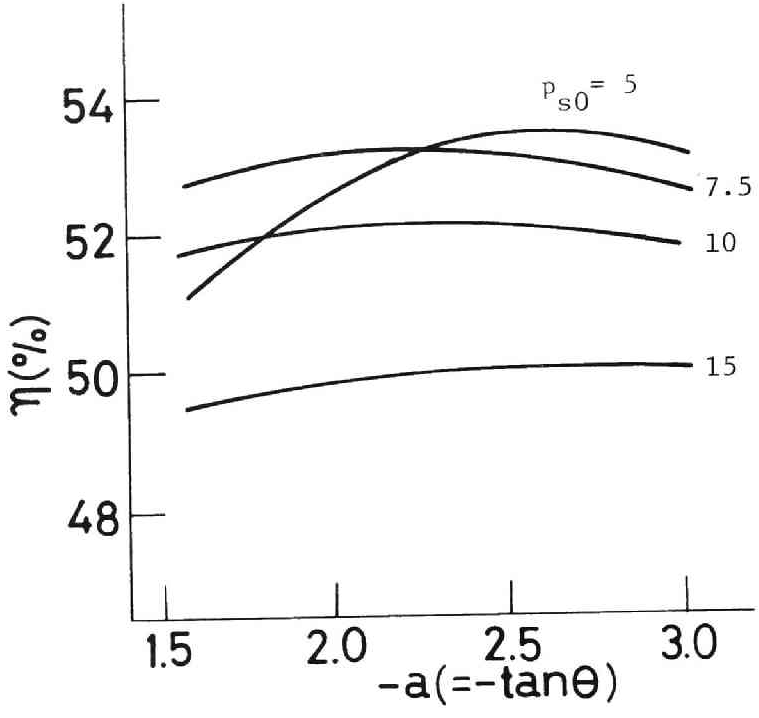

Fig. 1.6. Influence of p_{s0} and a on η.

3.3.4 Influence of inlet stagnation temperature

Figure 1.7 shows the influences of T_{s0} and a on η in the case of p_{s0} = 10 atm and L = 10 m. The figure indicates that the value of η increases by about 1.6 % per increase of 100 K of T_{s0} and that the maximum value of η is little dependent on a in the range of $|a| > 1.5$. These indicate that T_{s0} should be elevated more than 1900 K for obtaining $\eta > 50$ %.

3.3.5 Influence of applied magnetic flux density

In Fig.1.8, the influences of a and B on η are shown when

T_{s0} = 2000 K, p_{s0} = 7.5 atm, and L = 10 m.

From the figure, it is seen that $|a_{opt}|$ becomes large with increasing B, for example, a_{opt} = -1.8, -1.95, and -2.2 for B = 6, 8, and 10 T, respectively.

Moreover, the maximum value of η exceeds 50 % for $B>$ about 6 T, and it increases with increasing B by the rate of about 1 % per 1 T. The rate of increase of η by B does not become so much in the case where the ionization instability is considered as in this thesis, though the output power increases in proportion to B^2 if the ionization instability does not occur.

3.3.6 Distribution of various quantities in optimum duct

In Figs. 1.9 and 1.10, there are plotted the distributions of

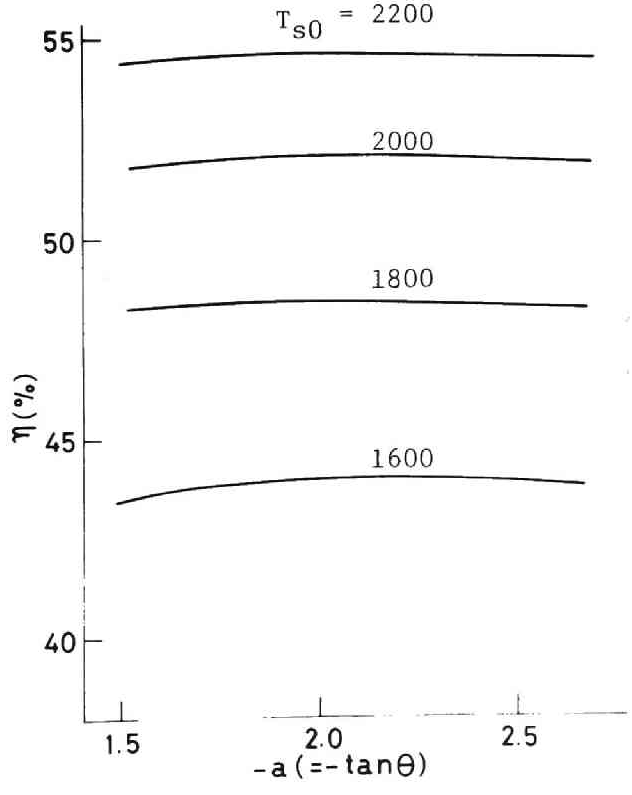

Fig. 1.7. Influence of T_{s0} and a on η.

the quantities in the optimum generator duct [see Table 1.2], which gives the maximum efficiency η, where B = 10 T, p_{s0} = 10 atm, and T_{s0} = 2000 K. In this case, we have η = 52.1 %, η_i = 73.6 %, η_{MHD} = 44.0 %, and P_w = 52.3 MW/m^3 as listed in Table 1.2. Figure 1.8 shows that T_e decreases uniformly from T_{e0} = 2000 to T_{e1} = 1900 K, and so the difference $T_{e1} - T_{e0}$ is only about 5 % of T_{e0}. Therefore T_e may be regarded as almost constant. σ_{eff} decreases from 1.16 to 0.31 ℧/m and inversely β increases from 4.8 to 32.2. Also J_x changes its sign in the latter half of the generator duct, both $-E_x$ and E_y have their peaks there, and $|E_x|$ does not exceed 9kV/m. Next, the ratio of the inlet cross section to the exit A_1/A_0 is 8.38.

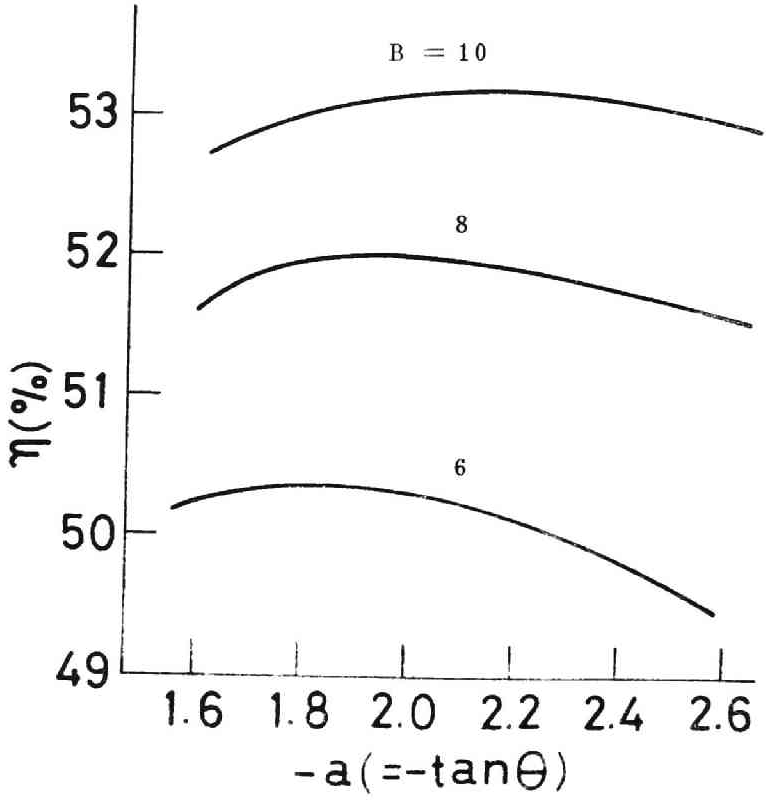

Fig. 1.8. Influence of B and a on η.

3.4 Optimization of Faraday Type Generator

In the performance analysis of the Faraday type generator, M_0 and T_{e0} are assumed constant along the flow, and the same numerical conditions as for the diagonal type listed in Table 1.1 are used.

The duct length of the optimum duct becomes about 10 m under the given conditions. Also are obtained T_{eopt} = 1970 K, M_{opt} = 1.34, η = 52.3 %, η_i = 74.4 %, η_{MHD} = 44.4 %, and P_w = 56.1 MW/m^3 in the case of T_{s0} = 2000 K and p_{s0} = 10 atm as shown in Table 1.2, where T_{eopt} is an electron temperature which maximizes η.

The distributions of the quantities in the optimum duct of the Faraday type generator are plotted in Figs.1.11 and 1.12, which

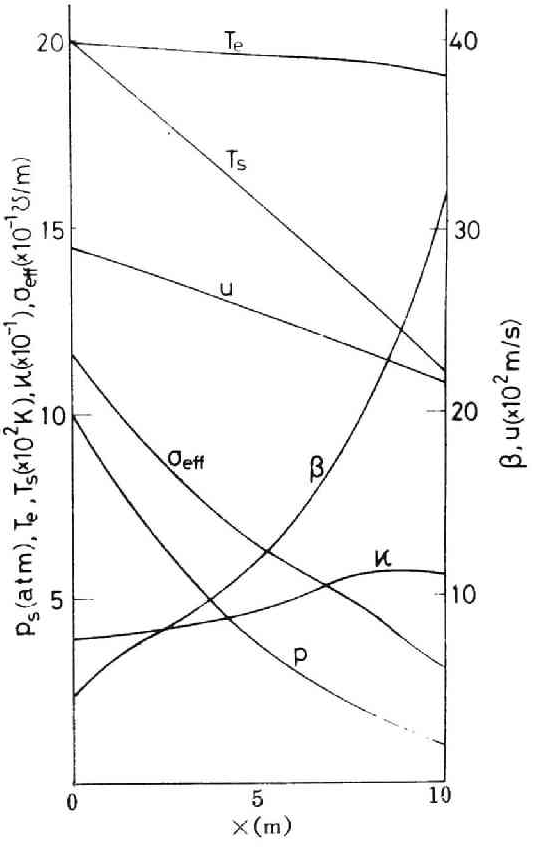

Fig. 1.9. Variation of quantities along the diagonal type generator duct (I).

show that σ_{eff} decreases from 0.81 to 0.36 $\mho$/m and β increases from 6.3 to 32.4 along the duct. Also $|E_x|$ exceeds 10 kV/m in the first half of the duct and A_1/A_0 becomes 7.01.

3.5 Comparison between Diagonal and Faraday Type Generators

As shown in the previous sections, the values of the various quantities in the optimum generator ducts in the case of T_{s0} = 2000 K and p_{s0} = 10 atm are listed in Table 1.2. As seen in the table, η, η_i, and P_w of the diagonal type generator become about 0.2 %, 0.8 %, and 3.8 MW/m^3, respectively, smaller than those of the Faraday type, and V'_{sc} of the former becomes only a little

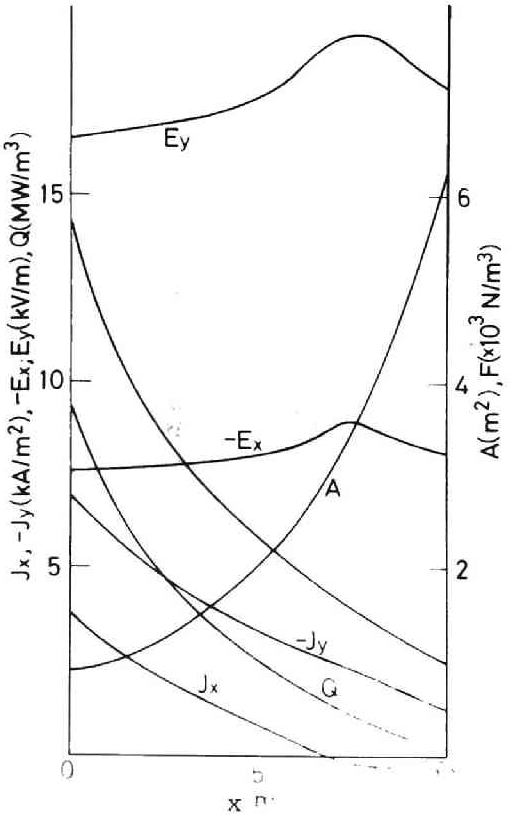

Fig. 1.10. Variation of quantities along the diagonal type generator duct (II).

larger than that of the latter. In both type generators, the optimum duct length L_{opt}, which makes η maximum, is nearly equal, M_{opt} becomes supersonic, and M_{opt} of the diagonal type is a little lower than that of the Faraday type generator. Next, $|E_x|$ in the former is below 9 kV/m, but that in the latter exceeds 10 kV/m.

In the open cycle MHD generation, the performances of the diagonal type generator are a little inferior to those of the Faraday type generator [1.23]. On the other hand, the difference of the performance between both type generators in the closed cycle MHD generation is fairly smaller than that in the open cycle. Consequently, it can be said that the performances of the diagonal type generator sufficiently approach to those of the Faraday type.

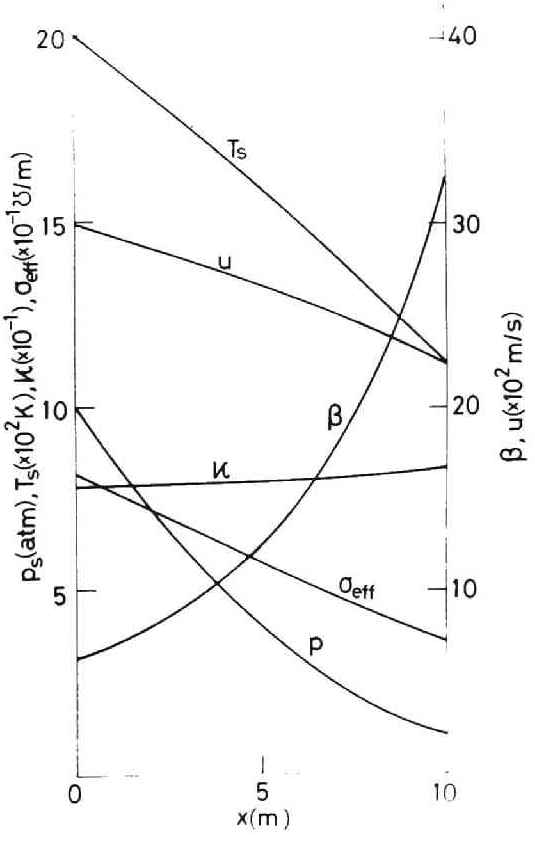

Fig. 1.11. Variation of quantities along the Faraday type generator duct (I).

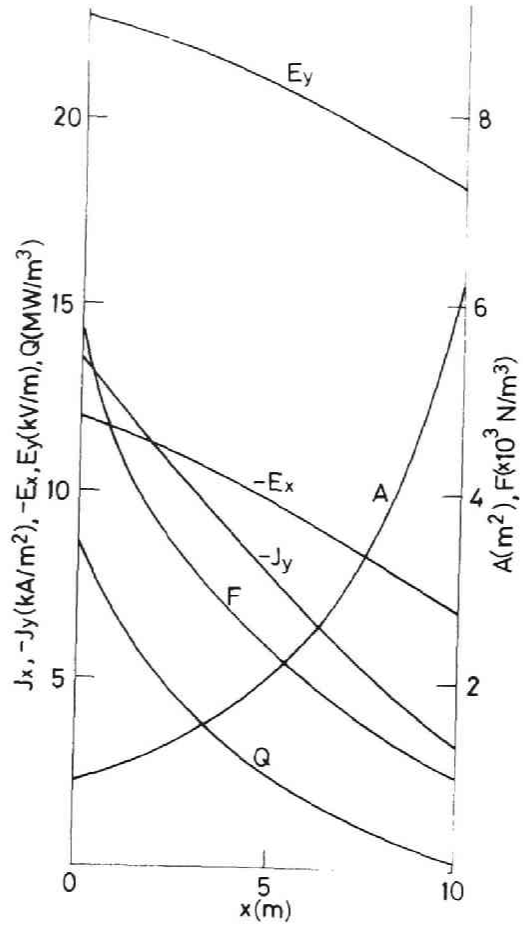

Fig. 1.12. Variation of quantities along the Faraday type generator duct (II).

Table 1.2 Values of various quantities in optimum duct

		Diagonal Faraday				Diagonal Faraday	
α		-2.2		P_w	(MW/m^3)	52.3	56.1
I	(kA)	16.2		P_{MHD}	(MW)	1310	1320
T_e	(K)	1950	1970	P_{st}	(MW)	453	478
M_0		1.38	1.34	P_c	(MW)	594	593
L	(m)	10.0	10.0	P_t	(MW)	1143	1179
η	(%)	52.1	52.3	A_1/A_0		8.38	7.01
η_i	(%)	73.6	74.4	V'_{sc}	(m^2)	36.3	35.8
η_{MHD}	(%)	44.0	44.5				

3.6 Concluding Remarks

The main conclusions, which were derived from the above described numerical analysis, are as follows.

(1) When the ionization instability of the nonequilibrium plasma is assumed to occur, the total thermal efficiency of the MHD-steam plant with the diagonal type generator exceeds 52 % in the case of B = 10 T, p_{s0} = 10 atm, and T_{s0} = 2000 K.

(2) The optimum values of the Mach number and the inclination parameter are considerably influenced by the value of B, p_{s0}, or T_{s0}, and we have M_{opt} = 1.38 and a_{opt} = -2.2 in the case of B = 10 T, p_{s0} = 10 atm, and T_{s0} = 2000 K.

(3) The optimum duct length of the diagonal type generator is nearly equal to that of the Faraday type generator, and about 10 m. In this connection, the variation of the thermal efficiency by L is small.

(4) The smaller p_{s0} is, the larger η and a_{opt} are. The small p_{s0} gives the very large $|a_{opt}|$.

(5) The total thermal efficiency increases by about 1.6 % per increase of 100 K of T_{s0} and it reaches about 50 % at T_{s0} = 1900 K.

(6) The efficiency decreases by about 1.0 % per decrease of 1 T of B, but it exceeds 50 % still in the case of B = 6 T.

(7) The performances of the diagonal type generator can sufficiently approach to those of the Faraday type, and the thermal efficiency of the former is only 0.2 % lower than that of the latter. In both types, a quantities proportional to the volume of the superconducting wire is almost equal each other.

Thus, it may be thought that the diagonal type nonequilibrium plasma MHD generator will be practically used in future in view of the total thermal efficiency of the MHD-steam power plant.

PART II

TWO-DIMENSIONAL ANALYSES OF DIAGONAL TYPE NONEQUILIBRIUM PLASMA MHD GENERATOR

CHAPTER 1
INTRODUCTION

Electrical characteristics of MHD generators can be totally investigated by a quasi one-dimensional theory. However, in the generator duct, there usually occurs two- or three-dimensional phenomena, which cannot be analyzed by the above theory, such as current concentration at the electrode end and end effects. These have large influence on the generator performance. Accordingly, at least, a two-dimensional analysis of the generator becomes necessary for grasping more accurately the performance.

The two- or three-dimensional current and potential distributions in the Faraday type generator have been investigated in fair detail by Hurwitz [1.1], Celinski [1.3], Oliver [2.1], Argyropoulos [2.2], Lengyel [2.3], and many others, and its electrical characteristics have been considerably clarified. Those distributions in the Hall type generator have been studied by Denzel [2.4], Tanaka [2.5], et al. Moreover, the generator characteristics of a diagonal type MHD generator have been a little discussed by a two -dimensional analysis by Kaidalov [2.6], et al., but the detailed analysis has not been made.

Therefore, the auther et al. have investigated some basic electrical characteristics of the diagonal type nonequilibrium plasma MHD generator [2.7] to [.12], two methods of improving the characteristics [2.13] to [2.15], the end effects in the generator [2.16] to [2.20], influences of difference between internal and external connections of the diagonal electrodes on the generator characteristics [2.21], [2.22], etc.

In this part, the electrical characteristics of the diagonal type nonequilibrium plasma generator will be investigated by two -dimensional analyses.

In Chapter 2, there are introduced the basic equations, which are used in the analyses, such as the Maxwell equations, the gen-

eralized Ohm's law, and the energy equation for electrons. Applying the stream and potential functions to the basic equations, the nonlinear two-dimensional partial differential equations to be numerically solved are obtained. Next, boundary and subsidiary conditions are shown, which are required for calculations of the current and potential distributions in the diagonal type generator. Further, for quantitative estimation of the electrical efficiency, the specific Hall voltage, an expression of grade of the current concentration at an electrode end, etc. are derived.

In Chapter 3, the basic electrical characteristics of the generator such as an electrical efficiency and a specific Hall voltage are investigated by a two-dimensional analysis. When the electrical conductivity and the Hall parameter are assumed constant, the current distribution is evaluated, and influences of the load factor, the Hall parameter, and the inclination parameter on the distribution are investigated. Then, influences of the inclination parameter, the Hall parameter, etc. on the electrical characteristics are studied. Next, when the electrical conductivity and the Hall parameter vary spatially, the distributions of current, potential, and electron temperature are shown, and influences of the load factor and the inclination parameter on the current distribution are discussed. Then, influences of the duct size and the temperatures of the gas plasma and the duct wall on the electrical characteristics are investigated.

In Chapter 4, effects of a resistive electrode and a distribution of the applied magnetic flux on the electrical characteristics of the generator are studied by a two-dimensional analysis. The configuration of the resistive electrode and the distribution of magnetic flux used in this chapter are shown. Next, influences of the conductivity and configuration of a wedge-shaped resistive electrode on the current concentration at the electrode, electrical efficiency, etc. are investigated. Next, the electrical characteristics of the generator with the attenuation of magnetic flux in

the region near the duct wall are compared with those of the generator with the constant magnetic flux.

In Chapter 5, end effects of the generator are investigated by a two-dimensional analysis. First, when electrical conductivity and electron mobility are assumed constant, influences of the attenuation of magnetic flux and type and position of the output electrodes on the current distribution, the internal resistance, etc. in the end regions are studied. Next, when nonuniformity of electrical conductivity and electron mobility are considered, effects of the attenuation of magnetic flux on the current distribution, the internal resistance, the ballast resistance, etc. are investigated.

In Chapter 6, effects of internal or external connection of electrodes in a diagonal type generator are investigated by a two-dimensional analysis in the duct cross section perpendicular to the plasma flow. First, the two-dimensional differential equations in the above cross section are derived from the basic equations in Chapter 2, and the boundary and subsidiary conditions are introduced. Next, numerical calculation results of the current and potential distributions in the generators with internally and externally connected electrodes are comparatively studied. Then, influences of the load factor, the duct wall temperature, and the inclination parameter on the current distribution, electrical efficiency, etc. are discussed.

CHAPTER 2
TWO-DIMENSIONAL THEORY

2.1 Introduction

As already noted, for grasping accurately the generator characteristics considering current concentration at the electrode end, etc., at least, a two-dimensional analysis of the generator is needed.

In this chapter, the basic equations are introduced such as the Maxwell equations, the generalized Ohm's law, and the energy equation for electrons. The nonlinear partial differential equations are derived by applying the stream and potential functions. Next, the boundary and subsidiary conditions are presented, which are required for the diagonal type generator. Further, the electrical efficiency, the specific Hall voltage, and expression of grade of the current concentration at an electrode end, etc. are derived.

2.2 Basic Equation

2.2.1 Basic equation

In a two-dimensional analysis of the electrical characteristics of the diagonal type nonequilibrium plasma MHD generator, it is assumed that the electric quantities such as the current density, electric field, etc. vary with x and y [see Fig.2.1] in Chapters 3 to 5, and in particular, do periodically in the period of the electrode pitch s in the x direction viz. along the gas flow in Chapters 3 and 4, and that the gas velocity and temperature in Chapters 3 to 5 depend on only y according to Eqs.(2.8) and (2.9) and the pressure is constant.

The Maxwell equations for the electromagnetic field, the continuity equation of electrons, the generalized Ohm's law, the energy equation of electrons, etc. are used as the basic equations

for the gas plasma in MHD duct.

First, the Maxwell equations are written as

$$\nabla \times \boldsymbol{E} = 0, \qquad \nabla \cdot \boldsymbol{J} = 0, \qquad \nabla \cdot \boldsymbol{B} = 0, \tag{2.1}$$

where $\boldsymbol{E}$, $\boldsymbol{J}$, and $\boldsymbol{B}$ are the electric field intensity, current density, and magnetic flux density or magnetic induction vectors, respectively.

Next, the continuity equation for the electrons is

$$\left.\begin{aligned} & u\partial n_e/\partial x = n_e(n_{es}^2 - n_e^2)\nu_r, \\ \text{where} \quad & \\ & \nu_r = 1.09\times10^{-20} T_e^{-9/2} \end{aligned}\right\}, \tag{2.2}$$

is the three body recombination coefficient, n_e the electron density, n_{es} the electron density obtained by the following Saha's equation

$$\left.\begin{aligned} & n_{es}^2 = n_s(2\pi m_e kT_e/h'^2)^{3/2} exp(-eV_i'/kT_e), \\ \text{in which} \quad & \\ & n_s = n_{s0} - n_{es}, \end{aligned}\right\}, \tag{2.3}$$

n_s and n_{s0} are the seed atom density and the original one before ionization, respectively, and u the x component of gas velocity.

The generalized Ohm's law is written as

$$\boldsymbol{J} = \sigma(\boldsymbol{E} + \boldsymbol{u}\times\boldsymbol{B} + \nabla p_e/en_e) - \beta\boldsymbol{J}\times\boldsymbol{B}/B + \beta\beta_i(\boldsymbol{J}\times\boldsymbol{B})\times\boldsymbol{B}/B^2, \tag{2.4}$$

which is nothing but the momentum equation for electrons, where $\boldsymbol{u}$ is the gas velocity vector, $p_e = n_e kT_e$ the electron partial pressure, and β_i the Hall parameter for ion [see Eq.(2.12)].

The energy equation for electrons is given by

$$u\partial\{(3/2kT_e + eV_i')n_e\}/\partial x = J^2/\sigma - 3/2kn_e m_e(T_e - T)$$

$$x(\nu_{es}/m_s + \nu_{e0}/m_0 + \nu_{ei}/m_i) - \nabla(kn_e T_e)\cdot J/en_e, \quad (2.5)$$

where

$$\left.\begin{aligned} \nu_{es} &= (8kT_e/\pi m_e)^{1/2} n_s Q_s, \\ \nu_{e0} &= (8kT_e/\pi m_e)^{1/2} n_0 Q_0, \\ \nu_{ei} &= (8kT_e/\pi m_e)^{1/2} n_e Q_{ei}, \end{aligned}\right\} , \quad (2.6)$$

m_s, m_0, and m_i are the masses of seed atom, parent gas atom, and ion, respectively, n_0 the parent gas density, Q_{ei} the collision cross section between electron and ion. In Eq.(2.5), the radiation term is neglected since the electron temperature is relatively low

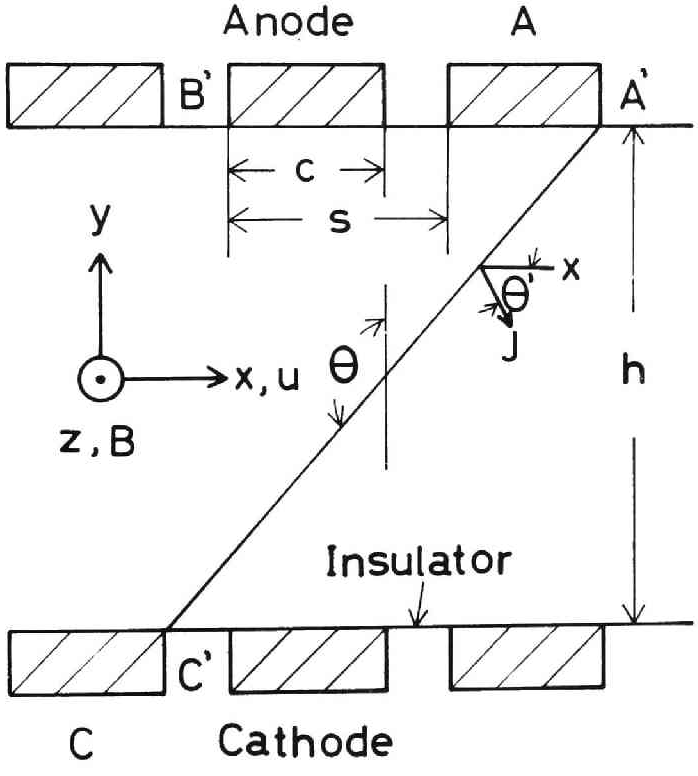

Fig. 2.1. Schema of diagonal type MHD generator duct for two-dimensional analysis.

under the numerical conditions in this thesis.

Next, we assume $\boldsymbol{E}$, $\boldsymbol{J}$, $\boldsymbol{B}$ and $\boldsymbol{u}$ as

$$\left.\begin{aligned} \boldsymbol{E} &= (E_x,\ E_y,\ 0), \qquad \boldsymbol{J} = (J_x,\ J_y,\ 0), \\ \boldsymbol{B} &= (\ 0,\ \ 0,\ B), \qquad \boldsymbol{u} = (\ u,\ \ 0,\ 0), \end{aligned}\right\}, \tag{2.7}$$

in the chapters except Chapter 6.

The secondary magnetic flux caused by $\boldsymbol{J}$ is assumed to become negligible in comparison with the applied magnetic flux, since the magnetic Reynolds number of the gas plasma is much smaller than unity under the operating conditions.

Next, as described previously, it is assumed that the gas velocity u and temperature T in Chapters 3 to 5 depend on only y according to the following relations,

$$u/u_0 = \{4y/h\cdot(1 - y/h)\}^m \tag{2.8}$$ [2.3]

and

$$(T - T_w)/(T_0 - T_w) = \{4y/h\cdot(1 - y/h)\}^{m'} \tag{2.9}$$ [2.3]

respectively, where h is the duct height, T_w the wall temperature, T_0 and u_0 the gas temperature and velocity at the center of flow, namely y=h/2, respectively, and m and m' constants.

Finally, the electrical conductivity σ, Hall parameters β and β_i for electrons and ions are given by

$$\sigma = n_e e^2/m_e \nu_e, \tag{2.10}$$

$$\beta = \mu_e B, \qquad \mu_e = e/m_e \nu_e, \tag{2.11}$$

$$\beta_i = eB(8kT/\pi m_s)^{1/2}\{Q_{i0}/(1 + m_s/m_0) + \varepsilon_s Q_{is}/\sqrt{2}\}^{-1}/3p, \tag{2.12}$$ [2.22]

where the average electron momentum transfer collision frequency ν_e is given by

$$\nu_e = (8kT_e/\pi m_e)^{1/2}(n_s Q_s + n_0 Q_0 + n_e Q_{ei}),$$

in which

$$\left.\begin{aligned} Q_{ei} &= 3.90(e^2/8\pi\varepsilon_0 kT_e)^2 \log\Lambda, \\ \Lambda &= 12\ (\varepsilon_0 kT_e/e^2)^{3/2} n_e^{-1/2}, \end{aligned}\right\}, \qquad (2.13)$$

[2.23]

and Q_{i0} and Q_{is} the collision cross sections between ions and parent gas atoms and between ions and seed atoms, respectively, μ_e the electron mobility, and ε_0 the permittivity of free space.

2.2.2 Stream and potential functions

To evaluate the current distribution in the MHD generator duct, we use the conventional stream function Ψ defined by

$$J_x = \partial\Psi/\partial y, \qquad J_y = -\partial\Psi/\partial x, \qquad (2.14)$$

which satisfy $\nabla \boldsymbol{J}=0$ in Eq.(2.1).

Also, to obtain the potential distribution, we adopt the potential function Φ defined by

$$\boldsymbol{E} = -\nabla\Phi, \qquad (2.15)$$

which satisfies $\nabla \times \boldsymbol{E}=0$ in Eq.(2.1).

Then, from Eqs.(2.1), (2.4), and (2.14) the following partial differential equation of the 2nd order for Ψ is derived.

$$\nabla^2\Psi + P\partial\Psi/\partial x + Q\partial\Psi/\partial y = R_1, \qquad (2.16)$$

where

$$\left.\begin{aligned} P &= \sigma/\varepsilon\cdot\{\partial(\varepsilon/\sigma)/\partial x - \partial(\beta/\sigma)/\partial y\}, \\ Q &= \sigma/\varepsilon\cdot\{\partial(\varepsilon/\sigma)/\partial y + \partial(\beta/\sigma)/\partial x\}, \\ R_1 &= \sigma/\varepsilon\cdot\{-\partial(\partial p_e/\partial y/en_e)/\partial x \\ &\quad + \partial(\partial p_e/\partial x/en_e)/\partial y\}, \end{aligned}\right\}, \qquad (2.17)$$

in which

$$\varepsilon = 1 + \beta\beta_i.$$

Also, from Eqs.(2.1), (2.4), and (2.15) the following equation for Φ is obtained,

$$\Phi^2 + P'\partial\Phi/\partial x + Q'\partial\Phi/\partial y = R', \tag{2.18}$$

where

$$\left.\begin{aligned} P' &= (\partial\sigma'/\partial x + \partial\sigma''/\partial y)/\sigma', \\ Q' &= (-\partial\sigma''/\partial x + \partial\sigma'/\partial y)/\sigma', \\ R' &= \partial\{\sigma(uB - \partial p_e/\partial y/en_e) + \sigma'\partial p_e/\partial x/en_e\} \\ &\quad /\partial x/\sigma' + \partial\{\sigma''\partial p_e/\partial x/en_e + \sigma'(-uB \\ &\quad +\partial p_e/\partial y/en_e)\}/\partial y/\sigma' \end{aligned}\right\}, \tag{2.19}$$

in which

$$\sigma' = \sigma\varepsilon/(\varepsilon^2 + \beta^2), \qquad \sigma'' = \sigma\beta/(\varepsilon^2 + \beta^2).$$

In these equations P, P', etc. are the functions of Ψ or Φ and so both Eqs.(2.16) and (2.18) become nonlinear equations.

2.3 Boudary and Subsidiary Conditions

For solving Eqs.(2.16) and (2.18), we need boundary conditions on an electrode surface and an insulating wall, periodicity conditions, and two subsidiary conditions peculiar to the diagonal type generator.

First, the boundary condition on the insulating wall is

$$J_y = 0. \tag{2.20}$$

Using Eqs.(2.4), (2.7), (2.14), and (2.15), this equation is changed into the following equation

$$\Psi = \text{const.} \tag{2.21}$$

or

$$\begin{aligned} &\varepsilon(E_y + \partial p_e/\partial y/en_e) + \beta(E_x + \partial p_e/\partial x/en_e) \\ &= \varepsilon(-\partial\Phi/\partial y + \partial p_e/\partial y/en_e) + \beta(-\partial\Phi/\partial x \\ &\quad + \partial p_e/\partial x/en_e) = 0. \end{aligned} \tag{2.22}$$

Next, the boundary condition on a good conductor electrode surface is

$$E_x = 0. \tag{2.23}$$

Using Eqs.(2.4), (2.7), (2.14), and (2.15), the above equation is transformed into the following equation

$$\varepsilon J_x/\sigma + \beta J_y/\sigma - \partial p_e/\partial x/en_e$$

$$=(\varepsilon\partial\Psi/\partial y - \beta\partial\Psi/\partial x - \sigma\partial p_e/\partial x/en_e)/\sigma = 0 \tag{2.25}$$

or

$$\Phi = \text{const.} \tag{2.25}$$

Next, the periodicity conditions for $\boldsymbol{J}$ and $\boldsymbol{E}$ are given

$$\boldsymbol{J}(x+s) = \boldsymbol{J}(x), \qquad \boldsymbol{E}(x+s) = \boldsymbol{E}(x). \tag{2.26}$$

By Eqs.(2.14) and (2.15), these equations are rewritten as

$$\Psi(x+s) = \Psi(x) + I'_y, \qquad \Phi(x+s) = \Phi(x) + V'_x, \tag{2.27}$$

respectively, where I'_y is the current flowing into an electrode and V'_x the potential difference per electrode pitch s in the x direction.

Finally, in the diagonal type generator, the potential difference must be zero between the electrodes C and A short-circuited each other in Fig.2.1. Accordingly, the first subsidiary condition becomes

$$\int_C^A \boldsymbol{E}\cdot d\boldsymbol{s} = 0, \tag{2.28}$$

where $d\boldsymbol{s}$ is the line element vector on an optional integral path from C to A.

Next, the current which runs through an arbitrary surface S crossing the insulating wall surfaces C' and A' is equal to the load current I. This gives the following second subsidiary condition

$$\int_S \boldsymbol{J}\cdot d\boldsymbol{S} = I, \tag{2.29}$$

where $d\boldsymbol{S}$ is the element vector of the surface S.

The current and potential distributions in the diagonal type generator duct can be obtained by solving numerically Eqs.(2.16) and (2.18) under the conditions (2.20) to (2.29).

2.4 Formulation of Electrical Characteristics

As the quantities which are used for the estimation of the generator performance, we adopt the electrical efficiency η_e given by

$$\eta_e = -\int_0^s \boldsymbol{E}\cdot\boldsymbol{J}dx / \int_0^s (\boldsymbol{J}\times\boldsymbol{B})\cdot\boldsymbol{u}dx \tag{2.30}$$

and the specific Hall voltage Q_H defined by

$$Q_H = V_H/V_{ideal}. \tag{2.31}$$

In this equation, V_H and V_{ideal} are the Hall and ideal potential differences per one electrode pitch s, which are given by

$$V_H = -\int_0^s E_x dx \tag{2.32}$$

and

$$V_{ideal} = (\langle\beta\rangle - a)uB\kappa s/(1 + a^2), \tag{2.33}*$$

respectively, where

$$\kappa = 1 - I(1 + \beta_{eff}^2)/\{hw\sigma_{eff}\langle u\rangle B(\beta_{eff} - a)\}. \tag{2.34}*$$

In this equation, w is the duct width in the z direction, and σ_{eff} and β_{eff} the effective conductivity and Hall parameter, which are obtained by the following relations

$$\left.\begin{aligned} J_x = {} & \sigma_{eff}/(1 + \beta_{eff}^2)\cdot\{(1 - a\beta_{eff})\langle E_x\rangle \\ & + \langle u\rangle B\beta_{eff}\}, \end{aligned}\right\} \tag{2.35}*$$

---

* See Appendix II.

$$J_y = \sigma_{eff}/(1 + \beta_{eff}^2)\cdot\{(\beta_{eff} + a)\langle E_x\rangle - \langle u\rangle B\}. \quad \Big| \tag{2.33}$$

In Eqs.(2.33) to (2.35), $\langle\ \rangle$ shows the average value per one electrode pitch s.

Moreover, a grade of the current concentration at an electrode end is estimated by the following relations

$$J_{peak}/\langle J\rangle_{el}, \tag{2.36}$$

where J_{peak} and $\langle J\rangle_{el}$ are the maximum and average current dinsity on the electrode. In this connection, $J_{peak}/\langle J\rangle_{el} = 1$ shows that the current distribution on the electrode surface is completely uniform.

2.5 Numerical Calculation of Basic Equations

2.5.1 Normalized basic equations

Now putting

$$\left.\begin{aligned} &\xi = x/s, \quad \zeta = y/s, \quad \psi = \Psi/(I/w), \\ &T_e' = T_e/T_0, \quad n_e' = n_e/n_0, \end{aligned}\right\}, \tag{2.37}$$

where n_0 is the electron density obtained by Eq.(2.3) in the case of $T_e = T_0$.

Equations (2.16), (2.17), (2.21), (2.24), (2.27), and (2.5) are normalized as

$$\nabla^2\psi + P''\partial\psi/\partial\xi + P''\partial\psi/\partial\zeta + R'' = 0, \tag{2.38}$$

$$\left.\begin{aligned} P'' &= \sigma/\varepsilon\cdot\{\partial(\varepsilon/\sigma)/\partial\xi - \partial(\beta/\sigma)/\partial\zeta\}, \\ Q'' &= \sigma/\varepsilon\cdot\{\partial(\beta/\sigma)/\partial\xi + \partial(\varepsilon/\sigma)/\partial\zeta\}, \\ R'' &= wk\sigma T_0/(Ie\varepsilon n_e')\cdot(\partial T_e'/\partial\xi\cdot\partial n_e'/\partial\zeta \\ &\quad - \partial T_e'/\partial\zeta\cdot\partial n_e'/\partial\xi) + w/I\cdot\sigma/\varepsilon\cdot sw\partial B/\partial\xi, \end{aligned}\right\}, \tag{2.39}$$

$$\psi = \text{const.}, \tag{2.40}$$

$$\partial\psi/\partial\zeta = \beta/\varepsilon\cdot\partial\psi/\partial\xi + k/e\cdot\sigma/\varepsilon\cdot T_0/n_e'\cdot\partial(n_e'T_e')/\partial\xi, \tag{2.41}$$

$$\psi(\xi+1,\zeta) = \psi(\xi,\zeta) + I'_y/(I/w), \tag{2.42}$$

$$3n_0T_0m_e\delta kn'_e\sigma(T'_e - T/T_0)(\nu_{es}/m_s + \nu_{e0}/m_0 + \nu_{ei}/m_i)/2 = (I/sw)^2\{(\partial\psi/\partial\xi)^2 + (\partial\psi/\partial\zeta)^2\}, \tag{2.43}$$

respectively.

2.5.2 Difference approximation of normalized basic equations

Defining

$$\psi_{ij} = \psi(x_i,y_j), \quad x_i = i\Delta, \quad y_j = j\Delta, \quad i,j = 1,2,--- \tag{2.44}$$

by the central difference approximation, Eqs.(2.38) and (2.41) are transformed to

$$\left.\begin{aligned} &(1 + \Delta P_{ij}/2)\psi_{i+1,j} - 4\psi_{i,j} + (1 - \Delta P_{ij}/2) \\ &\times \psi_{i-1,j} + (1 + \Delta Q_{ij}/2)\psi_{i,j+1} \\ &+ (1 - \Delta Q_{ij}/2)\psi_{i,j-1} + \Delta^2 R_{ij} = 0 \\ &i,j = 1,2,--- \end{aligned}\right\}, \tag{2.45}$$

$$\left.\begin{aligned} &\psi_{i,j+1} - \psi_{i,j-1} - \beta/\varepsilon\cdot(\psi_{i+1,j} - \psi_{i-1,j}) \\ &+ kwT_0\sigma/(eIn'_e\varepsilon)\cdot(n'_{e\ i+1,j}T'_{e\ i+1,j} \\ &- n'_{e\ i-1,j}T'_{e\ i-1,j}), \\ &i,j = 1,2,--- \end{aligned}\right\}, \tag{2.46}$$

where P_{ij}, Q_{ij}, R_{ij}, n'_{eij}, and T'_{eij} are the values of P'', Q'', R'', n'_e, and T'_e at a point (x_i, y_j), respectively. Here $\psi_{i,j-1}|_{j=1}$ and $\psi_{i,j=1}|_{j=h/\Delta}$, which can not exist physically, can be easily eliminated from Eqs.(2.45) and (2.46) for the electrode surfaces.

The rectangular region s x h is subdivided by 20 x 40 rectangular meshes of an equal size. In this connection, it has been

ascertained that the calculation results by those meshes agree very well with that by 50 x 100 rectangular meshes.

In addition, with respect to the numerical example in this thesis, it has been seen that if the forward or backward difference approximation is applied to the electrode surface, it is very difficult to find out the converging solutions of the basic equations.

2.5.3 Relaxation parameter** in SOR method

The simultaneous difference equations (2.45) can be solved under Eqs.(2.46), (2.40), and (2.42) by means of the SOR method (successive over-relaxation method). However, for converging the calculation of the strong current concentration which rises often at an electrode end in an MHD generator duct, the basic difference equations require a considerably smaller relaxation parameter $\omega = \omega^*$ (= 0.1 to 0.4) than the conventional value. Therefore the digital computation cannot rapidly converge and wastes a long time.

Accordingly, the above small value $\omega = \omega^*$ is used only for the numerical calculation near the electrode. On the other hand, within the duct, the other relaxation parameter $\omega = \omega_0$ (=1 to 2) of the conventional magnitude is used to accelerate the calculation. Moreover, if the residuals of the solutions of the difference equations decrease, ω_0 is increased by a suitable value ω', and conversely if they increase, ω_0 is reduced by another suitable value ω''.

For example, when $\omega^*=0.3$ and $\omega_0 = \omega^*$, the repetition calculation of 4451 times was required for the residuals to become smaller than 10^{-3}, but when $\omega^*=0.3$ and $\omega_0=1.0$ to 1.84 ($\omega'=0.002$ and $\omega''=0.02$) only the repetition of 592 times was done. In these examples, the numerical solutions agreed very well with those by a conformal mapping [1.6] or the equivalent circuit in the case where σ, β, and u were constant.

** See Appendix III.

2.6 Concluding Remarks

In this chapter, a two-dimensional theory for analysis of the diagonal type MHD generator has been introduced. The main conclusions are as follows.

(1) The nonlinear partial differential equations were derived from the basic equation, by which the current and potential distributions in the MHD generator duct can be numerically calculated.

(2) The electrical efficiency, the specific Hall voltage, etc. were derived, by which the electrical characteristics of the diagonal type generator can be estimated.

(3) The method of numerical calculation of the basic equations was introduced, which includes the normalized basic equations, the difference basic equations, and the modified SOR method.

CHAPTER 3
BASIC ELECTRICAL CHARACTERISTICS

3.1 Introduction

The two- or three-dimensional analyses of the current and potential distributions, etc. in the Faraday type generator duct have been carried out by many researchers [2.1] to [2.3] et al., and its basic electrical characteristics have been fairly clarified.

However, the usual Faraday type generator is a current-controlled generator, and on the other hand, the diagonal type generator is a potential-controlled one because of the diagonal connections of electrodes. Therefore, the electrical characteristics of the diagonal type generator duct differ fairly from those of the Faraday type so that they must be clarified independently for the practical use of the diagonal type generator.

In this chapter, first, when the electrical conductivity or the Hall parameter are assumed constant in the generator duct, the current distribution is evaluated and influences of the load factor, etc. on it are investigated. The current distribution in the diagonal type generator is compared with that in the Faraday or Hall type generators. Then, influences of the inclination parameter, the Hall parameter, etc. on the electrical characteristics such as electrical efficiency of the diagonal type generator are studied. Next, when the electrical conductivity or the Hall parameter vary spatially, the distributions of current, potential, and electron temperature are evaluated and influences of the load factor and the inclination parameter on the current distribution are discussed. Then, the influences of the duct size and the temperatures of plasma and duct wall on the electrical characteristics of generator duct are investigated.

These investigations are carried out by means of the theory described in Chapter 2. In this connection, the Saha equilibrium

is assumed in the cumerical calculations, since the gas is assumed to be a subsonic flow.

3.2 Numerical Conditions

The numerical analysis in this chapter is carried out for the diagonal type MHD generator with a cesium-seeded helium plasma in nonequilibrium ionization in which

$$\left.\begin{aligned} & h = 0.2, \quad w = 0.1, \quad s = 0.1, \quad c = 0.06 \text{ m}, \\ & B = 4, 5 \text{ T}, \quad u_0 = 2000 \text{ m/s}, \quad T_0 = 1700 \\ & \quad \text{to } 2000 \text{ K}, \quad p = 5 \text{ atm}, \quad \varepsilon_s = 0.3 \text{ \%}, \\ & \delta = 5, \quad m = m' = 1/7 \end{aligned}\right\}, \quad (2.47)$$

where ε_s is the seed fraction of the cesium, and it is assumed that the duct size is related to the somewhat large experimental duct, and the gas velocity is subsonic.

3.3 Numerical Calculation Processes

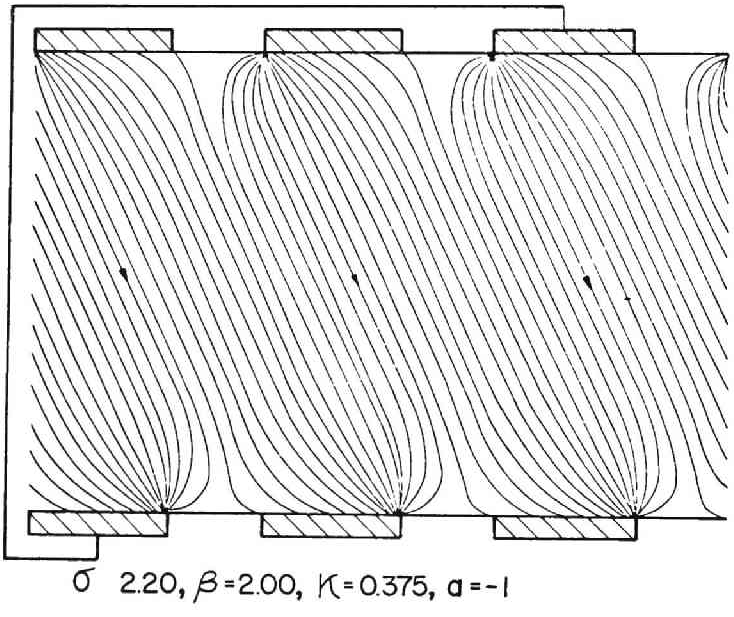

Fig. 2.2. Current distribution for constant σ and β (1).

The value of the stream function ψ is determined by solving the basic difference equations (2.44) and (2.45) under the boundary conditions (2.40) and (2.46) and the subsidiary conditions (2.28) and (2.29) by the modified SOR method. The calculation processes are as follows.

(1) The values of ψ on the insulators are plausibly assumed to satisfy the subsidiary condition (2.29).

(2) The reasonable values of I, σ, β, ε, n_e, and T_e are given, and then the value of ψ is obtained by solving the difference equation (2.45) under the conditions (2.40), (2.42), and (2.46) by the SOR method.

(3) Using the Newton-Raphson method, the value of T_e' is calculated by Eq.(2.43), in which the value of ψ obtained in the above process (2) is used. Then, by Eqs.(2.10), (2.11), etc. σ, β, and

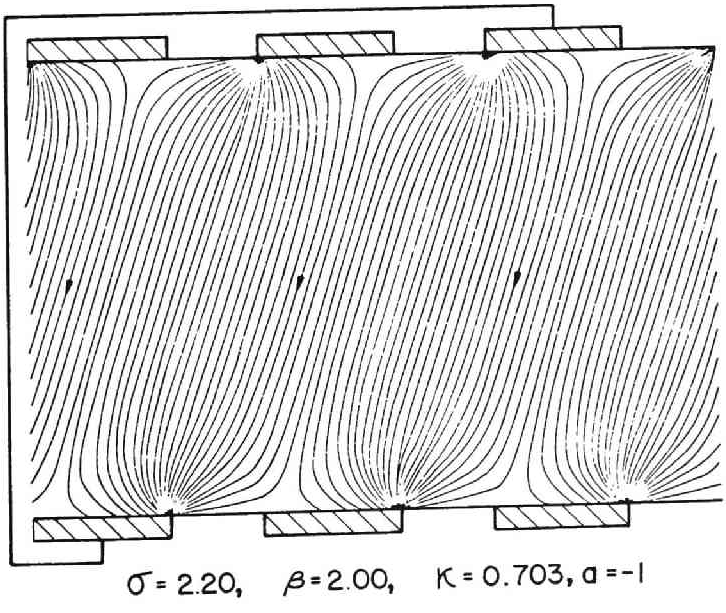

Fig. 2.3. Current distribution for constant σ and β (2).

n_e are calculated.

(4) The digital computation in the processes (1) to (3) are repeated until ψ converges to a constant value for I given in the process (2).

(5) To satisfy the subsidiary condition (2.28) the previous value of I is changed to a new value. After many repetitions of the processes (2) to (4), the desirable value of ψ is acquired.

In addition, the potential Φ can be obtained by the similar processes.

3.4 When Electrical Conductivity and Hall Parameter Are Assumed Constant

3.4.1 Current distribution and influence of load factor

In this section, the current distribution, influences of the load factor, the Hall parameter, etc. are discussed when σ and β are assumed constant in the generator duct.

When σ and β are spatially constant, P, Q, and R_1 in Eq.(2.16)

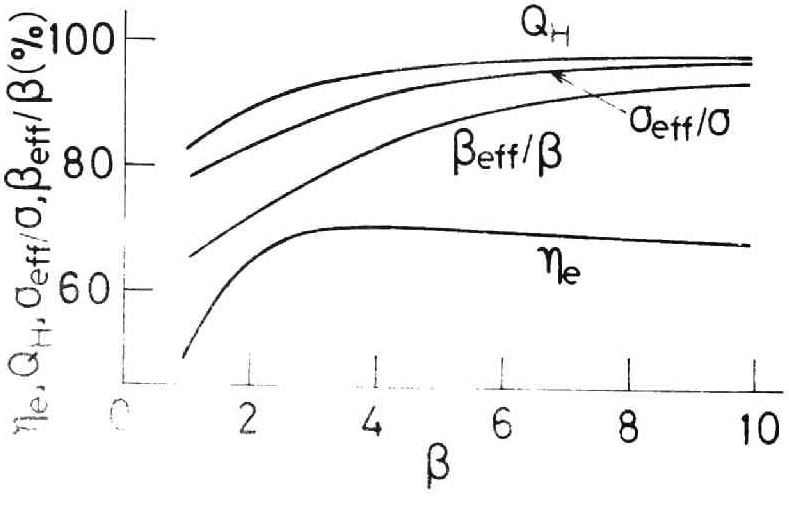

Fig. 2.4. Influence of β on η_e, Q_H, σ_{eff}/σ and β_{eff}/β.

become zero, and the equation reduces to the Laplace equation

$$\nabla^2\psi = 0. \tag{2.48}$$

If values of σ and β are assumed, the numerical solution of Eq.(2.48) is found through the calculation processes (1), (2), and (4) described in Section 3.3, and then the current distribution in the duct is obtained.

In Figs. 2.2 and 2.3, the current distributions are plotted in the case of $\kappa = 0.375$; $J = 0.532$ A/cm^2 and $\kappa = 0.703$; $J = 0.684$ A/cm^2, respectively, where $\sigma = 2.2$ ℧/m, $\beta = 2$, $B = 4$T, and $a = -1$ ($\theta = 135°$). These figures show that the current distribution in the diagonal type generator remarkably varies with κ. That is , the current flows from an upstream anode to a downstream cathode when $\kappa < \kappa^*$. On the other hand, it does from a downstream anode to an upstream cathode when $\kappa > \kappa^*$, where

$$\kappa^* = \kappa|_{<J_x>=0} = (1 - a\beta_{eff})(\beta_{eff} - a) / \{\beta_{eff}(1 + a^2)\}. \tag{2.49}$$

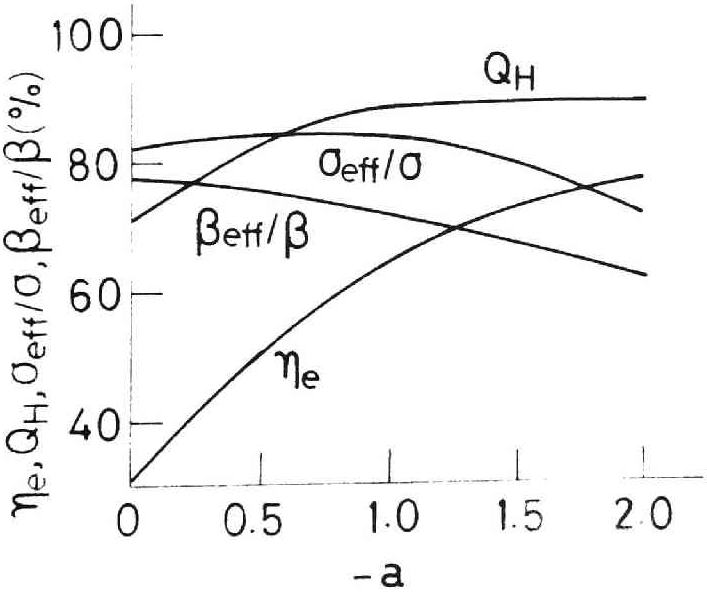

Fig. 2.5. Influence of a on η_e, Q_H, σ_{eff}/σ, and β_{eff}/β.

In this connection, the load current flows from the inlet to the exit of the generator duct in all cases, since an anode and cathode are diagonally connected.

This is explained by the following. Using Eqs.(2.35), the tangent of the angle θ' between the direction of a average current density $\langle J \rangle$ and the x-axis [see Fig.2.1] is expressed by the following equations

$$\begin{aligned} \tan\theta' &= -\langle J_y \rangle / \langle J_x \rangle \\ &= -\{\beta_{eff}\langle E_x \rangle + \langle E_y \rangle - \langle u \rangle B\} \\ &\quad /\{\langle E_x \rangle - \beta_{eff}(\langle E_y \rangle - \langle u \rangle B)\} \\ &= \{1 + a^2 + (\beta_{eff} - a)(\beta_{eff} + a)\kappa\} \\ &\quad /\{\beta_{eff}(1 + a^2) - (1 - a\beta_{eff}) \\ &\quad \times (\beta_{eff} - a)\kappa\}. \end{aligned} \tag{2.50}$$

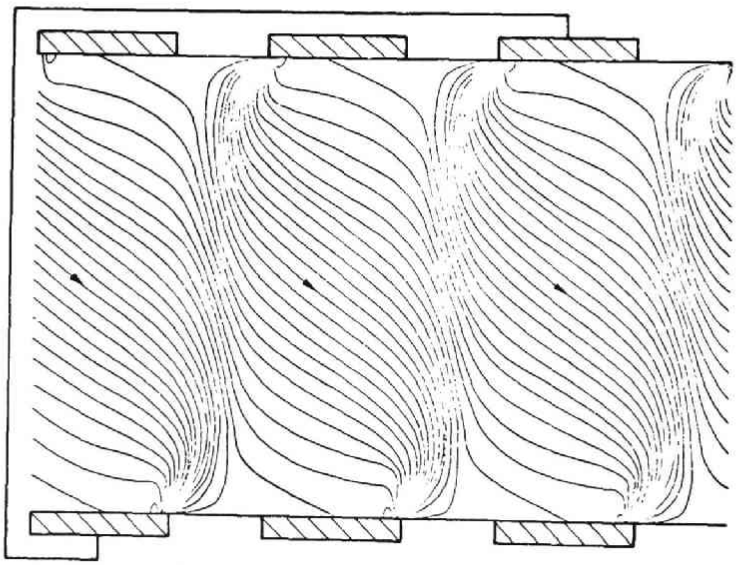

Fig. 2.6. Current distribution for nonuniform σ and β (1).

Accordingly,

$$\partial(\tan\theta')/\partial\kappa = (1 + a^2)(1 + \beta_{eff}^2)(\beta_{eff} - a)$$
$$/\{\beta_{eff}(1 + a^2) - (1 - a\beta_{eff})$$
$$\times (\beta_{eff} - a)\kappa\}^2 > 0. \qquad (2.51)$$

This equation shows that θ' increases with κ. Namely, when κ is small, θ' is small and the current runs from an upstream anode to a downstream cathode. On the contrary, when κ becomes large, θ' does large and the current from a downstream anode to an upstream cathode.

Moreover, since the duct must operate as a generator, the load factor $\kappa > 0$. Therefore, we obtain the condition $\theta' > \tan^{-1} 1/\beta_{eff}$ from Eq.(2.50), and also the load current I has to flow from the inlet to the exit of the duct, consequently we obtain $\theta' < 3\pi/2 - \theta$. Thus, we have the following constraint

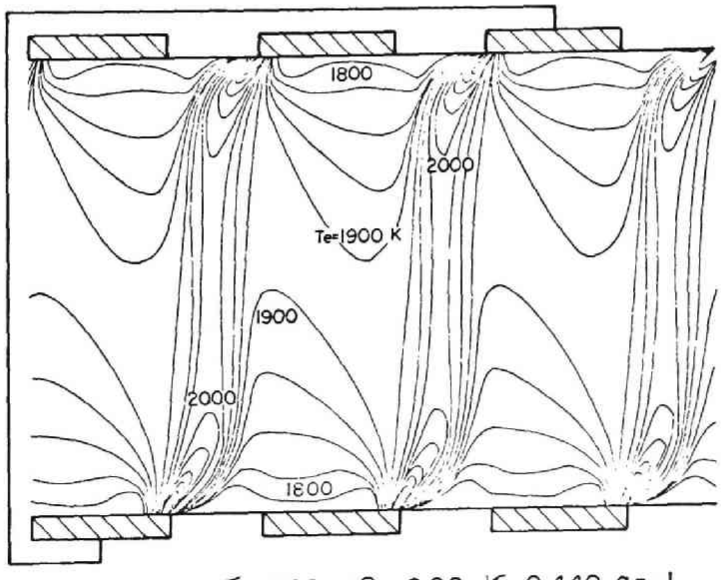

Fig. 2.7. Electron temperature distribution corresponding to current distribution in Fig. 2.6.

$$tan^{-1} 1/\beta_{eff} < \theta' < 3\pi/2 - \theta \qquad (2.52)$$

for θ' in the generator duct.

From the above description, it is understood that the current distribution in a diagonal type generator varies very widely with κ. On the other hand, since $\langle J_x \rangle = 0$ for the whole duct of the Faraday type generator and $\langle J_x \rangle > 0$ for the Hall type, the above -mentioned phenomena do not occur in both type ducts.

The state of the current concentration at the electrode end is fairly similar to that in the Faraday or Hall type generator shown in the references [2.1] ot [2.5].

3.4.2 Influence of Hall parameter on electrical efficiency and specific Hall voltage

The variations of η_e, Q_H, σ_{eff}/σ, and β_{eff}/β by β are shown in Fig.2.4 in the case of $\kappa = 0.5$, $B = 4T$, $a = -1$, and $\sigma = 2.0$℧/m. The figure shows that Q_H, σ_{eff}/σ, and β_{eff}/β increase with β, and

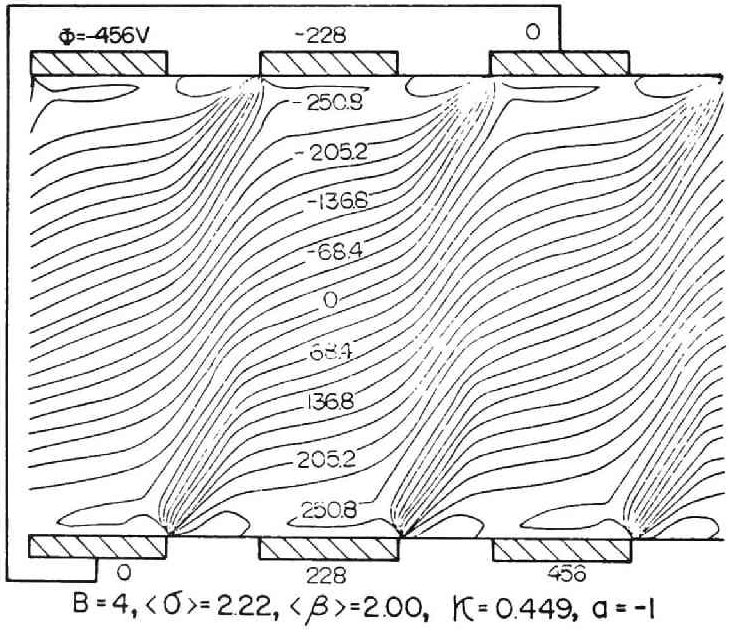

Fig. 2.8. Potential distribution corresponding to current distribution in Fig.2.6.

then they saturate. These are because V_H increases as β becomes large, but when β becomes larger the current concentration at electrode ends and the nonuniformity of the current distribution become intensive. η_e has the maximum value near $\beta = 4$.

3.4.3 Influence of inclination parameter on electrical efficiency and specific Hall voltage

The relations of η_e, Q_H, σ_{eff}/σ, and β_{eff}/β to a are plotted in Fig.2.5 in the case of $\kappa = 0.5$, $B = 4T$, $\sigma = 2.0$℧/m, and $\beta = 2$. It is seen that η_e and Q_H increase with $|a|$, and that those of the Hall type generator ($a = 0$ or $\theta = 90°$) become fairly small, namely its electrical characteristics are inferior to those of the diagonal type generator.

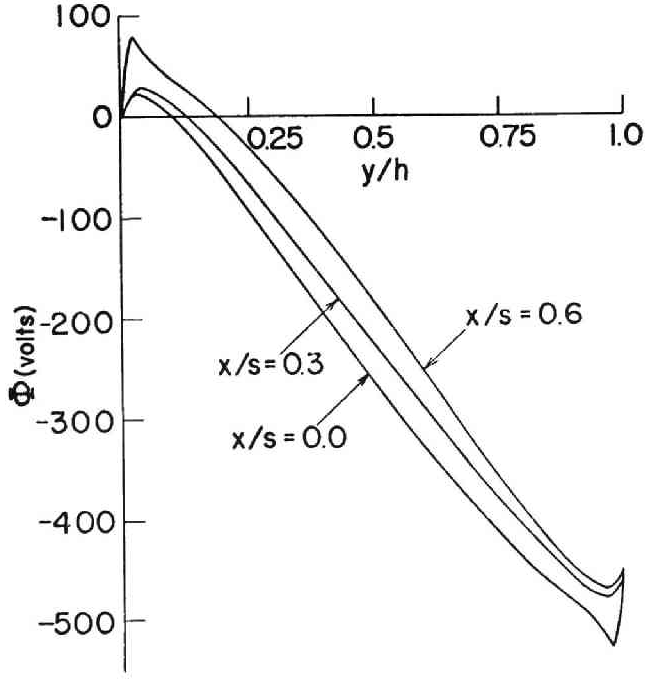

Fig. 2.9. Variation of electric potential Φ between confronted anode and cathode corresponding to current distribution in Fig.2.6.

3.5 When Nonuniformity of Electrical Conductivity and Hall Parameter Are Considered

3.5.1 Current, electron temperature, and potential distributions

In this section, the current, electron temperature, and potential distributions are evaluated and influences of β, a, h, T_0, and T_w on the generator characteristics is studied when σ, β, and β_i vary according to Eqs.(2.10) to (2.12). In addition, it was made clear by the numerical calculation results that two terms of the ion-slip $\beta\beta_i(\boldsymbol{J}\times\boldsymbol{B})\times\boldsymbol{B}/B^2$ and the gradient of the electron pressure $\nabla p_e/en_e$ in Eq.(2.4) are much smaller than the other two terms under the numerical conditions in this thesis.

In Figs. 2.6, 2.7, and 2.8 are plotted the distributions of current, electron temperature, and potential, respectively, and in Fig.2.9 the variation of potential Φ between a pair of confronted

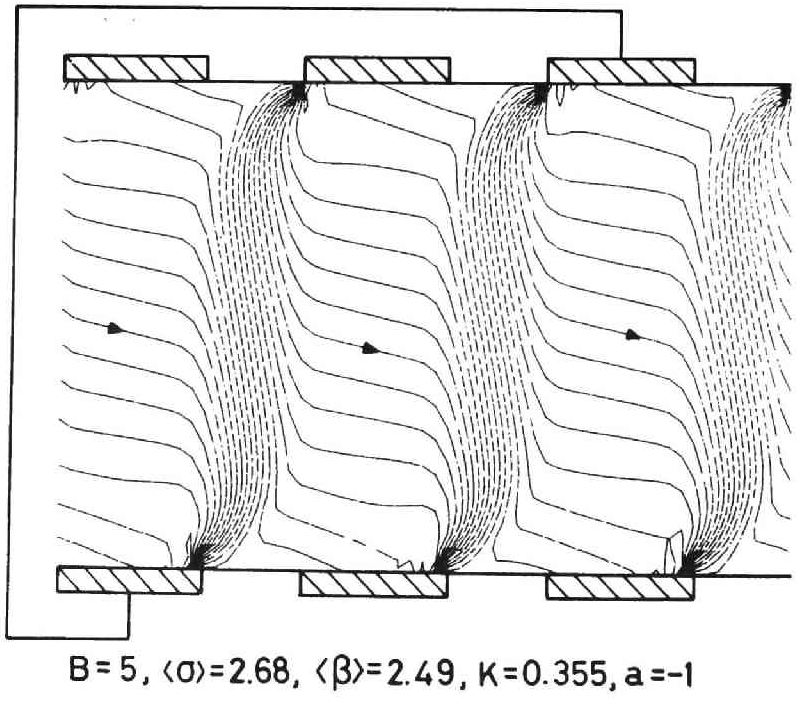

Fig. 2.10. Current distribution for nonuniform σ and β (2).

anode and cathode in the case of κ = 0.499, B = 4T, a = -1, T_0 = 1800 K, T_w = 1600 K, $\langle\sigma\rangle$ = 2.2 $\mho$/m, $\langle\beta\rangle$ = 2.00, and $\langle J\rangle$ = 0.468 A/cm^2. By comparison between Fig.2.6 and 2.2, it is found that the current concentration at the electrode end in the case of nonuniform σ and β becomes more intensive than that in the case of constant σ and β, and that the eddy current is induced on the electrode surfaces. The phenomena similar to these arise in the Faraday type generator [2.2]. This is because the Joule heating due to current concentration makes T_e and therefore σ high in the case of the nonuniform σ and β.

As seen in Fig.2.2, the current distribution is almost uniform in the main flow where the gas velocity becomes almost constant, and its nonuniformity in the x direction does not yet occur there. However, in Fig.2.6, the nonuniformity in the x direction appears clearly in the main flow.

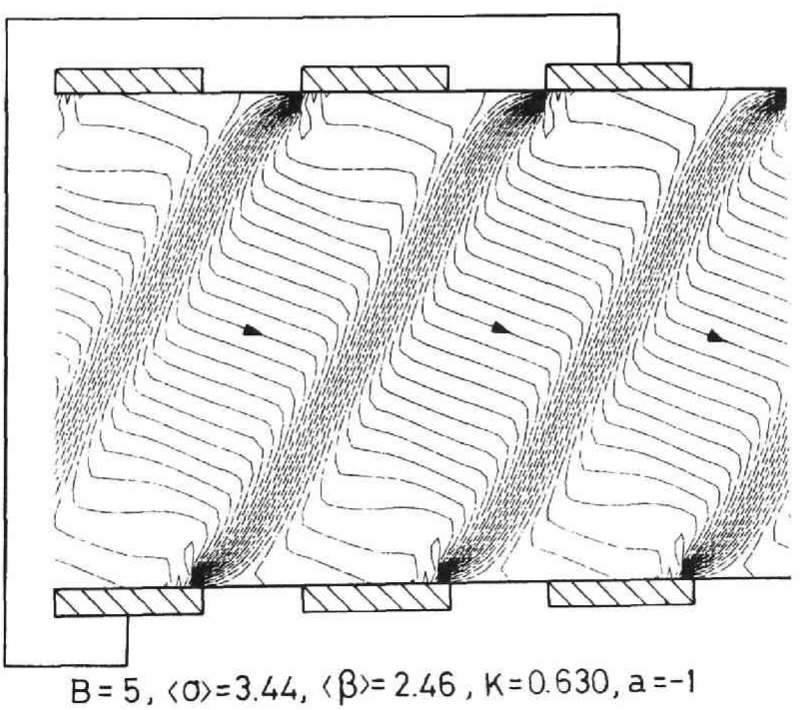

Fig. 2.11. Current distribution for nonuniform σ and β (3).

Next, Fig.2.7 shows that the distribution of the electron temperature becomes very nonuniform and T_e varies from 1600 to 2200 K. In addition, σ varies 0.019 to 7.72 ℧/m and β 1.63 to 2.03.

It is seen from the potential distribution between the confronted anode and cathode in Fig.2.9 that the electrode voltage drop is about 13 % of the potential difference between the confronted electrodes.

3.5.2 Influence of load factor on current distribution

In Fig.2.10, the current distribution is plotted for κ = 0.533, $\langle\sigma\rangle$ = 2.68 ℧/m, $\langle\beta\rangle$ = 2.49, and β_{crit} = 1.77, and in Fig. 2.11, that for κ = 0.630, $\langle\sigma\rangle$ = 3.44 ℧/m, $\langle\beta\rangle$ = 2.46, and β_{crit} = 1.61, where B = 5T, T_0 = 1800 K, and T_w = 1600 K.

In Fig.2.10 where κ is small, the current flows from an upstream anode to a downstream cathode, but in Fig.2.11 where κ is large, it runs from a downstream anode to an upstream cathode in

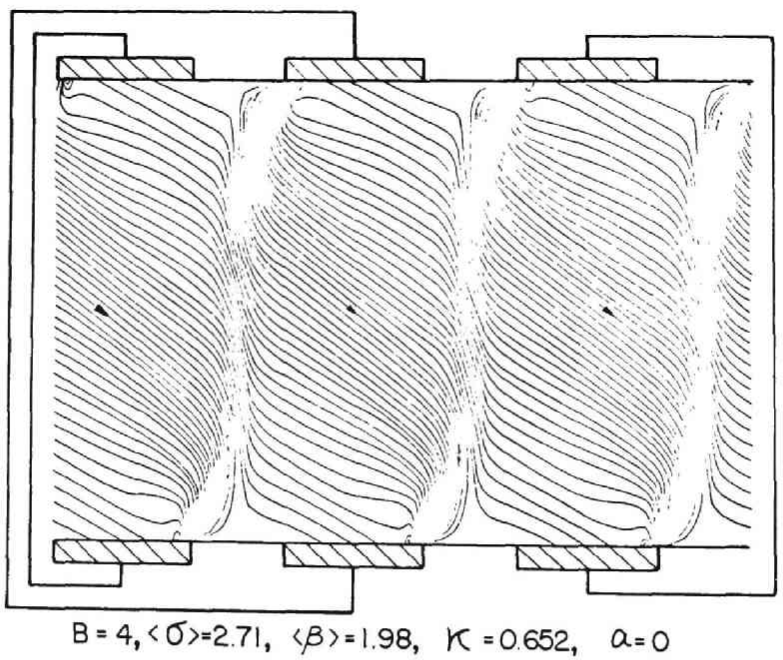

Fig. 2.12. Current distribution for nonuniform σ and β (4).

the similar way to the case of constant σ and β. Such phenomena cannot occur in the Faraday and Hall type generators. Also, from Figs.2.6, 2.10, and 2.11, it is seen that the state of the nonuniformity in the x direction in the main flow is changed with κ. Besides, as seen in Figs.2.10 and 2.11, when $<\beta>$ becomes high and exceeds β_{crit}, the streamer due to the ionization instability grows [1.11] to [1.13]. Moreover both figures indicate that the state of the streamers varies with κ, and hence the state of ionization instability does with κ.

3.5.3 Influence of inclination parameter on current distribution

In Figs.2.12 and 2.13, the current distributions are shown for κ = 0.652 and a = 0, and κ = 0.658 and a = -2, respectively, where B = 4T, T_0 = 1800 K, and T_w = 1600 K.

These figures tell that the current distribution varies remarkably by the values of a and that the current density increases with decreasing $|a|$. The reason for these is the following. From

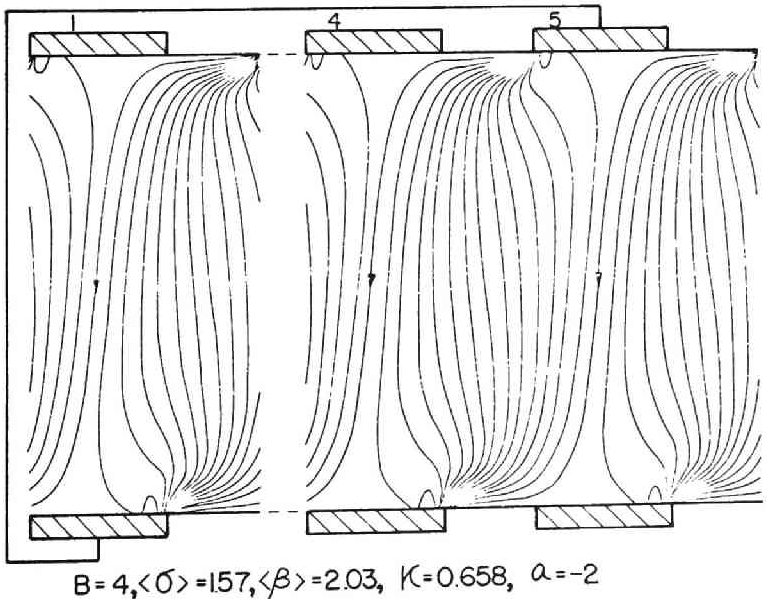

Fig. 2.13. Current distribution for nonuniform σ and β (5).

the subsidiary condition (2.29), the following equation is derived

$$\langle J_n \rangle = I/(wh\sqrt{1 + a^2}), \tag{2.53}$$

where $\langle J_n \rangle$ is the average value of the current density perpendicular to the cross-section C'A' in Fig.2.1. The above equation indicates that the current density in the Hall type duct ($a = 0$) is $(1 + a^2)^{1/2}$ times as large as that of the diagonal type ($|a| > 0$), even when the load current I is equal. Therefore, the current concentration, the nonuniformity of its distribution, etc. in the Hall type generator become more intensive than those in the diagonal type generator.

3.5.4 Influence of duct height on current distribution and electrical characteristics

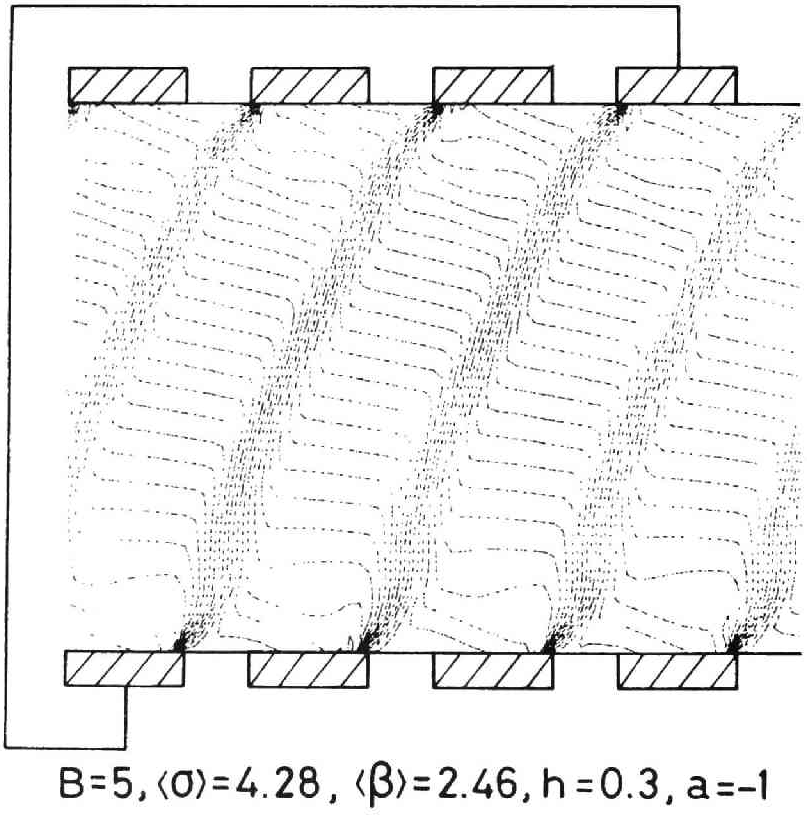

Fig. 2.14. Current distribution for nonuniform σ and β (6).

In the case of B = 5T, a = -1, T_0 = 1800 K, T_w = 1600 K, and I_x = 0A, Figs. 2.14 and 2.15 show the current distributions for h = 0.3 and 0.4 m, respectively, where the influence of the boundary layer are excluded in this article. From the figures, it is seen that the current distribution is not largely influenced by the duct size when a nonequilibrium ionization grows. In Fig.2.16, the variations of η_e, Q_H, $\sigma_{eff}/\langle\sigma\rangle$, and $\beta_{eff}/\langle\beta\rangle$ by h/s are plotted. As seen from the figure, η_e and Q_H are little dependent on h/s, while $\sigma_{eff}/\langle\sigma\rangle$ increases with h/s. This is explained by the following. In Figs.2.14 and 2.15, the current distribution has the repetition of the almost same pattern except the region near duct wall, and it is little influenced by the duct size, if the duct size is much larger than the size of the pattern. Accordingly, it is thought that our investigation can be sufficiently carried out by the

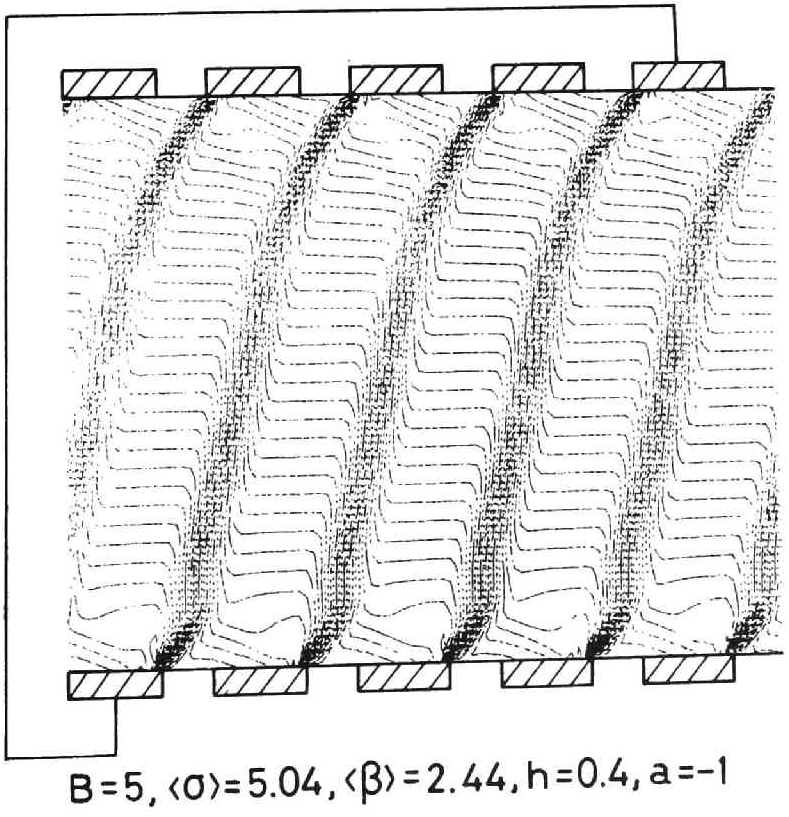

Fig. 2.15. Current distribution for nonuniform σ and β (7).

numerical analysis for h/s = 2.

3.5.5 Infuence of temperatures of central gas flow and duct wall on electrical characteristics

In Fig.2.17 the variations of η_e, Q_H, etc. by T_0 are plotted in the case of B = 4T, a = -1, $T_0 - T_w$ = 200 K, and $\kappa \fallingdotseq 0.5$. The figure tells that the changes of η_e and $\beta_{eff}/\langle\beta\rangle$ due to T_0 are large and they increase fairly with T_0, but on the other hand, the variations of Q_H and $\sigma_{eff}/\langle\sigma\rangle$ by T_0 is very small.

The reason of the above phenomena is shown below. When T_0 is low, nonequilibrium ionization occurs more intensively than when T_0 high, and consequently the nonuniformity of the current distribution becomes severe in the former case. Accordingly, η_e falls as T_0 decreases. On the other hand, the decrease of T_0 makes $\langle\sigma\rangle$ and $\langle J\rangle$ low, so that the effects of $\langle\sigma\rangle$ and $\langle J\rangle$ on Q_H offset each other, since V_H depends on $\langle J\rangle/\langle\sigma\rangle$. V_H or Q_H are scarcely changed

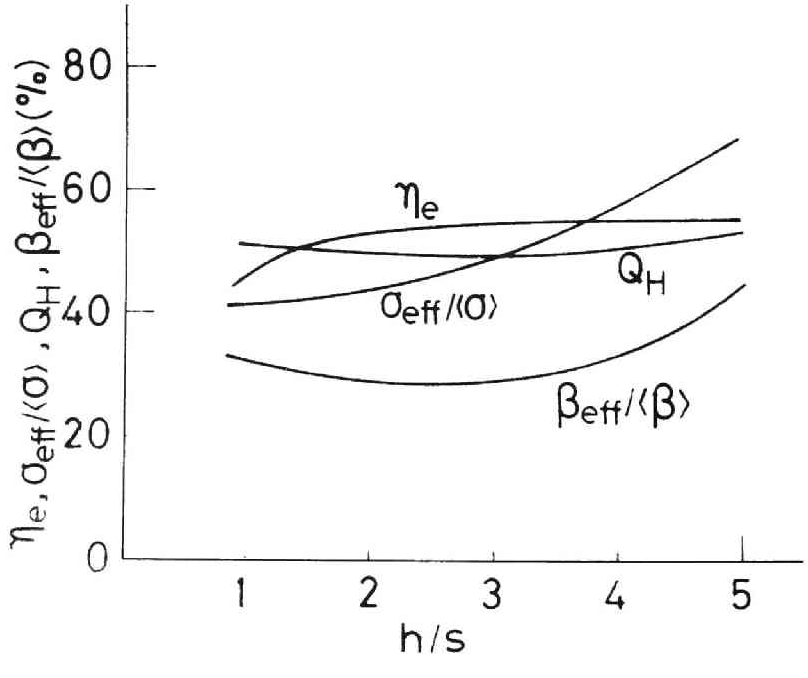

Fig. 2.16. Influence of h/s on η_e, Q_H, $\sigma_{eff}/\langle\sigma\rangle$, and $\beta_{eff}/\langle\beta\rangle$.

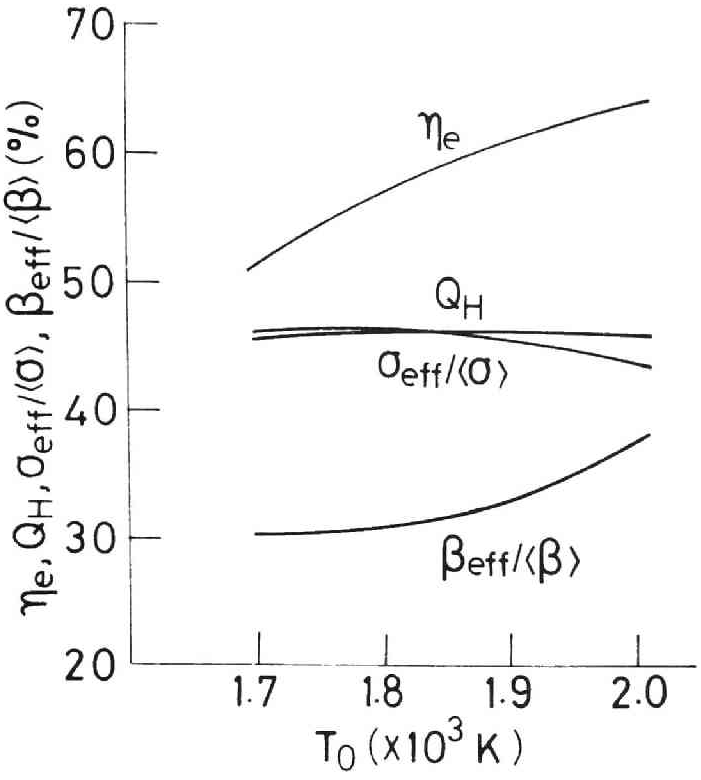

Fig. 2.17. Influence of T_0 on η_e, Q_H, $\sigma_{eff}/\langle\sigma\rangle$, and $\beta_{eff}/\langle\beta\rangle$.

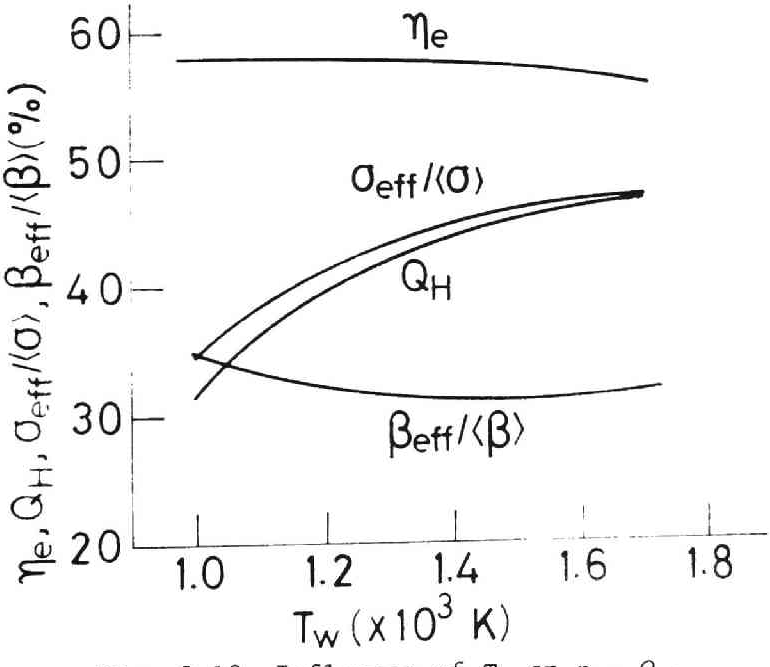

Fig. 2.18. Influence of T_w on η_e, Q_H, $\sigma_{eff}/\langle\sigma\rangle$, and $\beta_{eff}/\langle\beta\rangle$ (1).

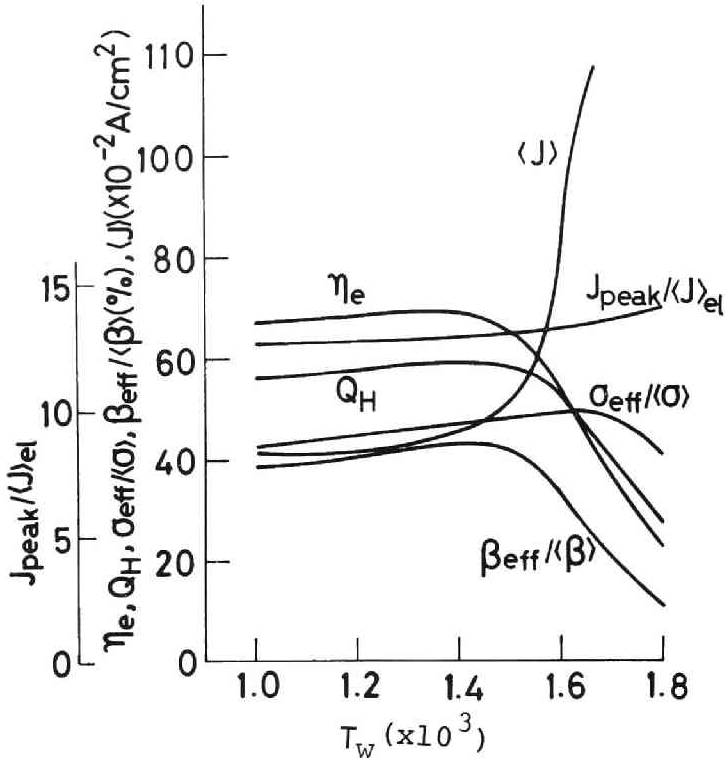

Fig. 2.19. Influence of T_w on η_e, Q_H, $\sigma_{eff}/\langle\sigma\rangle$, and $\beta_{eff}/\langle\beta\rangle$ (2).

by T_0.

Next, Fig.2.18 shows the variations of η_e, Q_H, $\sigma_{eff}/\langle\sigma\rangle$, and $\beta_{eff}/\langle\beta\rangle$ by T_w in the case of B = 4T, a = -1, T_0 = 1800 K, and κ = 0.5. It is seen that η_e and $\beta_{eff}/\langle\beta\rangle$ decrease slightly, and on the other hand, Q_H and $\sigma_{eff}/\langle\sigma\rangle$ increase fairly with T_w. These can be explained as follows. The intensive current concentration at the electrode ends already grows and the current distribution in the duct varies only a little with T_w. Therefore, T_w has only a little influence on η_e which is much influenced by the current distribution as seen from Eq.(2.30). On the other hand, the drop due to thermal boundary layer increases with decreasing T_w, while the degree of decrease of $\langle\sigma\rangle$ is small because T_0 is assumed constant. V_H, on which $\langle J\rangle/\langle\sigma\rangle$ has a large influence, namely Q_H decreases with lowering T_w.

Moreover, in Fig.2.19 the influence of T_w on η_e, Q_H, etc. is plotted in the case of B = 5T, a = -1, T_0 = 1800 K, and I_x = 0. The layer of the low electrical conductivity due to the decrease of T_w is apt to make the current distribution uniform, for example the value of $J_{peak}/\langle J \rangle_{el}$ changes from 14.0 to 12.6 as T_w decreases from 1800 to 1000 K, and also to prevent the current from flowing in the case of B = 5T, where the higher degree of the nonequilibrium ionization occurs. Accordingly, the electrical characteristics become best when $T_0 - T_w$ = 300 to 400 K in the case of ionization instability.

3.6 Concluding Remarks

The basic electrical characteristics of the diagonal type generator have been investigated by a two-dimensional analysis. The main results are as follows.

(1) The current concentration at the electrode end is fairly similar to that in the Faraday and the Hall type generators.

(2) The current distribution in the diagonal type generator is remarkably affected by the values of the load factor and the inclination parameter, which differs from the states in the Faraday and the Hall type ducts.

(3) In the main flow, the large nonuniformity of the current distribution in the x direction grows if nonequilibrium ionization is made strong. The state of the nonuniformity is varied remarkably by the values of the load factor and the inclination parameter.

(4) The effects of the duct height on the electrical characteristics become small as the nonequilibrium ionization instability grows.

(5) The electrical characteristics of the generator degrades as the temperatures of the central gas flow and the duct wall low er, where the former and the latter affect mainly the electrical efficiency and the specific Hall voltage, respectively.

CHAPTER 4

EFFECTS OF RESISTIVE ELECTRODE AND DISTRIBUTION OF APPLIED MAGNETIC FLUX ON ELECTRICAL CHARACTERISTICS

4.1 Introduction

As shown from the results which have been obtained in Chapter 3, the current concentration at the electrode ends makes the current distribution in the generator duct nonuniform, and the Joule heating by the concentration may damage the electrodes and break down the insulation between the adjacent electrodes.

The current concentration is caused by short-circuiting of the axial Hall electric field through a good conductor electrode. For the Faraday type generator, as one way removing the concentration, the use of a resistive electrode has been proposed and already its effects have been investigated in fair detail [2.25] to [2.28]. As another way, reduction of the applied magnetic flux in the direction perpendicular to both the flux density and the gas velocity in a region near the duct wall has been thought out and its effects have been discussed, too [2.29].

On the other hand, their influences on the current concentration at the electrode ends and the performance characteristics of the diagonal type generator have been yet little investigated. However, as found in Chapter 3, the current distribution in the diagonal type generator duct varies remarkably with the load factor, , , which noticeably differes from that in the Faraday type. Accordingly, it is necessary to study their effects on the performance characteristics of the diagonal type generator.

In this chapter, influences of resistive electrode and attenuation of the magnetic flux density in the neighbourhood of the duct wall on the performance characteristics of the diagonal type generator with nonequilibrium ionization plasma are investigated

by a two-dimensional analysis. The configuration of resistive electrode and the distribution of magnetic flux adopted in this thesis are shown. Next, current distributions are calculated, and the influence of conductivity and configuration of wedge-shaped resistive electrode on the current concentration and electrical efficiency is investigated. Besides, the electrical characteristics of generator with the attenuation of the magnetic flux density in the region near duct wall are compared with those of the generator with the constant magnetic flux density.

4.2 Effects of Resistive Electrode

4.2.1 Basic equations in resistive electrode

The basic equations for the gas plasma in the generator duct has been already shown in Section 2.1. In this article, only the basic equations in a resistive electrode are introduced.

The basic equations in the resistive electrode are the Maxwell equations

$$\nabla \times \boldsymbol{E}' = 0, \qquad \nabla \cdot \boldsymbol{J}' = 0, \tag{2.54}$$

and Ohm's law

$$\boldsymbol{J}' = \sigma_e \boldsymbol{E}', \tag{2.55}$$

where $\boldsymbol{E}'$ and $\boldsymbol{J}'$ are the electric field intensity and current density vectors in the resistive electrode, respectively, and σ_e the conductivity of the electrode [see Fig.2.20]. They are assumed as

$$\left.\begin{aligned} &\boldsymbol{E}' = (E_x', E_y', 0), \qquad \boldsymbol{J}' = (J_x', J_y', 0) \\ &\sigma_e = \text{const.} \end{aligned}\right\}, \tag{2.56}$$

Using a stream function Ψ' of the same type as Ψ in Eqs. (2.14), which is derived as

$$J_x' = \partial\Psi'/\partial y, \qquad J_y' = -\partial\Psi'/\partial x, \tag{2.57}$$

to evaluate the current distribution in the resistive electrode,

the following Laplace equation

$$\nabla^2\psi' = 0 \tag{2.58}$$

can be obtained.

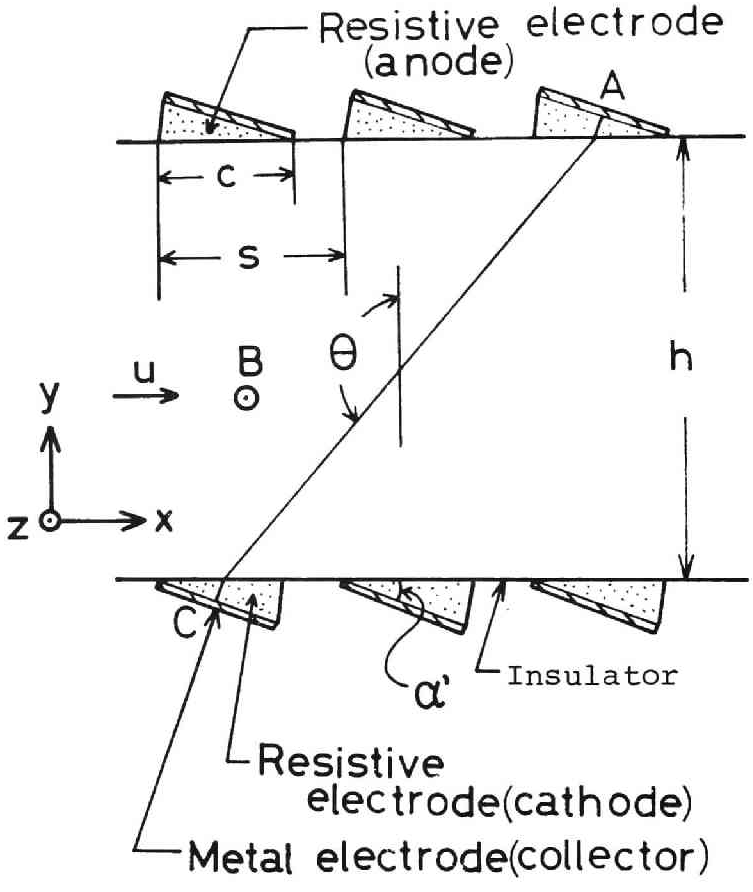

Fig. 2.20. Schema of diagonal type generator duct with resistive electrodes.

4.2.2 Boundary and subsidiary conditions

The boundary condition (2.23) on the electrode surface in Chapter 2 is replaced by the following two equations.

$$E_x' = E_x, \qquad J_y' = J_y. \tag{2.59}$$

Using the stream functions Ψ and Ψ', these equations are trans-

formed as

$$\left.\begin{aligned} \partial\Psi'/\partial y &= \sigma_e(\varepsilon\partial\Psi/\partial y/\sigma - \beta\partial\Psi/\partial x/\sigma \\ &\quad - \partial p_e/\partial x/en_e), \\ \Psi' &= \Psi, \end{aligned}\right\} , \quad (2.60)$$

respectively. The other boundary and subsidiary conditions are the same as Eqs.(2.21) and (2.27) to (2.29) in Chapter 2; A and C in Eq.(2.28) must be replaced by collectors A and C in Fig.2.20.

4.2.3 Configuration of resistive electrode

When let us express the angle between $\boldsymbol{J}'$ and the normal of the boundary surface between the gas plasma and the resistive electrode with α', the angle of intersection between an equipotential surface in the resistive electrode and the boundary surface is α' as seen from Fig.2.21, since $\boldsymbol{E}'$ and $\boldsymbol{J}'$ are parallel each other.

This indicates that a collector should be arranged on an equipotential surface [2.25], which is made of a good conductor. The configuration of resistive electrode can be assumed to be the wedge shape as shown in Fig.2.20.

Then, Eqs.(2.4), (2.55), and (2.59) yield

$$tan\alpha' = \sigma_e(\beta - tan\alpha)/\sigma, \quad (2.61)$$

[2.25]

where α is an angle between $\boldsymbol{J}$ and the normal of the boundary surface [see Fig.2.21].

4.2.4 Numerical conditions

In this chapter, the numerical calculation is made for the diagonal type generator with cesium-seeded helium plasma in nonequilibrium ionization.

Numerical conditions are given by

$$\left.\begin{aligned} &h = 0.2, \quad w = 0.1, \quad s = 0.1, \quad c = 0.06 \text{ m}, \\ &B = 4 \text{ to } 6 \text{ T}, \quad u_0 = 2000 \text{ m/s}, \quad T_0 = 1800, \end{aligned}\right\}, \quad (2.62)$$

T_w = 1600 K, p = 5 atm, ε_s = 0.3 %,

δ = 5, $m = m'$ = 1/7, θ = 135°.

The values of B, B_w, α', δ_B, σ_e, and κ are varied and influences of those variations on the current distribution, the electrical characteristics, etc. are investigated.

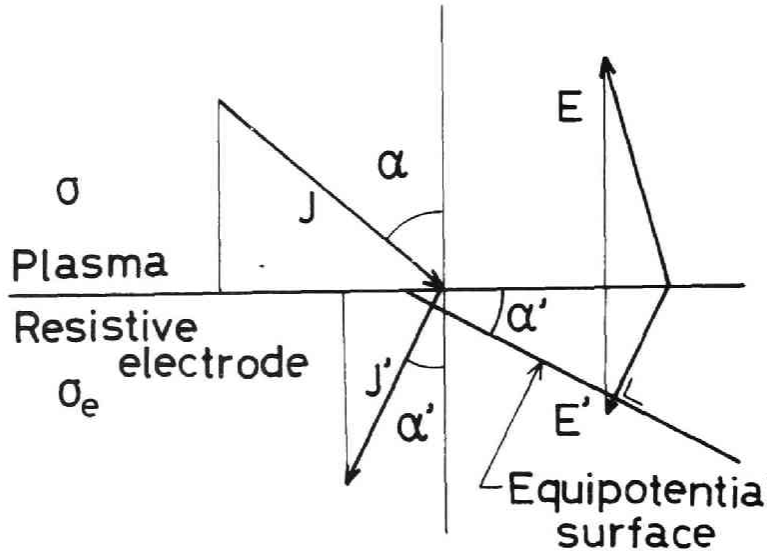

Fig. 2.21. Schetch of electrical quantities in plasma and resistive electrodes.

4.2.5 Effect of resistive electrode

As shown in Fig.2.11, the intensive current concentration occurs at the end of a good conductor electrode, and there $J_{peak}/\langle J\rangle_{el}$ = 13.3.

Figure 2.22 shows the current distribution in the generator duct with the resistive electrodes, where B = 5T, κ = 0.744, a = -1, σ_e = 0.4 ℧/m, α' = 30°, $\langle\sigma\rangle$ = 1.71 ℧/m, $\langle\beta\rangle$ = 2.53, and β_{crit} = 3.81. The figure indicates that the excessive current concentration at the electrode end as seen in Fig.2.11 can be eliminated by use of the resistive electrode. In this case $J_{peak}/\langle J\rangle_{el}$ = 1.46.

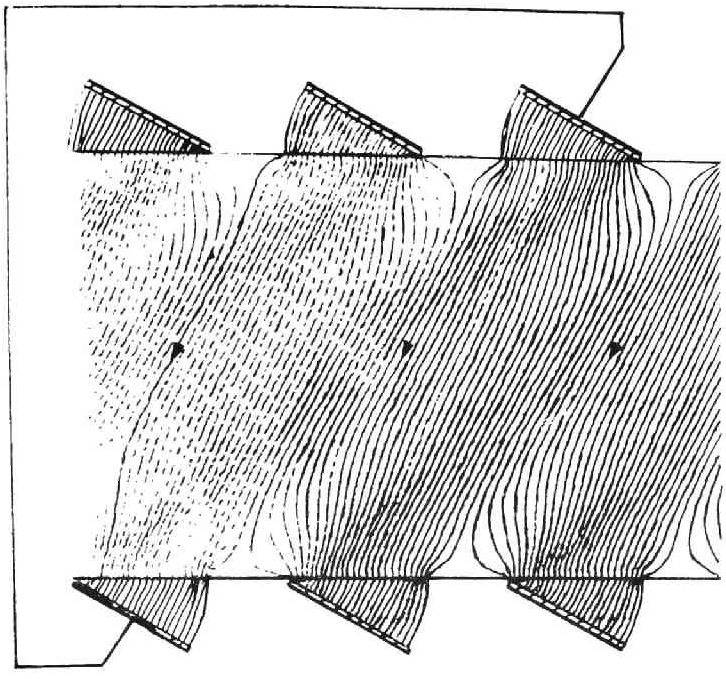

Fig. 2.22. Current distribution in generator duct with resistive electrodes (1).

Next, Fig.2.23 represents the current distribution in the case of B = 6T, κ = 0.273, σ_e = 0.4 ℧/m, α' = 30°, $\langle\sigma\rangle$ = 1.50 ℧/m, $\langle\beta\rangle$ = 3.06, and β_{crit} = 3.29. The current distribution becomes a little more nonuniform than that in Fig.2.22, but a streamer does not grow yet.

Figure 2.24 shows the current distribution for B = 6T, κ = 0.716, σ_e = 0.4 ℧/m, α' = 30°, $\langle\sigma\rangle$ = 1.94 ℧/m, $\langle\beta\rangle$ = 3.02, and β_{crit} = 2.17. From the figure we see that the current scarcely concentrates at the electrode end, though the streamer occurs. These denote that the wedge-shaped resistive electrode can suppress occurence of the current concentration at the electrode end in the same way as the Faraday type generator, and also that it can suppress the growth of streamer in the gas plasma to some ex-

tent.

In Fig.2.25 is presented the influence of κ on $J/\langle J\rangle_{el}$ on the electrode surface when B = 5T, α' = 30°, and σ_e = 0.4 ℧/m. Under these numerical conditions, the variation of $J_{peak}/\langle J\rangle_{el}$ by κ is small and the values of $J_{peak}/\langle J\rangle_{el}$ become smaller than 1.46, although κ varies from 0.281 to 0.744. These show that the resistive electrode can hold its validity against a large variation of κ, though the current distribution remarkably varies by κ in a diagonal type generator.

In Figs.2.26 and 2.27, the variations of η_e, Q_H, $J_{peak}/\langle J\rangle_{el}$, I, P, $\sigma_{eff}/\langle\sigma\rangle$, and $\beta_{eff}/\langle\beta\rangle$ by σ_e are plotted for α' = 5° and 30°, respectively, where B = 4T and κ = 0.5. Figure 2.26, where α' is small, shows that the current concentration at the electrode end is largely weakened, and η_e and Q_H increase a little with de-

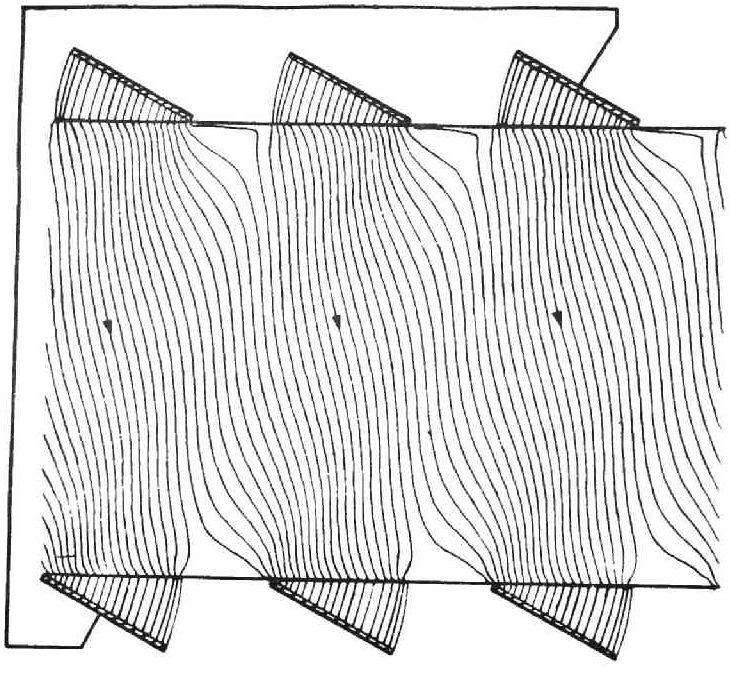

Fig. 2.23. Current distribution in generator duct with resistive electrodes (2).

creasing σ_e, but I and P decrease. Figure 2.27 tells that current concentration is most removed at σ_e = 0.5 ℧/m. This value of σ_e roughly coincides with the value obtained from Eq.(2.61) under the above numerical conditions.

Moreover, Figs.2.26 and 2.27 inform that the variation of η_e, Q_H, etc. is small in the σ_e range of about 0.1 to 1 ℧/m, and thus the use of the resistive electrode will not degrade the electrical characteristics of the generator. σ_e = 0.1 to 1 ℧/m will be suitable for the resistive electrode. In this connection, many investigations of electrode materials have been carried out, and the electrical conductivity of ZrO_2-CeO_2 mixture or spinels has been found to show above-mentioned values [2.30] and [2.31].

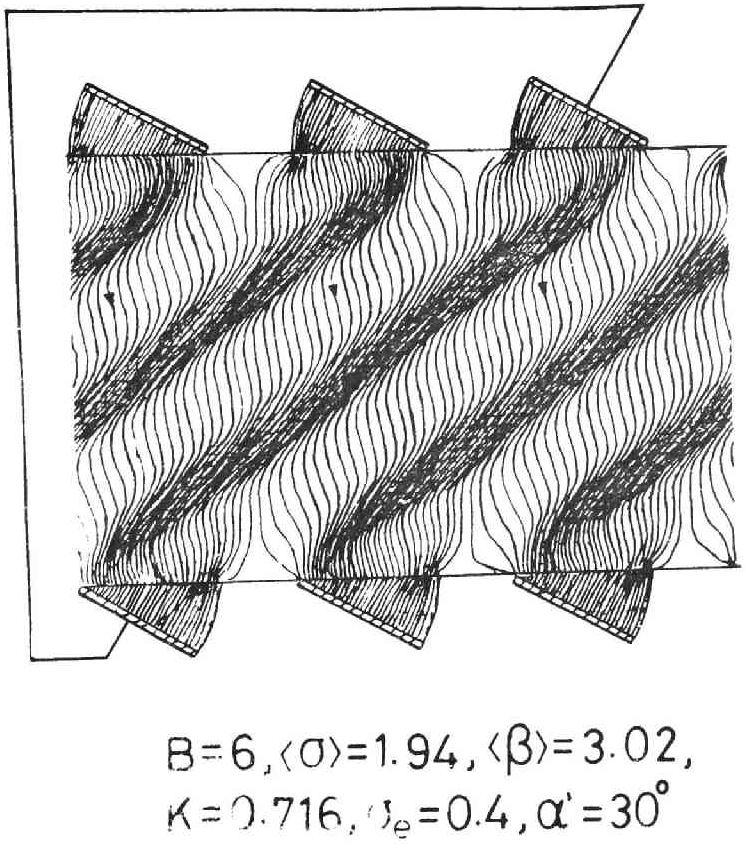

Fig. 2.24. Current distribution in generator duct with resistive electrodes (3).

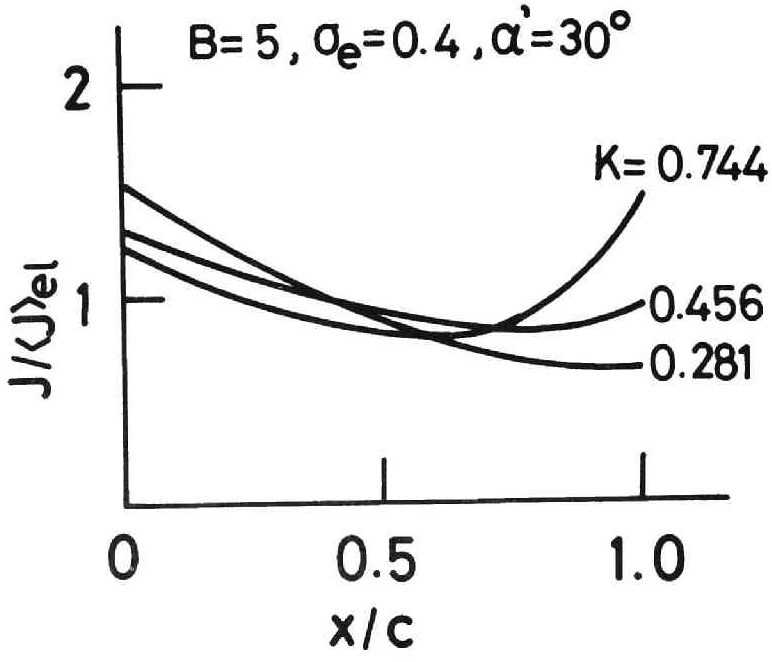

Fig. 2.25. Influence of κ on $J/\langle J\rangle_{el}$ on electrode surface.

4.3 Effects of Distribution of Applied Magnetic Flux

4.3.1 Distribution of applied magnetic flux

It has been proposed to eliminate the current concentration at the electrode ends by an attenuation of the magnetic induction at the region near duct wall in the y direction, where the Hall effect decreases because of a low magnetic flux density [2.29].

Distribution of the applied magnetic flux B is assumed to be given by the expression

$$B = \begin{cases} \{(B_0 - B_w)/\delta_B\}y/h + B_w, & 0 < y/h < \delta_B \\ B_0, & \delta_B < y/h < 1 - \delta_B \\ -\{(B_0 - B_w)\delta_B\}y/h + \{B_0 - (1 - \delta_B)B_w\}/\delta_B, & \\ \quad 1 - \delta_B < y/h < 1, & \end{cases}, \quad (2.63)$$

as shown in Fig.2.28 where B_w is the magnetic flux density at the duct wall, and δ_B is the length shown in the figure. The distri-

bution of megnetic flux can have approximately the above configuration when the generator duct protrudes from the magnet in the y direction.

4.3.2 Effects of distribution of applied magnetic flux

The current distributions in the duct are plotted in Figs. 2.29, 2.30, and 2.31 in the case of κ = 0.114, 0.362, and 0.617, respectively, where B_0 = 5T, B_w = 2T, and δ_B = 0.1. These figures show that the streamers are formed in the x, y, and negative x directions for κ = 0.114, 0.362, and 0.617, respectively. Namely, the current distribution in the diagonal type duct is very dependent on the value of κ.

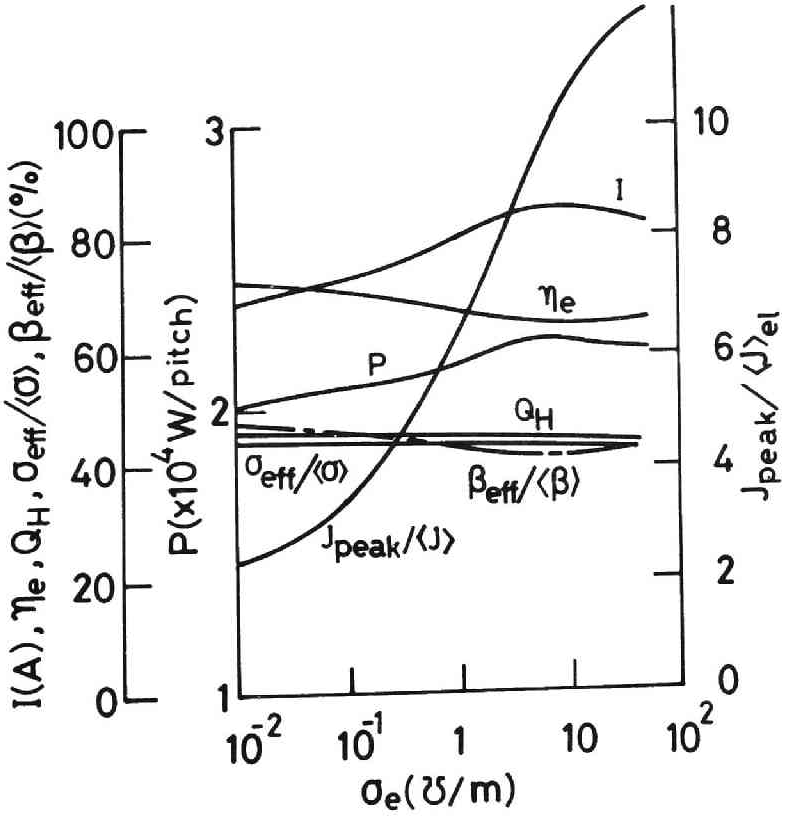

Fig. 2.26. Influence of σ_e on η_e, Q_H, etc. (1).

In Comparison with Fig.2.11 which shows the current distribution for κ = 0.630 and $B_w = B_0$ = 5T, Fig.2.29 tells that the circulating current near the electrodes is eliminated and the current distribution there becomes uniform to some extent when B_w is small, but the current still concentrates at electrode end and the main streamer is influenced little by B_w. Furthermore, as seen in Figs. 2.30 and 2.31, the new streamer occurs in the neighborhood of the insulating walls in parallel with the insulating walls when κ is large.

Figure 2.32 shows influences of B_w on the generator performance when κ = 0.6 and B_0 = 5T. The figure indicates that $J_{peak}/\langle J\rangle_{el}$ decreases with B_w and its value for B_w = 0 is about 75 % of that for $B_w = B_0$, but η_e, Q_H, etc. are affected little by B_w. The current concentration at the electrode end can be eliminated to some extent by decreasing B_w, but the main streamer is hardly dependent on B_w. Consequently, the generator performance is affected

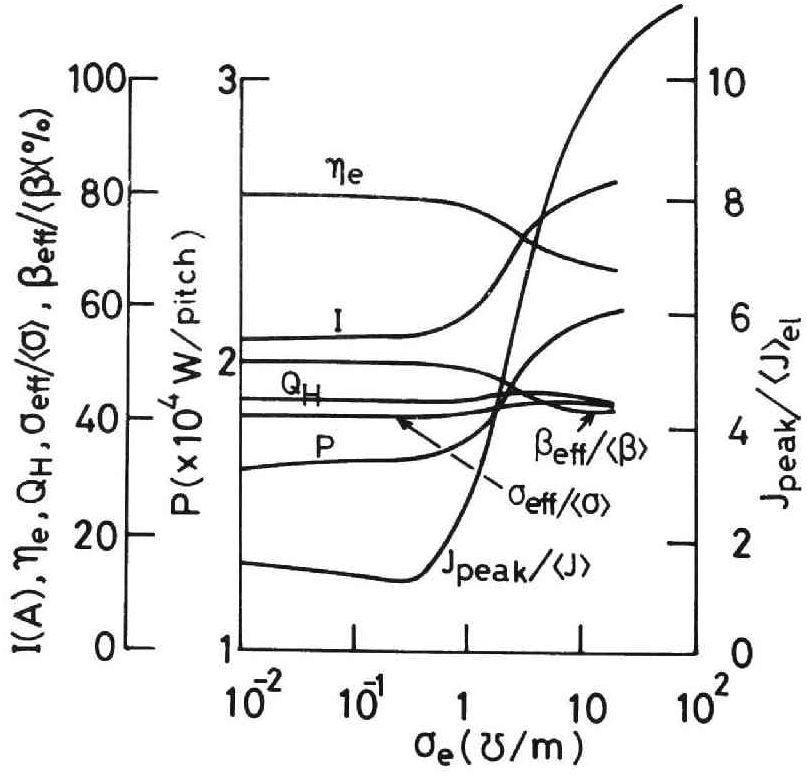

Fig. 2.27. Influence of σ_e on η_e, Q_H, etc. (2).

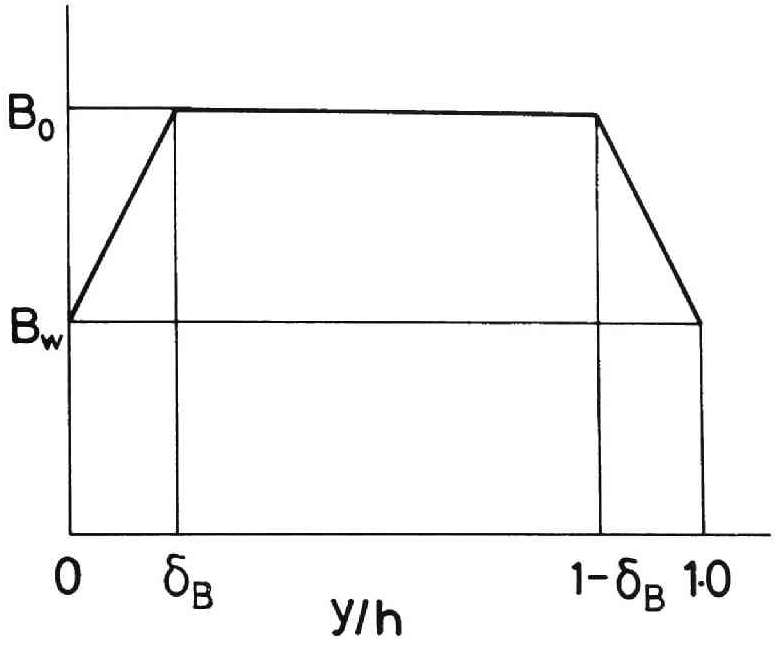

Fig. 2.28. Distribution of applied magnetic flux.

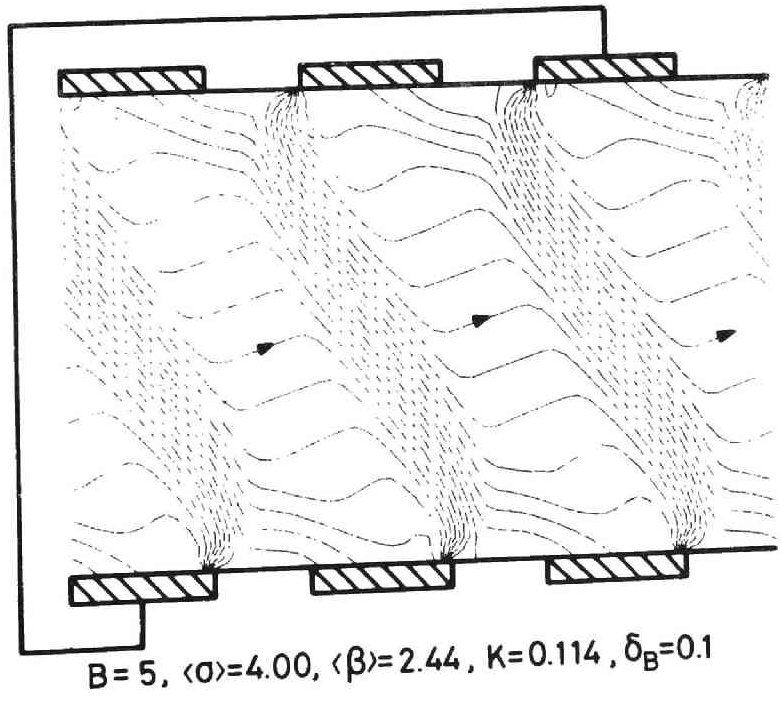

Fig. 2.29. Current distribution in generator duct (1).

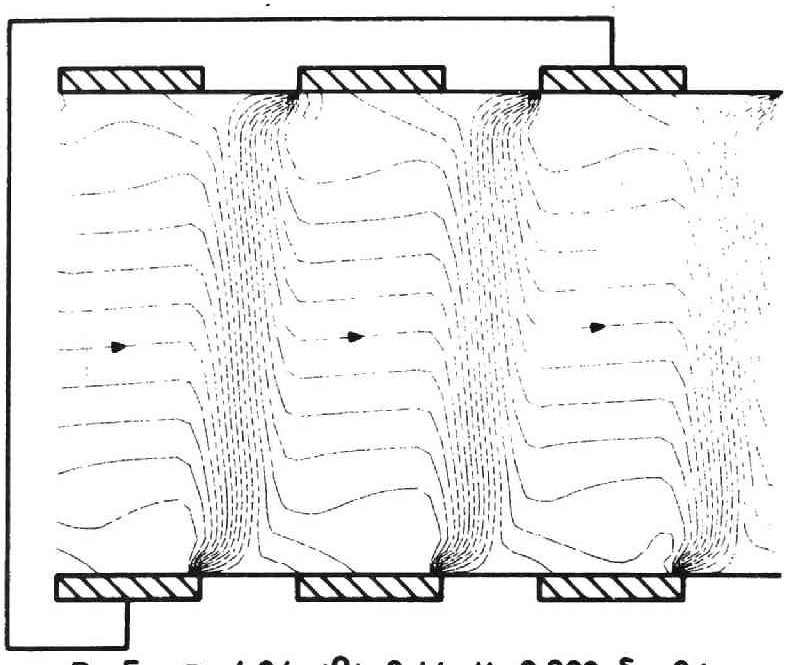

Fig. 2.30. Current distribution in generator duct (2).

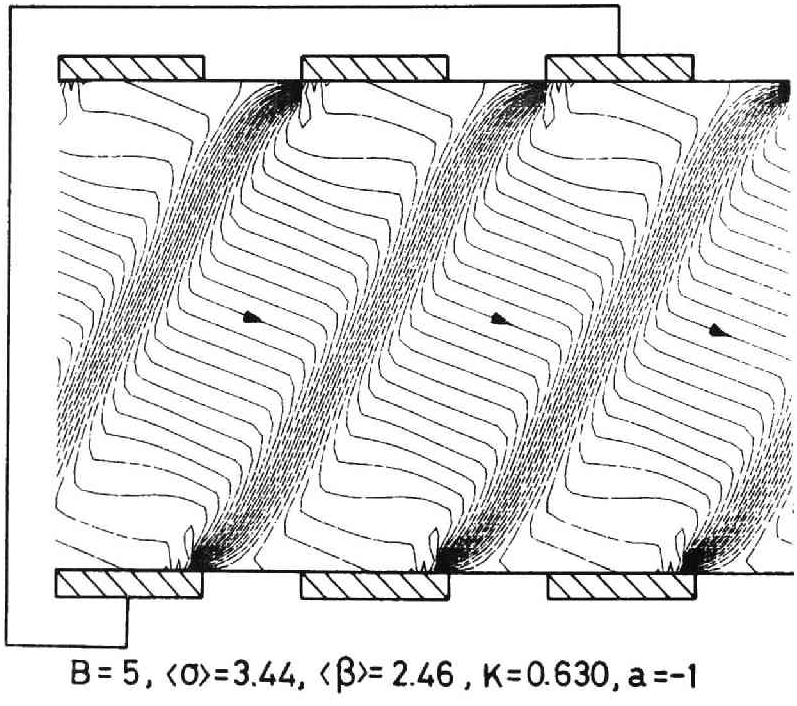

Fig. 2.31. Current distribution in generator duct (3).

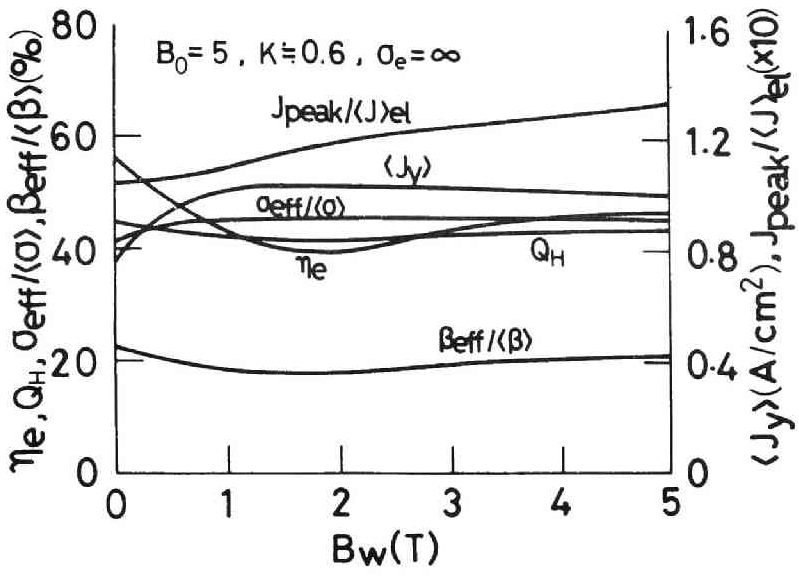

Fig. 2.32. Influence of B_w on η_e, Q_H, etc.

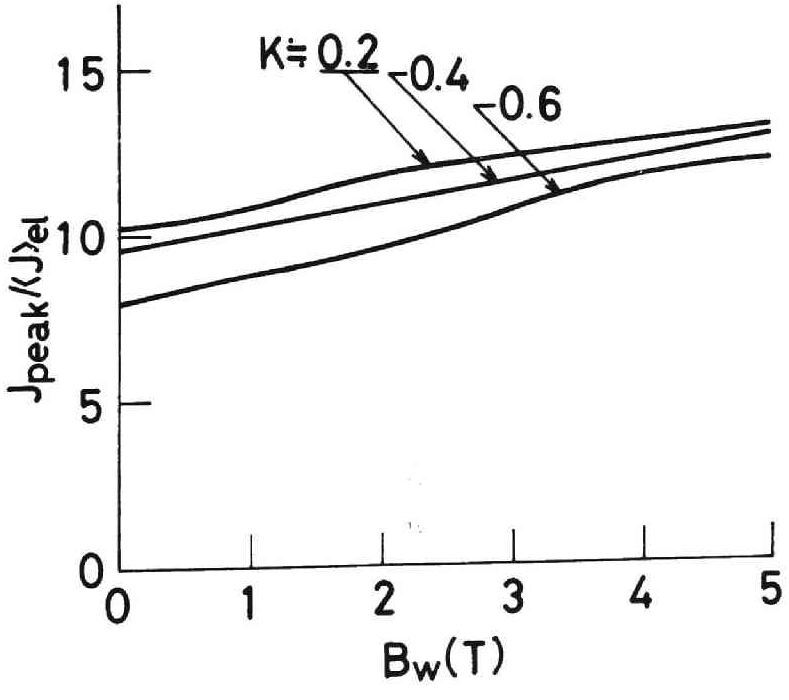

Fig. 2.33. Influence of B_w and κ on $J_{peak}/\langle J\rangle_{el}$.

little by attenuation of B in y direction near the duct wall.

From Fig.2.33, in which the variation of $J_{peak}/\langle J\rangle_{el}$ by κ is plotted, it is seen that $J_{peak}/\langle J\rangle_{el}$ becomes about 65.0, 72.5, and 75.0 % of those for $B_w = B_0$, in the cases of $\kappa \fallingdotseq 0.2$, 0.4, and 0.6, respectively. This indicates that current concentration is eliminated better as κ is small.

Furthermore, it was ascertained that $J_{peak}/\langle J\rangle_{el}$ becomes 10.9, 11.2, and 10.6 for $\delta_B = 0.1$, 0.2, and 0.4, respectively, when $B_0 =$ 5T, $B_w = 2$T, and $\kappa \fallingdotseq 0.4$. This shows that variation of $J_{peak}/\langle J\rangle_{el}$ by δ_B is small. In addition, a little short-circuit current flows between the adjacent electrodes when $\delta_B = 0.4$.

4.4 Concluding Remarks

The effects of wedge-shaped electrode and attenuation of magnetic flux density in the region near duct wall on the performance of the diagonal type MHD generator with nonequilibrium plasma have been numerically investigated. The main results are as follows.

(1) The wedge-shaped resistive electrode can largely remove the current concentration at the electrode ends of the diagonal type MHD generator with nonequilibrium plasma.

(2) It is not necessary to vary the conductivity of the resistive electrode according to the load factor, although the current distribution is varied remarkably by the load factor in the diagonal type generator.

(3) The generator characteristics such as the electrical efficiency and the specific Hall voltage are not degraded by the use of wedge-shaped resistive electrode.

(4) Attenuation of magnetic flux density in the region near the duct wall can eliminate the current concentration to some extent.

(5) The elimination of the current concentration varies with the load factor and decreases with increasing the load factor.

CHAPTER 5
END EFFECTS

5.1 Introduction

An eddy current is apt to be generated in the end regions of a generator, since spatial differences of the induced electromotive forces are created there in the direction of attenuation of the magnetic flux dinsity. It distorts a normal current distribution in the generator duct ends and degrades the total electrical charcteristics of the generator. These may be intensive especially in the diagonal type generator, because the output electrodes are arranged in the inlet and exit regions of generator duct.

The end effects in the Faraday type generator have been analyzed in fair detail [2.32] to [2.34]. On the other hand, those in the diagonal type have been only a little discussed [2.35] to [2.37]. Accordingly, the end effects in the diagonal type generator are studied by a two-dimensional analysis.

In this chapter, the arrangement of the output electrodes and the distribution of the applied magnetic flux are shown, which are used for the numerical investigation. Then, in the case of constant electrical conductivity and electron mobility, by the numerical analysis are investigated influences of the attenuation of the magnetic flux density and the types and position of output electrodes on the current distribution in the end regions, the potential difference between adjacent electrodes, the internal resistance, etc. in the end regions.

Next, in the case of variable conductivity and electron mobility, effects of the attenuation of magnetic flux density on the current distribution, the internal resistance, the ballast resistance, etc. are studied.

In addition, the current distribution in the inlet region becomes symmetric with the distribution in the exit region on the assumptions made in this thesis.

5.2 Arrangement of Output Electrodes and Distribution of Applied Magnetic Flux

5.2.1 Arrangement of output electrodes

(1) Arrangement of output electrodes

Among various types of arrangements of the output electrodes which have been proposed for the diagonal type generator, the effects of three types shown in Figs.2.34, 2.35(a), and (b), which we call hereafter A, B, and C types for the convenience, will be investigated in this chapter. As seen in the figures, in A type the two electrodes E_1 and E_2 which are shorted each other, in B type two pairs of the diagonally connected end electrodes, and in C type two pairs of the Hall connected electrodes are equipped as the output electrodes, respectively. Of cource, the anode A_i and cathode C_i ($i = 1,2,---, n$) except the output electrodes are connected diagonally.

(2) Subsidiary conditions of end region

The subsidiary and periodicity conditions (2.28) and (2.29) are replaced by

$$V_i = -\int_{C_i}^{A_i} \boldsymbol{E}\cdot d\boldsymbol{s}=0, \quad i = 1,2,---,n, \tag{2.64}$$

$$\int_{S_i} \boldsymbol{J}\cdot d\boldsymbol{S} = I, \quad i = 1,2,---,n, \tag{2.65}$$

respectively.

In this connection, behind the n-th electrode pair A_n and C_n [see Fig.2.34], the electric quantities are assumed to vary periodically with one electrode pitch s along the gas flow. Then, the periodicity condition (2.27) is rewritten as

$$\Psi(x_1) = \Psi(x_1 - s) + I_y^{(n)}, \tag{2.66}$$

where x_1 is the x co-ordinate of the right edge of the insulating wall C'_n in Fig.2.34.

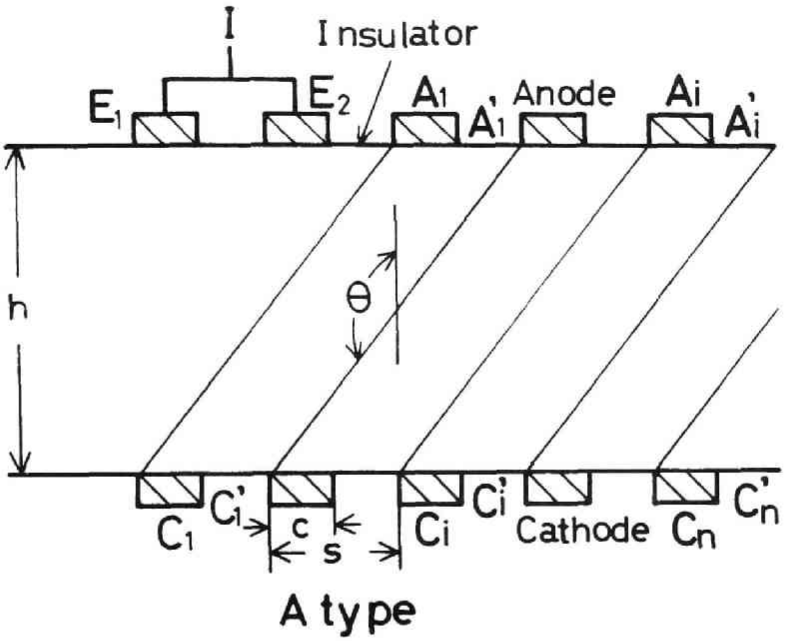

Fig. 2.34. Coordinate system and end region of diagonal type MHD generator duct (A type).

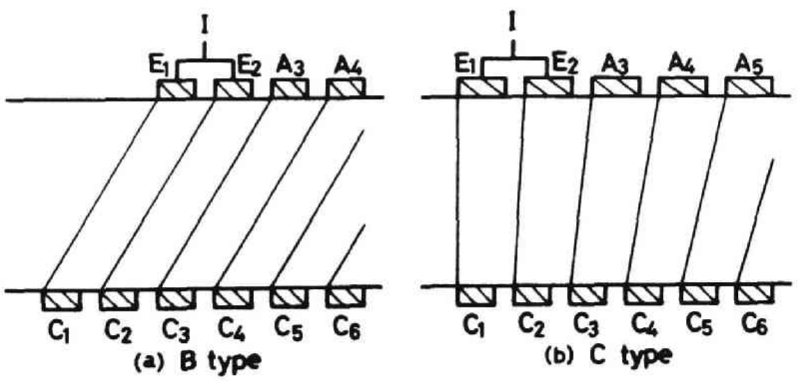

Fig. 2.35. Duct end geometries (B and C types).

Next, From Eqs.(2.14) and (2.65), we can derive the following equations

$$\left.\begin{aligned} &\psi_i^{A'} - \psi_i^{C'} = 1, \quad i = 1,2,\cdots,n \\ &\psi = \Psi/(I/w), \end{aligned}\right\} , \tag{2.67}$$

where $\psi_i^{A'}$ and $\psi_i^{C'}$ are the values of ψ on the insulating wall surfaces A_i' and C_i', respectively, in Fig.2.34.

First, if the values of I and w are assumed and $\psi_i^{A'}$ is given a plausible value, the value of $\psi_i^{C'}$ is decided by Eq.(2.67). When Eq.(2.16) is digitally solved by those values of $\psi_i^{A'}$ and $\psi_i^{C'}$ and the appropriately assumed values of u, σ, and β, we can obtain the numerical solution of ψ. By applying the solution to Eqs.(2.4) and (2.7), we can find the values of E_x and E_y. Further, by substituting the values of E_x and E_y into the integral $V_i = -\int_{C_i}^{Ai} \boldsymbol{E}\cdot d\boldsymbol{s}$ in Eq.(2.64), we can decide the value of V_i, but yet the value of V_i obtained is not necessarily equal to zero.

So let us consider the average resistance between the electrodes A_i and C_i

$$R_i' = h/\{\langle\sigma\rangle_i cw\cos(\pi-\theta)\}, \quad i = 1,2,---,n, \tag{2.68}$$

where $\langle\sigma\rangle_i$ is the average electrical conductivity of gas plasma. We assume that an imaginary current defined by

$$I_i = V_i/R_i', \quad i = 1,2,---,n, \tag{2.69}$$

flows through the resistance R_i'. To make V_i zero, it is necessary to flow the inverse current $-I_i$ through R_i'. Therefore, newly it is required to increase the current $w(\psi_{i+1}^{A'} - \psi_i^{A'})$ running into the anode A_i by $-I_i$.

Again beginning with the new modified value of $\psi_i^{A'}$, we must repeat the above-mentioned calculation process. When V_i becomes adequately small after many repetitions of the above-mentioned process, then we can obtain a satisfactory numerical solution of ψ.

5.2.2 Distribution of applied magnetic flux

For effective use of the magnet the MHD generator duct will be arranged in the attenuation domain of the magnetic induction B. In order to investigate the influence of attenuation of B on the current distribution in the generator, we assume that B is constant in the central domain and decreases linearly from the left

edge of the j-th electrode in the end regions of the generator.

5.3 When Electrical Conductivity and Electron Mobility Are Assumed Constant

5.3.1 Numerical conditions

As a numerical example, we analyze the current and potential distributions in a diagonal type MHD generator duct, in which

$$\left.\begin{array}{l} h = 0.3, \quad w = 0.3, \quad s = 0.075, \quad c = 0.056 \text{ m}, \\ B_0 = 4 \text{ T}, \quad I = 150 \text{ A}, \quad u_0 = 800 \text{ m/s}, \quad n = 9, \\ \sigma = 5.0 \text{ ℧/m}, \quad \mu_e = 0.5 \text{ and } 1.0, \quad \theta = 153°, \end{array}\right\}, \quad (2.70)$$

where B_0 is the magnetic flux density in the central region of the duct, and the five configurations of B are assumed as shown in Fig.2.36, in which g is the gradient of B and j=8.

In addition, the numerical results obtained in this section can be available for the open cycle generator.

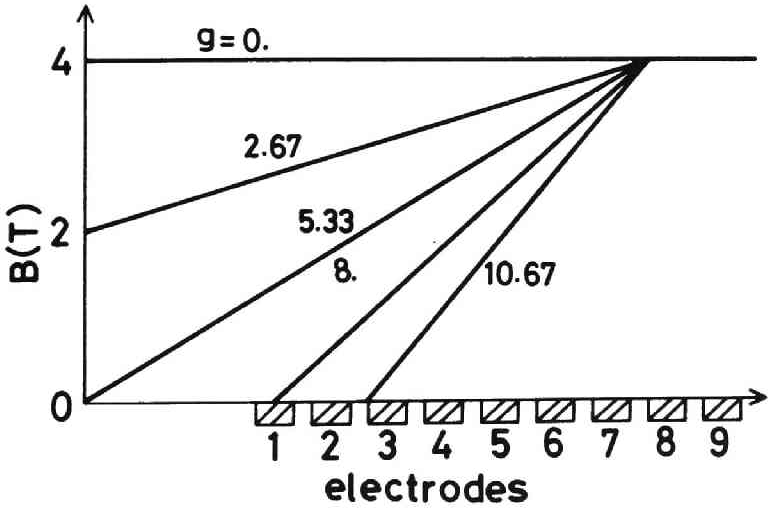

Fig. 2.36. Distribution of applied magnetic flux for j=8.

5.3.2 Effects of type of output electrodes and distribution of applied magnetic flux

(1) Current distribution

In Figs.2.37 to 2.40, are plotted the current distributions in the duct of the A type arrangement in the cases of g = 0, 5.33, 8, and 10.6 T/m , respectively, and j = 8. In the figures and the later Figs.2.41 to 2.44, the contour interval of current stream lines is 1/8 of the load current I.

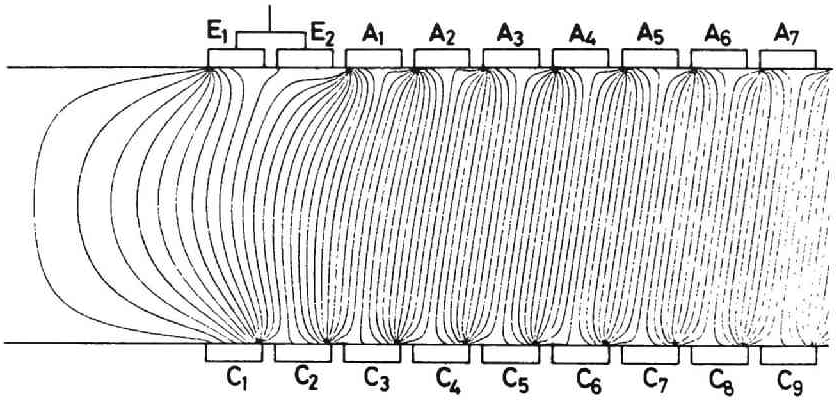

Fig. 2.37. Current distribution for g = 0 and j = 8 (A type).

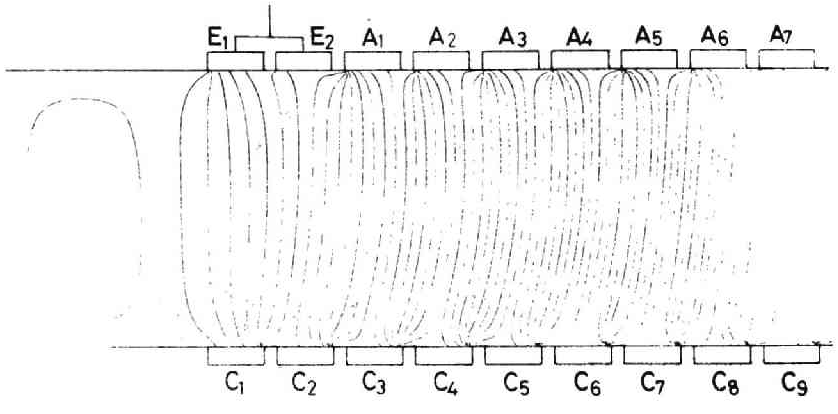

Fig. 2.38. Current distribution for g = 5.33 and j = 8 (A type).

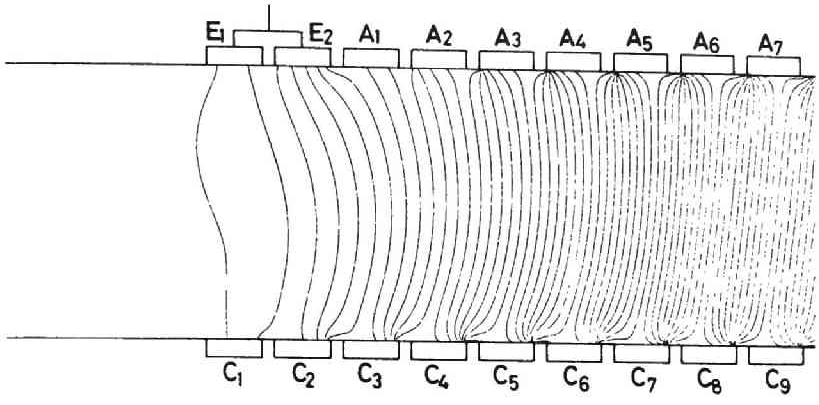

Fig. 2.39. Current distribution for g = 8 and j = 8 (A type).

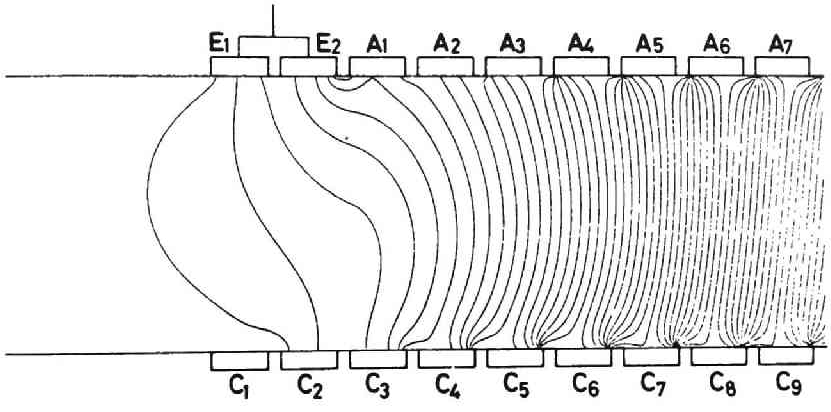

Fig. 2.40. Current distribution for g = 10.67 and j = 8 (A type).

From Fig.2.37, it is seen that the current concentrates only at the left end of the first output electrode E_1 and the second electrode E_2 acts little as the output electrode, and also that the large circulating current flows through the first electrode pair A_1-C_1 which are diagonally connected, when the magnetic flux density B does not attenuate.

Next, Fig.2.38 shows that in the case of g = 5.33 the current distribution on the output electrodes becomes fairly uniform, but

an eddy current occurs in the duct end region, whose rate is about 13.3 % of I.

Figure 2.39 indicates that the nearly equal currents flow into both output electrodes, and the current distribution on the electrodes becomes very uniform when B decreases with g = 8. The figure also tells that the current concentration at the output electrode ends weakens, because β becomes small in the area suffering a spatial attenuation of B. Further in this case, the eddy current vanishes.

Next, from Fig.2.40 we see that a new nonuniform current distribution occurs when B is rapidly attenuated by g = 10.67. For example, the current stream is pushed toward the central part of duct and a shorting current flows between E_2 and A_1.

Figures 2.38 to 2.40 inform that arranging the output electrodes within the attenuating domain of the applied magnetic flux density B has no appreciable influence on the current distribution in the central part of generator.

Next, Figs.2.41 and 2.42 show the current distributions in the ducts of the B and C type arrangements, respectively, in the case of g = 5.33 and j = 8. It will be seen that the current distributions in both figures are similar to the distribution in Fig.2.38. The persentages of the eddy current I_{eddy} in Figs.2.41 and 2.42 are about 21.1 and 9.1 % of I, respectively, and the B type arrangement induces a little larger eddy current than the other type arrangements. This is because the B type duct is not equipped with the output electrodes on the upper side in the inlet.

Figures 2.43 and 2.44 show the current distributions in the A type duct in the case of j = 6 and 4, respectively, and g = 8.

Figures 2.39, 2.43, and 2.44 also show that the current distribution varies with the positions of the output electrodes for the same gradient g, and getting the output electrodes nearer the

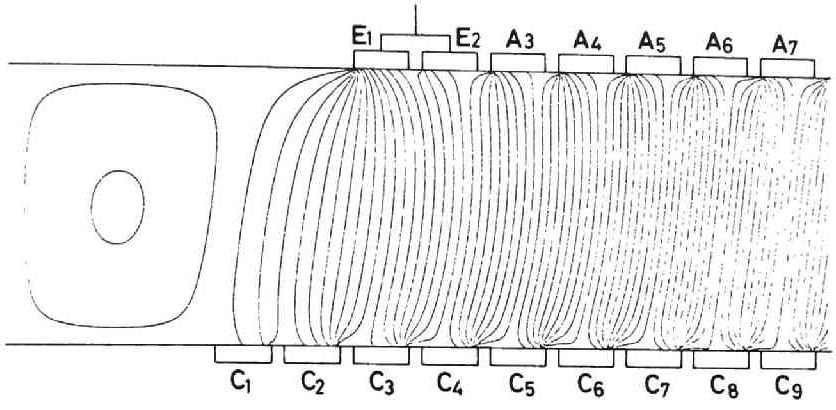

Fig. 2.41. Current distribution for g = 5.33 and j = 8 (B type).

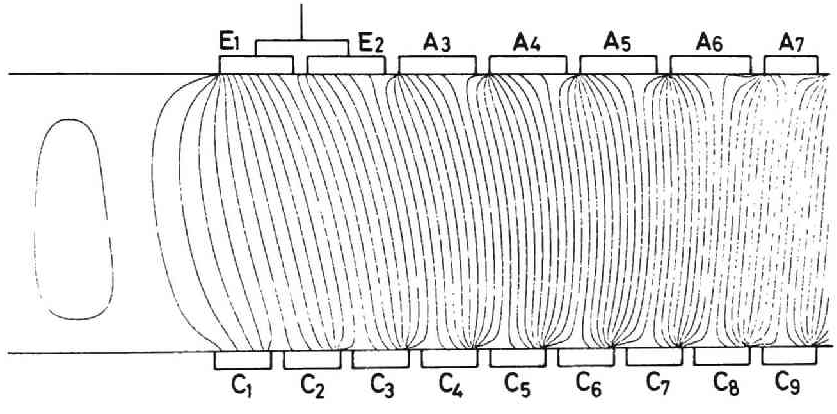

Fig. 2.42. Current distribution for g = 5.33 and j = 8 (C type).

domain of constant B makes eddy current large. In this connection, Table 2.1 shows the calculated values of I_{eddy}/I for the j = 8, 6, and 4, where I_{eddy} is the eddy current in the duct end.

In addition, when μ_e = 1.0, the percentage of I_{eddy}/I becomes about 12.5, 22.8, and 10.0 % in A, B, and C type, respectively, which are nearly equal to the percentages when μ_e = 0.5.

(2) Internal resistance and current concentraion

For quantitative estimation of the end effects of the generator, the internal resistance R_i of the end regions and the rate $J_{peak}/\langle J\rangle_{el}$ of the current concentration on the output electrodes are calculated by

$$R_i = (V_0 - V)/I \tag{2.71}$$

and Eq.(2.36), respectively, where V_0 is no-load potential difference between the output electrodes and the n-th electrode and V

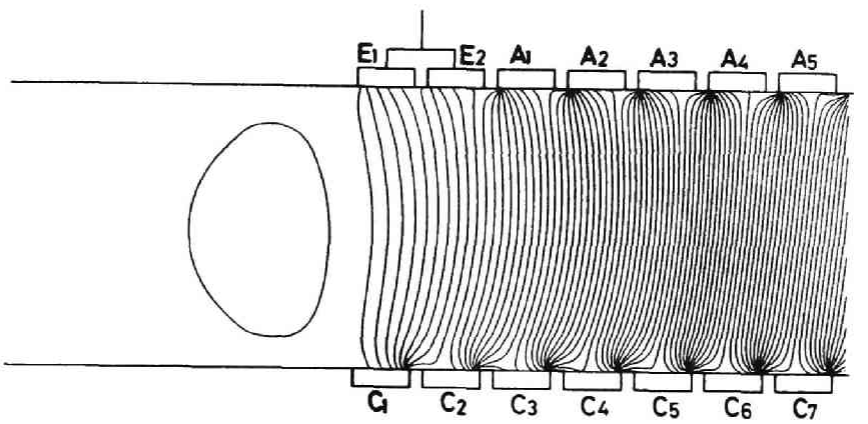

Fig. 2.43. Current distribution for g = 8 and j = 6 (A type).

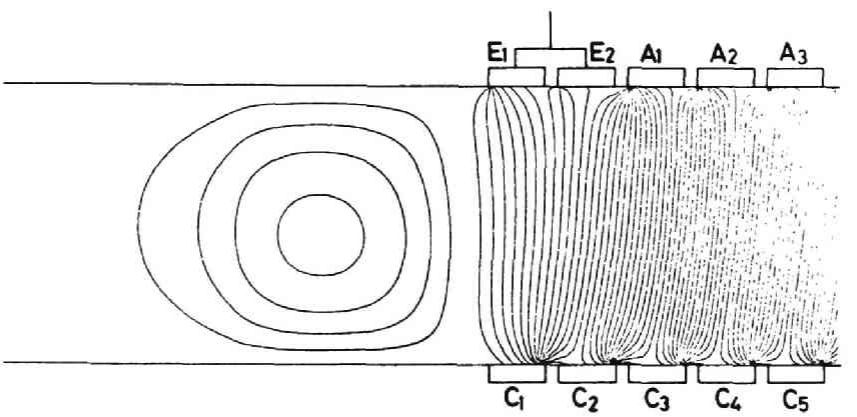

Fig. 2.44. Current distribution for g = 8 and j = 4 (A type).

Table 2.1 R_i, $J_{peak}/\langle J \rangle_{el}$, I_{eddy}, and V_{el} for j = 8, 6, and 4 (A type)

J	$R_i(\Omega)$	$J_{peak}/\langle J \rangle_{el}$	I_{eddy}/I	$V_{el}(V)$
8	5.10	1.63	0.	34.5
6	11.52	2.84	0.200	85.5
4	16.93	6.00	0.433	234.

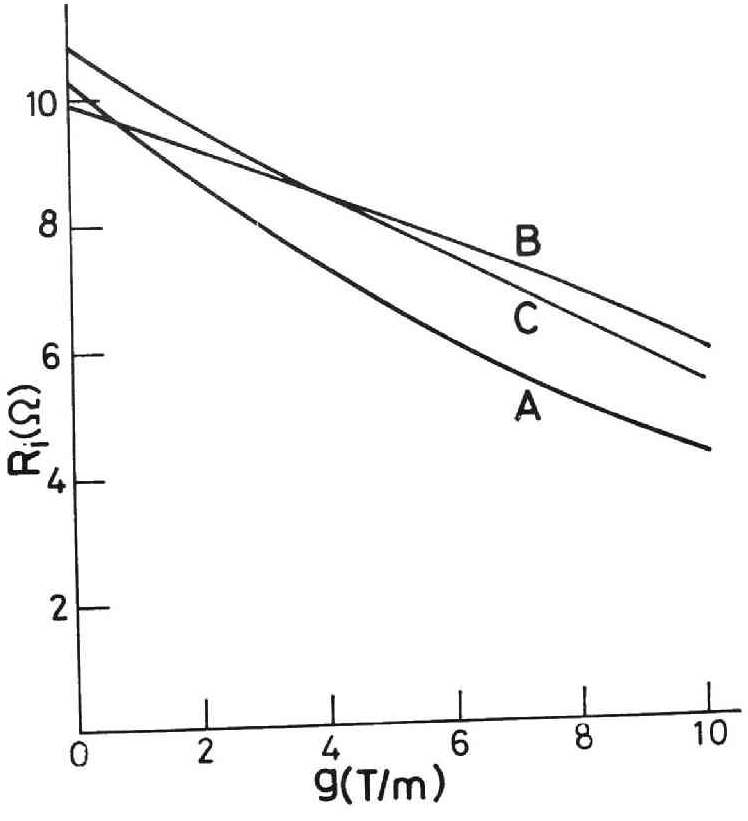

Fig. 2.45. Variation of internal resistance by g for j = 8.

the potential difference between these electrodes.

Table 2.1 shows the values of R_i and $J_{peak}/\langle J\rangle_{el}$, which are obtained with respect to Figs.2.39, 2.43, and 2.44, respectively. In Fig.2.45 is plotted the variation of R_i against g in the ducts of the A, B, and C type arrangements in the case of j = 8. The figure indicates that R_i decreases with g in all types, and for instance, the values of R_i for g = 8.0 become 49.8, 69.7, and 58.3 % of those for g = 0 in the A, B, and C type ducts, respectively.

Figure 2.46 shows the relation between $J_{peak}/\langle J\rangle_{el}$ and g. From the figure it is seen that in any type of duct the current

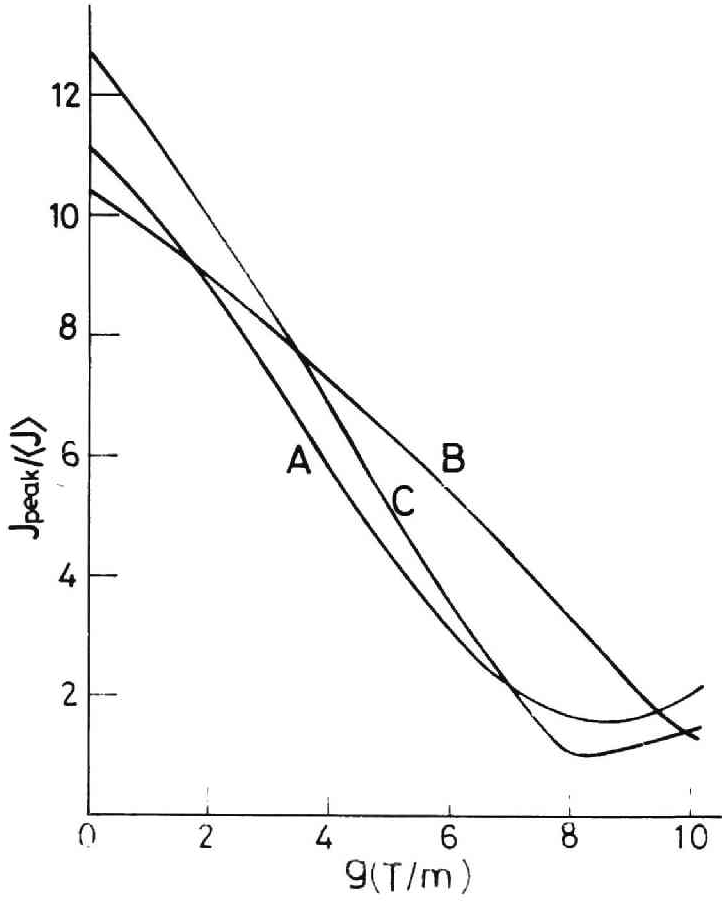

Fig. 2.46. Variation of current concentration on output electrodes by g for j = 8.

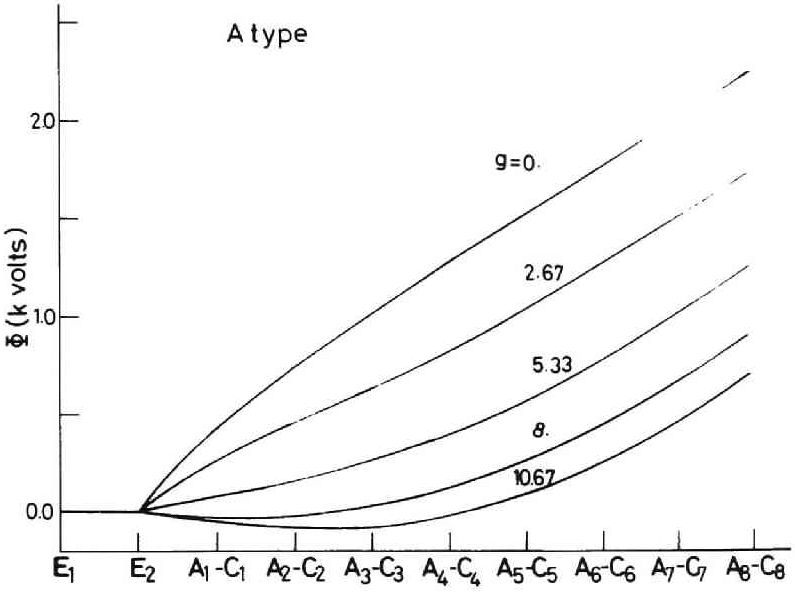

Fig. 2.47. Variation of potential difference for j = 8 (A type).

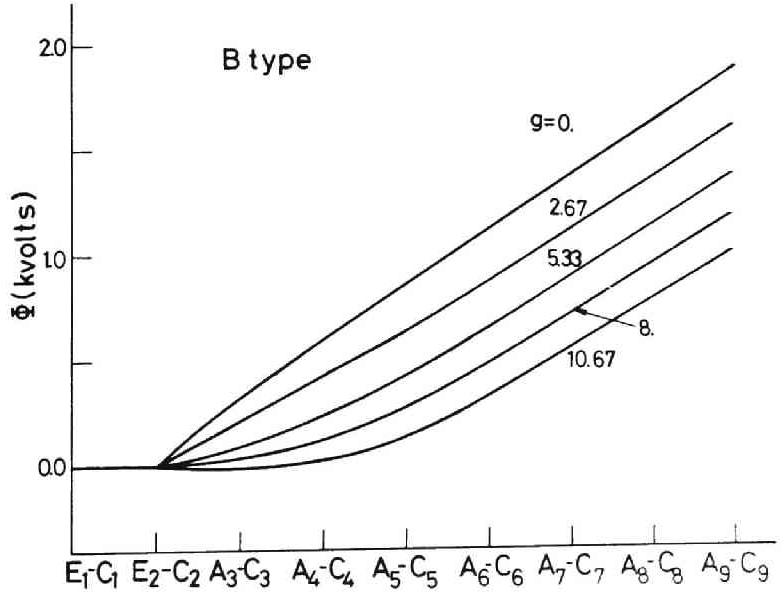

Fig. 2.48. Variation of potential difference for j = 8 (B type).

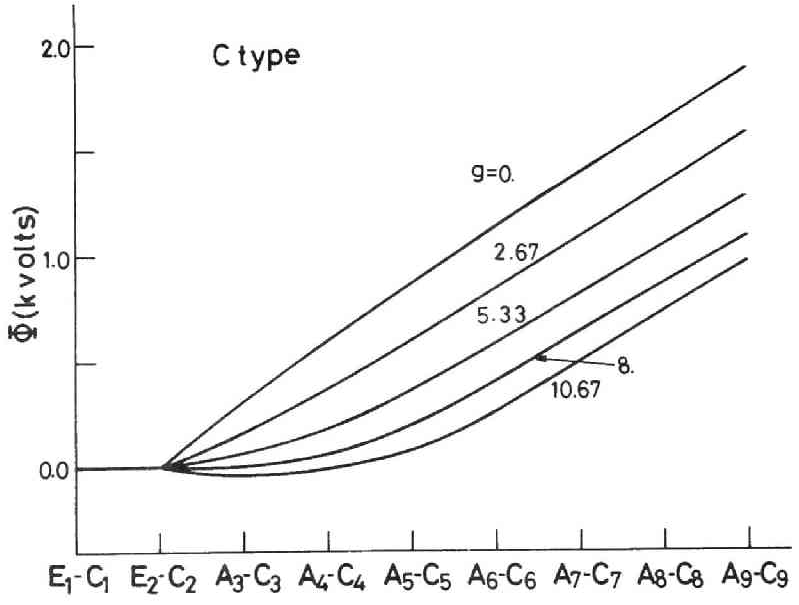

Fig. 2.49. Variation of potential difference for j = 8 (C type).

concentration considerably weakens in keeping with the attenuation of B. This indicates that arranging the output electrodes in the attenuation area of the magnetic flux density is useful to guard the output electrodes.

(3) Potential distribution

In Figs.2.47 to 2.49 are plotted the calculated results of the potential differences

$$\Phi = - \int_{E_1}^{A_i} \boldsymbol{E} \cdot d\boldsymbol{s}, \quad i = 1,2,---,n \tag{2.72}$$

between each electrode pair A_1-C_1 to A_8-C_8 and the electrode E_1 in the A, B, and C type arrangements, respectively. In the above equation, $d\boldsymbol{s}$ is a line element vector on an optional integral path from E_1 to A_1.

Figure 2.47 shows that the relatively large potential differ-

ence arises between the adjacent electrodes when B does not attenuate in the duct end, and accordingly large ballast resistors are necessary to use effectively the electrodes E_1 and E_2 as the output electrodes. On the other hand, the potential difference becomes smaller as g becomes larger, and in the range of g = 5.33 to 8, the potential difference between the adjacent electrodes E_2 and A_1 is almost negligible. Thus, by a proper attenuation of B, more output electrodes than two can be used without large ballast resistors.

From Figs.2.48 and 2.49, it is seen that the potential distributions in the B and C type ducts are similar to that in the A type duct for g = 5.33 and j = 8.

Also Table 2.1 shows the potential difference V_{el} between E_2 and A_1 in the A type duct.

5.4 When Nonuniformity of Electrical Conductivity and Electron Mobility Are Considered

5.4.1 Numerical conditions and ballast resistance

Numerical analysis is carried out for the diagonal type MHD generator with the nonequilibrium plasma, in which

$$\left.\begin{aligned} & h = 0.2, \quad w = 0.1, \quad s = 0.1, \quad c = 0.06 \text{ m}, \\ & B_0 = 4 \text{ and } 5 \text{ T}, \quad u_0 = 2000 \text{ m/s}, \\ & T_0 = 1800 \text{ K}, \quad T_w = 1600 \text{ K}, \quad p = 5 \text{ atm}, \\ & \varepsilon_s = 0.3 \%, \quad \delta = 5, \quad m = m' = 1/7, \\ & g = 0 \text{ to } 10 \text{ T/m}. \end{aligned}\right\} , \quad (2.73)$$

Also in this section, it is assumed that the applied magnetic flux has the six configurations and j = 5. The numerical calculation is carried out for the A type arrangement in this section with reference to the results obtained in the previous section 5.3. Then, the load current I is assumed to flow equally into both output

electrodes E_1 and E_2 through a ballast resistance R_b defined by

$$R_b = -\int_{E_1}^{E_2} \boldsymbol{E}\cdot d\boldsymbol{s}/I. \tag{2.74}$$

5.4.2 Effects of distribution of magnetic flux

(1) Current distribution

In Figs.2.50, 2.51, and 2.52, the current distributions are plotted in the case of g = 0, 6, and 10 T/m, respectively, B_0 = 4T and I = 70 A, where the contour interval of the current streamlines is 1/20 of the load current I. In the figures, $\langle J\rangle_{el}$ = 0.583 A/cm^2, $\langle\sigma\rangle$ = 1.84 $\mho$/m, and β_{crit} = 2.48, where the values of $\langle\sigma\rangle$ and β_{crit} are calculated in the n-th electrode region.

Figure 2.50 shows that the current concentration at the output electrode ends is very intensive when g = 0, viz. B is constant. On the other hand, Figs.2.51 and 2.52 indicate that the concentration weakens as g increases, since β becomes small in the area suffering a spatial reduction of B. Also it is seen that the current flowing into a diagonally connected electrode pair reduces with increasing g in the entrance region of duct, for instance, the currents of about 60, 25, and 15 % of I flow into C_1 for g =

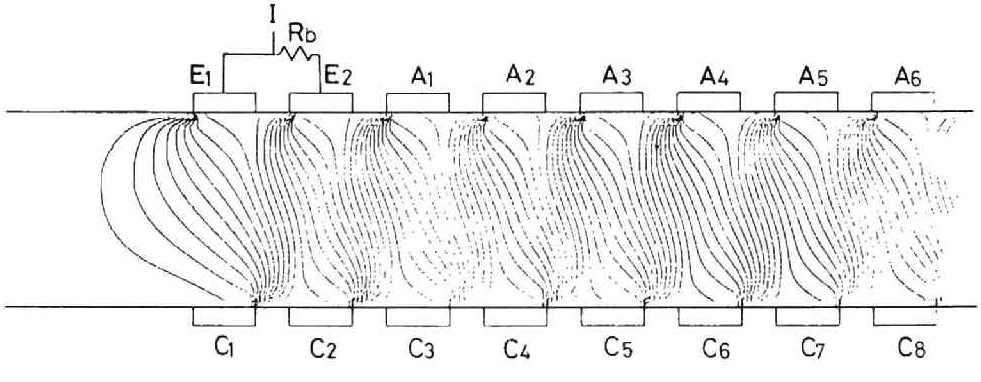

Fig. 2.50. Current distribution for g = 0, B_0 = 4, and j = 5.

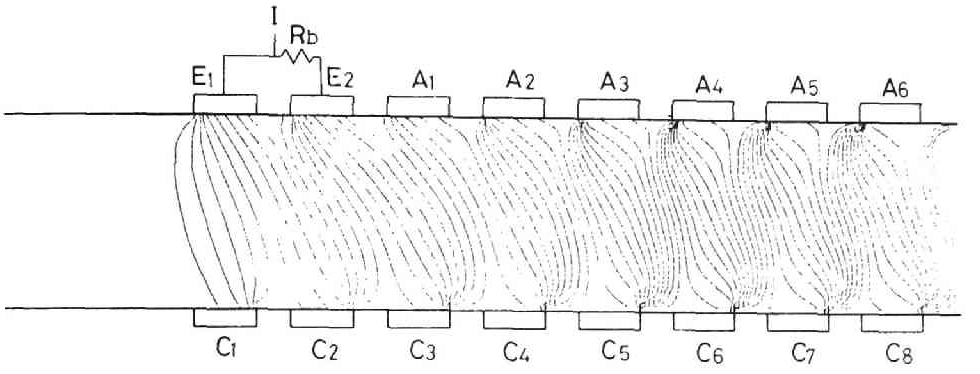

Fig. 2.51. Current distribution for $g = 6$, $B_0 = 4$, and $j = 5$.

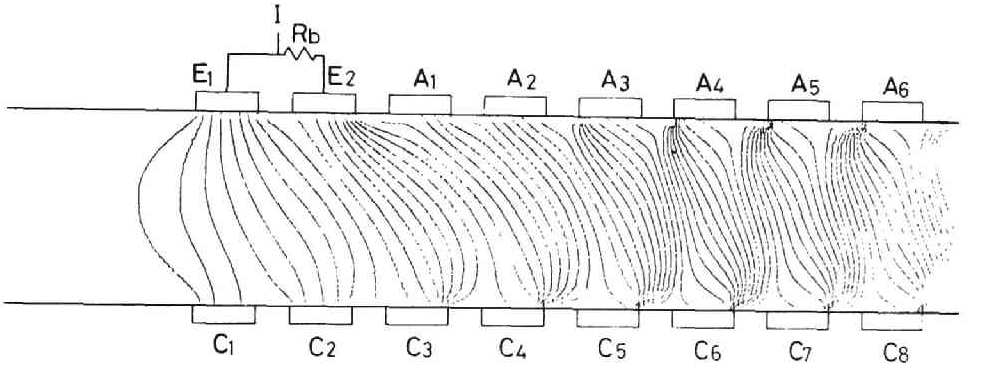

Fig. 2.52. Current distribution for $g = 10$, $B_0 = 4$, and $j = 5$.

0, 6, and 10 T/m, respectively. Also the figures show that the eddy current is not induced when the output electrodes are disposed in the attenuation domain of B [2.33], and that arranging the output electrodes within the attenuation domain has little appreciable influence on the current distribution in the central part of generator duct. These results are similar to the ones when electrical conductivity and electron mobility are assumed constant.

(2) Internal resistance and current concentration

Figure 2.53 shows the variations of R_i/R_{i0}, R_b/R_{b0}, and

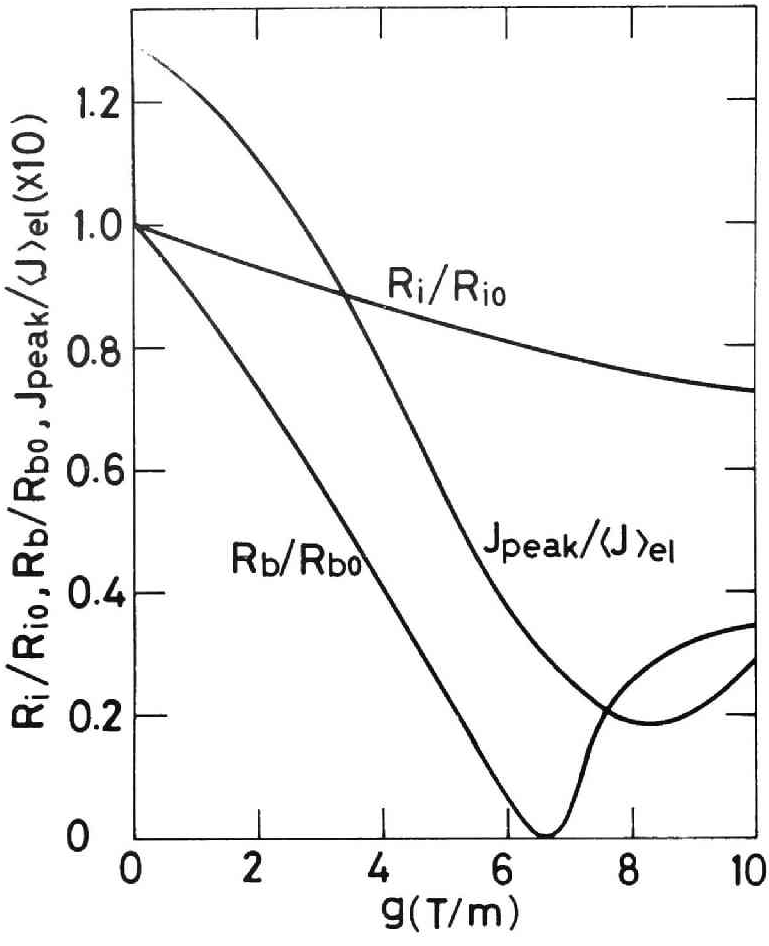

Fig. 2.53. Influence of g on R_i/R_{i0}, R_b/R_{b0}, and $J_{peak}/\langle J\rangle_{el}$ for $B_0 = 4$.

$J_{peak}/\langle J\rangle_{el}$ by g, where R_{i0} and R_{b0} are R_i and R_b for $g = 0$, respectively, and $B = 4$T. From the figure, it is seen that R_i decreases with g, for instance, R_i for $g = 6$ becomes about 80 % of R_{i0}, and that $J_{peak}/\langle J\rangle_{el}$ first decreases with g, reaches the minumum value 1.90 at $g = 8$ T/m, and next increases with g. This shows that the current concentration at the output electrode ends is almost diminished when $g = 8$ T/m. Accordingly, arranging the output electrodes in the attenuation area of the magnetic flux density is useful to guard the output electrodes.

In Fig.2.54, the current distribution is plotted for $g = 6$

T/m, B_0 = 5T, I = 150 A, $\langle J \rangle_{el}$ = 1.25 A/cm^2, $\langle \sigma \rangle$ = 2.85 ℧/m, $\langle \beta \rangle$ = 2.48, and β_{crit} = 1.90. The figure indicates that the streamer is induced in the central part of generator, while the current distribution becomes successively uniform as B attenuates along the generator duct and the current concentration is almost swept away near the output electrodes. Therefore it is seen that arranging the output electrodes within the attenuating domain of B is effective also for the case where the streamer is generated in the central region of generator duct.

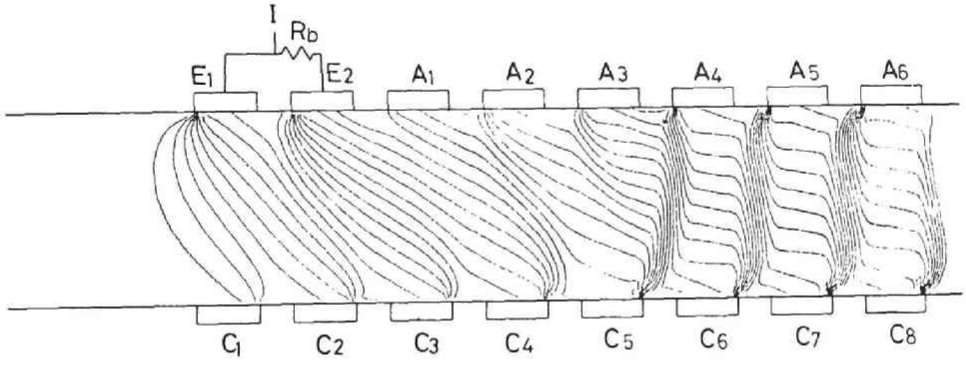

Fig. 2.54. Current distribution for g = 6, B_0 = 5, and j = 5.

(3) Potential distribution and ballast resistance

Figure 2.55 shows the variation of the potential difference between each electrode pair A_1-C_1 to A_8-C_8 and the electrode E_1 in the case of B = 4T. From the figures, it is seen that the relatively large potential difference arises between the two output electrodes E_1 and E_2 when B does not attenuate, namely g = 0. On the other hand, the potential difference becomes smaller as g becomes larger, it almost vanishes for g = 6, and the inverse difference appeares for g > 7. Also Fig.2.55 denotes that the potential differences in the central part of generator duct is little influenced by the decrease of the magnetic induction.

Figure 2.53 tells that R_b/R_{b0} decreases with g, becomes almost zero at g = 6.5, and then increases with g. Therefore, it is seen

that many output electrodes will require large ballast resistors when B does not attenuate or g exceeds 8 T/m, but they can be used without large ballast resistors in the range of g = 6 to 7 T/m.

In addition, the gradient of the magnetic flux density in the entrance of the apparatus decribed in Reference [1.3] is almost 8 T/m, and g = 6 to 7 T/m will be realized in the future super-conducting magnet.

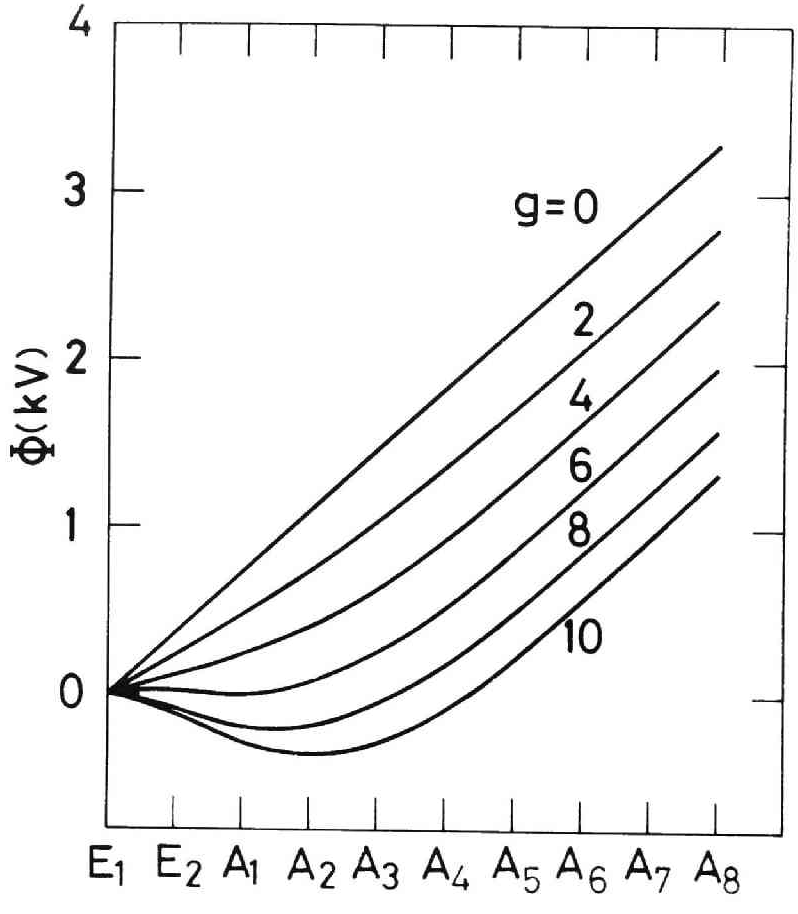

Fig. 2.55. Variation of potential difference for B_0 = 4.

5.5 Concluding Remarks

The main results obtained in this chapter are as follows.

(1) The variation of the type of output electrode arrangement has little effect on the current distribution in the generator. The selection of the type can be decided from a viewpoint of advantage in manufacturing.

(2) A suitable distribution of the magnetic flux can make the current distribution very uniform near the end region of generator duct, both when the streamer is not induced and when it is induced in the central region.

(3) Disposing the output electrodes within the attenuation area of magnetic flux density has little influence on the current distribution in the central part of generator duct.

(4) The internal resistance in the end region of the generator duct decreases as the magnetic flux attenuates.

(5) The current concentration at the output electrode ends can be fairly eliminated by attenuating magnetic flux.

(6) When the output electrodes are disposed in the region with a suitably decreased magnetic flux, the potential difference and the ballast resistance between two output electrodes become very small. Accordingly it is thought that many output electrodes can be used without large ballast resistors.

It was made clear that the output electrodes of the diagonal type MHD generator should be arranged in the attenuating region of magnetic flux, since arranging them in the region becomes useful not only for the improvement of the electrical characteristics in generator duct ends but also for the effective use of magnet.

CHAPTER 6

EFFECTS OF INTERNAL OR EXTERNAL CONNECTION OF ELECTRODES IN DIAGONAL TYPE GENERATOR

6.1 Introduction

In the diagonal type generator, a pair of anode and cathode to be shorted is connected internally or externally. What influence the difference between these connections gives the electrical characteristics of the generator must be studies to grasp sufficiently the generator performance. However, as it cannot be examined by the usual two-dimensional analysis for the vertical duct cross-section to magnetic flux, it has been little discussed [2.38]. .

In this chapter, by a two-dimensional analysis in the cross -section perpendicular to the plasma flow [2.39], [2.40], are investigated comparatively the current distribution, the electrical efficiency, etc. in the nonequilibrium plasma generators with the internally connected electrodes viz., the diagonal conducting wall (the so-called windframe generator) and those with the externally connected electrodes viz., the insulating sidewall, which let us call the DCW and the GIS, respectively, for simplicity. As in the previous chapters, numerical investigation is made for an example of the cesium-seeded helium in nonequilibrium ionization, where it is assumed that the ionization instability does not occur.

First, a two-dimensional differential equation in the duct cross-section perpendicular to the plasma flow is derived from the basic equations such as the Maxwell equations and the generalized Ohm's law, and then boundary and subsidiary conditions are shown for both the internal and external connections.

Next, the numerical calculation results of the current and potential distributions in the DCW and the GIS are comparatively studied. Then, influences of the load factor, the temperature of the duct wall, and the inclination parameter on the distributions,

the efficiency, the effective conductivity, etc. of the generator are investigated in detail.

6.2 Two-Dimensional Theory

6.2.1 Basic equations

In this chapter, it is assumed that the electrical quantities, such as the current and electric field, are independent of x and they vary with y and z [see Fig.2.56(a)], that the gas velocity and temperature depend on y and z according to Eqs.(2.86) and (2.87) presented later, and that the pressure is kept constant.

Next, $\boldsymbol{E}$, $\boldsymbol{J}$, $\boldsymbol{B}$, and $\boldsymbol{u}$ are assumed as

$$\left.\begin{aligned} \boldsymbol{E} &= (E_x, E_y, E_z), \quad \boldsymbol{J} = (J_x, J_y, J_z), \\ \boldsymbol{B} &= (0, 0, B), \quad \boldsymbol{u} = (u, 0, 0). \end{aligned}\right\}, \tag{2.75}$$

Then, $\nabla \times \boldsymbol{E} = 0$ in Eq.(2.1) and the assumption that the electrical quantities do not vary with x yield

$$E_x = \text{const.}, \tag{2.76}$$

thus E_x is regarded as a fundamental parameter in the calculation in this chapter.

When a stream function Ψ is defined newly by the following relations

$$J_y = -\partial\Psi/\partial z, \quad J_z = \partial\Psi/\partial y. \tag{2.77}$$

Then, from Eqs.(2.1), (2.4), (2.15), and (2.77), the following differential equations can be derived for Ψ and Φ.

$$\begin{aligned} &\partial^2\Psi/\partial y^2 + (\varepsilon^2 + \beta^2)/\varepsilon \cdot \partial^2\Psi/\partial z^2 \\ &+ \sigma\partial(1/\sigma)/\partial y \cdot \partial\Psi/\partial y + \sigma\partial(1/\sigma)/\partial z \cdot \partial\Psi/\partial z \\ &+ \sigma\partial\{(E_x + \partial p_e/\partial z/en_e)\beta/\varepsilon\}/\partial z \\ &+ \sigma\{\partial(1/en_e)/\partial z \cdot \partial p_e/\partial y - \partial(1/en_e)/\partial y \cdot \partial p_e/\partial z\} \\ &- \sigma\partial uB/\partial z = 0, \end{aligned} \tag{2.78}$$

$$\partial^2\Phi/\partial y^2 + (\varepsilon^2+\beta^2)/\varepsilon\cdot\partial^2\Phi/\partial z^2$$

$$+\partial\sigma'/\partial y\cdot\partial\Phi/\partial y/\sigma' + \partial\sigma/\partial z\cdot\partial\Phi/\partial z/\sigma'$$

$$- \partial(\partial p_e/\partial y/en_e)/\partial y - (\varepsilon^2+\beta^2)/\varepsilon\cdot\partial(\partial p_e/\partial z/en_e)/\partial z$$

$$-\partial\sigma'/\partial y/\sigma'\cdot\partial p_e/\partial y/en_e - \partial\sigma/\partial z/\sigma'\cdot\partial p_e/\partial z/en_e$$

$$+uB\partial\sigma'/\partial y/\sigma' + \partial uB/\partial y = 0, \qquad (2.79)$$

where

$$\sigma' = \varepsilon\sigma/(\varepsilon^2+\beta^2). \qquad (2.80)$$

In this connection,

$$J_x = \sigma/\varepsilon\cdot E_x + \partial\Psi/\partial z. \qquad (2.81)$$

In addition, the solution of Eq.(2.78) gives the orthographic projection of the current on the y-z plane by the definition of Eq.(2.77).

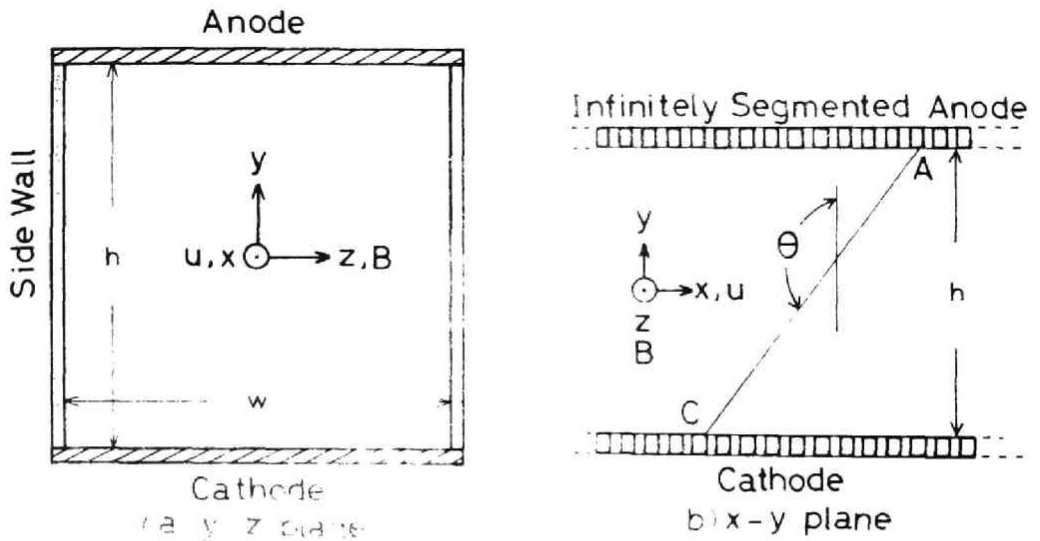

Fig. 2.56. Duct configuration of diagonal type generator.

6.2.2 Boundary and subsidiary conditions

Equations (2.78) and (2.79) require the boundary conditions on the electrode and insulating wall surfaces, and the subsidiary condition peculiar to the diagonal type generator.

First, the boundary condition on the electrode surfaces becomes

$$E_z = 0 \text{ at } y = 0 \text{ and } h. \tag{2.82}$$

Using Eqs.(2.4), (2.77), and (2.15), the above condition is changed with Ψ or Φ as

$$\left.\begin{aligned} &\partial\Psi/\partial y = \sigma/en_e \cdot \partial p_e/\partial z, \\ &\Phi = \text{const.}, \end{aligned}\right\} \quad \text{at } y = 0 \text{ and } h, \tag{2.82}'$$

respectively.

Next, from the assumption that the physical quantities are independent of x, the duct walls at z = 0 and w, which is the duct width in the z direction, become the infinite segmented electrodes in the DCW. Therefore, the boundary condition on the duct sidewalls is given by

$$E_y = aE_x, \quad a = \tan\theta. \tag{2.83}$$

By Eqs.(2.4), (2.15), and (2.77), Eq.(2.83) reduces to

$$\left.\begin{aligned} &\partial\Psi/\partial z = -\sigma'(a\varepsilon + \beta)E_x/\varepsilon - \sigma'\partial p_e/\partial y/en_e, \\ \text{or} \\ &\partial\Phi/\partial y = -aE_x, \quad \text{at } z = 0 \text{ and } w. \end{aligned}\right\}, \tag{2.83}'$$

In the generator of the GIS, the boundary condition is

$$J_z = 0, \quad \text{at } z = 0 \text{ and } w. \tag{2.84}$$

Substitution of Eqs.(2.4), (2.15), and (2.77) into Eq.(2.84) yields

$$\Psi = \text{const.}, \quad \Big)$$

or

$$\left.\begin{aligned} &\partial\Phi/\partial z = \partial p_e/\partial z/en_e. \end{aligned}\right\} \text{ at } z = 0 \text{ and } w. \qquad (2.84)'$$

Finally, in the diagonal type generator, the potential difference must be zero between a pair of the anode and cathode which are shorted each other. Hence, the subsidiary condition is given by

$$-\int_A^C \boldsymbol{E}\cdot d\boldsymbol{s} = 0, \qquad (2.85)$$

where $d\boldsymbol{s}$ is the line element vector on an optional integral path C to A [see Fig.2.56 (b)].

Using Eqs.(2.75) and (2.76), Eq.(2.85) reduces to

$$\int_0^h E_y dy = ahE_x. \qquad (2.85)'$$

6.2.3 Gas velocity and temperature distributions

As mentioned before, the gas velocity $\boldsymbol{u}$ has only the x component u, and u and T are assumed to vary in the y and z direction according to the relations

$$u/u_0 = \{4y/h\cdot(1 - y/h)\}^m\{4z/w\cdot(1 - z/w)\}^n \qquad (2.86)$$

and

$$(T - T_w)/(T_0 - T_w) = \{4y/h\cdot(1 - y/h)\}^{m'} \times\{4z/w\cdot(1 - z/w)\}^{n'}, \qquad (2.87)$$

where m, m', n, and n' are the constants, T_0 and u_0 the gas temperature and velocity, respectively, at the center of flow; namely at $y = h/2$ and $z = w/2$, and T_w the duct wall temperature.

6.2.4 Electrical efficiency

To estimate the performance characteristics of generator, the electrical efficiency

$$\eta_e = - \int_0^h \int_0^w \boldsymbol{E}\cdot\boldsymbol{J}dydz / \int_0^h \int_0^w (\boldsymbol{J}\times\boldsymbol{B})\cdot\boldsymbol{u}dydz \qquad (2.88)$$

is used. Also an effective electrical conductivity σ_{eff} and Hall parameter β_{eff} are evaluated, which are obtained by the definitions

$$\left.\begin{aligned} \sigma_{eff} &= <\boldsymbol{J}>^2/(<\boldsymbol{J}>\cdot<\boldsymbol{E}^*>), \\ \beta_{eff} &= |<\boldsymbol{J}>\times<\boldsymbol{E}^*>|/(<\boldsymbol{J}>\cdot<\boldsymbol{E}^*>), \end{aligned}\right\} , \qquad (2.89)$$

where $\boldsymbol{E}^* = \boldsymbol{E} + \boldsymbol{u}\times\boldsymbol{B}$ and $<\boldsymbol{J}>$ and $<\boldsymbol{E}^*>$ denote the avarage value of $\boldsymbol{J}$ and $\boldsymbol{E}^*$.

6.3 Numerical Investigations

6.3.1 Numerical conditions

Numerical conditions are given by

$$\left.\begin{aligned} &h = 0.2, \quad w = 0.2 \text{ m}, \quad B = 5 \text{ T}, \\ &u_0 = 2000 \text{ m/s}, \quad T_0 = 1800 \text{ K}, \\ &p = 5 \text{ atm}, \quad \varepsilon_s = 0.3 \%, \quad \delta = 5, \\ &m = m' = n = n' = 1/7. \end{aligned}\right\} , \qquad (2.90)$$

In addition, since the investigation in Chapter 3 has clarified that the terms of the ion-slip and the gradient of electron pressure are negligible under the present conditions, it can be assumed that $\varepsilon = 1$ and $\partial p_e/\partial y = \partial p_e/\partial z = 0$.

6.3.2 Influence of load factor

Figures 2.57 and 2.58 show the current and potential distributions on the y-z plane in the DCW, respectively, and Fig.2.59 presents the current distribution in the GIS, where $E_x = -800$ V/m, $T_w = 1600$ K, $\kappa = 0.053$, and $a = -1$ ($\theta = 135°$). Figure 2.57 indicates that some current flows into the conducting sidewall, namely $\boldsymbol{J}$ has not only the y component J_y but also the z component J_z near the

sidewall, and Fig.2.58 shows that the large electrode voltage drop occurs, when E_x and accordingly κ are small. Also Fig.2.59 shows that the current density becomes large in the central part of the duct cross-section and it is very small near the insulating sidewall.

In Figs.2.60 and 2.61, the current and potential distributions in the DCW are plotted, respectively, and in Fig.2.62, the current distribution in the GIS in the case of E_x = -8000 V/m, T_w = 1600 K, κ = 0.513, and a = -1. From Figs.2.60 and 2.61, it is seen that the current flowing into the conducting sidewall and the electrode voltage drop diminish against Figs.2.57 and 2.58. Also Fig.2.62 indicates that the current near the insulating sidewall tends to bend toward inside.

Next, Fig.2.63 gives the variation of η_e and $\sigma_{eff}/\langle\sigma\rangle$ by E_x in the case of T_w = 1600 K and a = -1, where $\langle\sigma\rangle$ is the average value of σ in

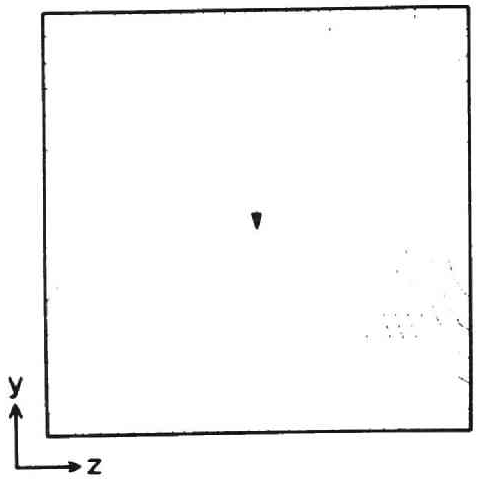

Fig. 2.57. Current distribution in the DCW when E_x = -800 V/m, T_w = 1600 K, and a = -1.

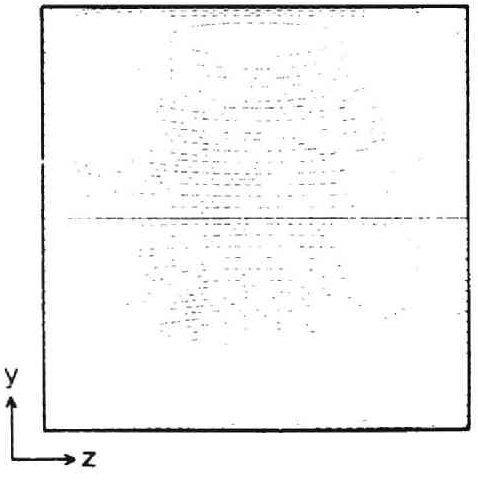

Fig. 2.58. Potential distribution in the DCW corresponding to current distribution in Fig.2.57.

the y-z plane. It shows that the magnitudes of η_e and $\sigma_{eff}/\langle\sigma\rangle$ of the DCW become a little larger than those of the GIS, and these differences increase with E_x. This is because the current in the DCW tends to flow not only in the middle area of the duct cross-section but also near the sidewall due to presence of the electrodes on the sidewall, and on the other hand, in the GIS it is difficult for the current to run near the sidewall because of the low temperature and low conductivity, and the current tends to gather in the middle area of the duct. In addition, the value of $\beta_{eff}/\langle\beta\rangle$ is nearly equal to unity in both the DCW and GIS, where $\langle\beta\rangle$ is the average value of β in the y-z plane, and it is not plotted in the figure.

Figure 2.64 shows the relations between E_x or κ and the x component I_x of the load current I, the

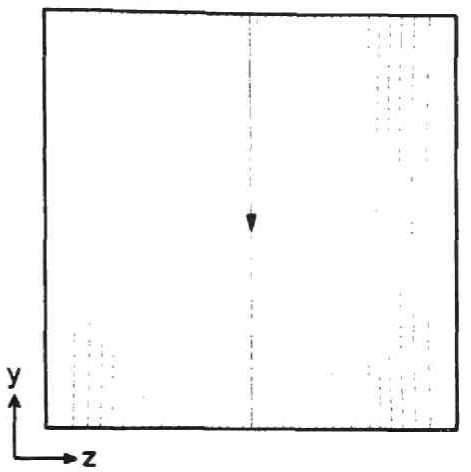

Fig. 2.59. Current distribution in the GIS under the same conditions as Fig.2.57.

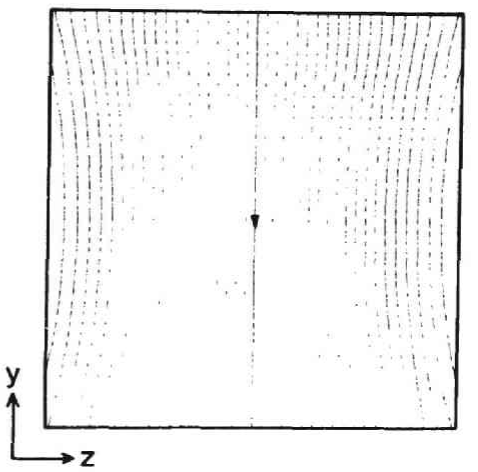

Fig. 2.60. Current distribution in the DCW when E_x = -8000 V/m, T_w = 1600 K, and a = -1.

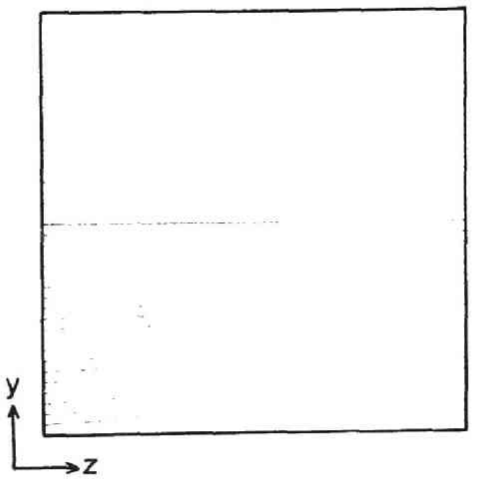

Fig. 2.61. Potential distribution in the DCW corresponding to current distribution in Fig.2.60.

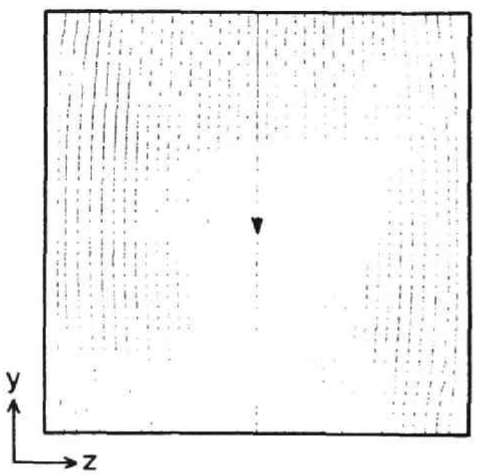

Fig. 2.62. Current distribution in the GIS under the same condition as Fig.2.60.

ratio i_z of the current flowing into one conducting sidewall to I', or the ratio v_D of electrode voltage drop to V_y in the DCW, where

$$\kappa = E_x/(E_x)_{open}$$
$$= -(1 + a^2)E_x/\{(\beta_{eff} - a)\langle u\rangle B\}, \tag{2.91}$$

$$\left.\begin{aligned} I &= I_x + I_y, \\ I_x &= \int_0^w\int_0^h J_x dydz, \quad I_y = ah\int_0^w J_y dz, \end{aligned}\right\} \tag{2.92}$$

$$i_z = \int_0^{h/2} J_z dy/I', \tag{2.93}$$

$$I' = \left|\int_0^w J_y dz\right| \quad \text{at } y = h/2, \tag{2.94}$$

$$V_y = -\int_0^h E_y dy. \tag{2.95}$$

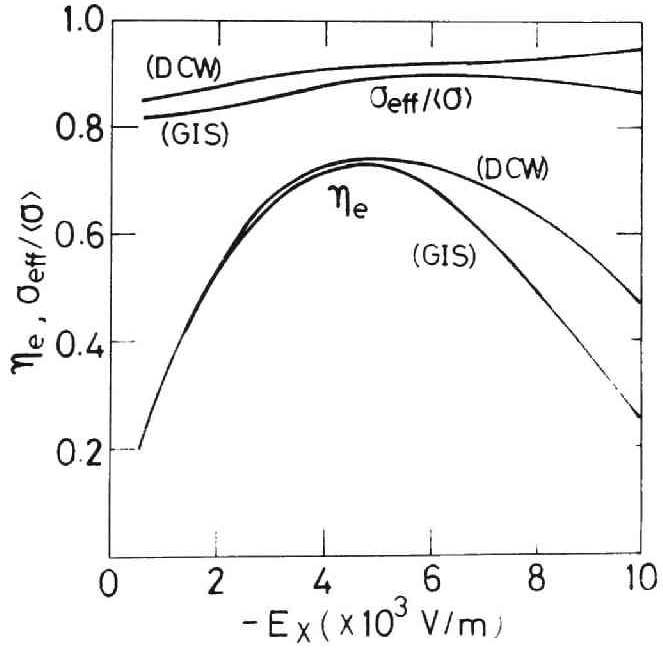

Fig. 2.63. Influence of E_x on η_e and $\sigma_{eff}/\langle\sigma\rangle$ when T_w = 1600 K and a = -1.

From the figure, it is found that the sign of I_x changes from positive to negative when E_x or κ becomes large, namely the direction of the current I_x is reversed. The values of κ and I_x in the DCW become nearly equal to those in the GIS. Then, i_z and v_D decrease and converge to a constant value when κ becomes large, for example, i_z = 14.3, 5.8, and 4.0 % for κ = 0.05, 0.5, and 0.7, respectively [see Figs.2.57 and 2.58].

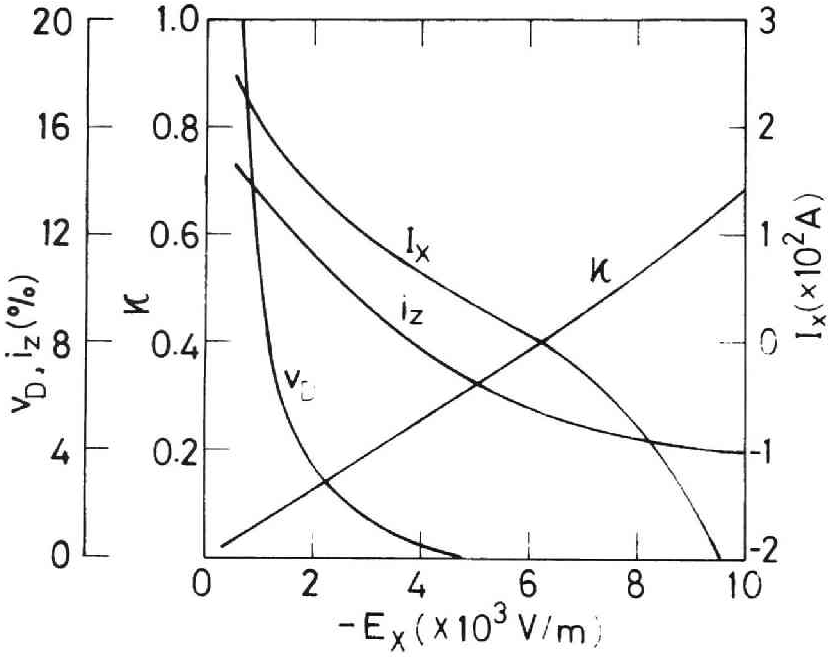

Fig. 2.64. Influence of E_x on I_x, i_z, v_D, and κ when T_w = 1600 K and a = -1.

6.3.3 Influence of duct wall temperature

Figure 2.65 shows the influence of duct wall temperature T_w on the electrical characteristics both of the DCW and of the GIS in the case of E_x = -5000 V/m and a = -1. From the figure, it is seen that the values of η_e and i_z are nearly independent of T_w, but $\sigma_{eff}/\langle\sigma\rangle$ and I_x increase with T_w, and also that η_e and $\sigma_{eff}/\langle\sigma\rangle$ of the DCW are a little larger than those of the GIS.

Figure 2.66 informs the influence of T_w on the performance

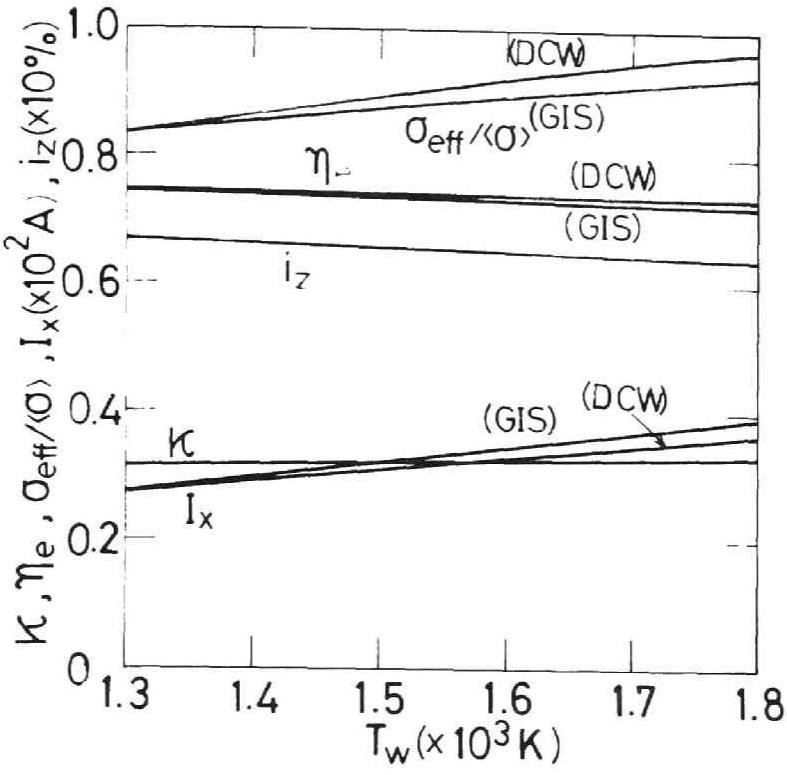

Fig. 2.65. Influence of T_w on I_x, i_z, η_e, κ, and $\sigma_{eff}/\langle\sigma\rangle$ when E_x = -5000 V/m and a = -1.

characteristics of the DCW when E_x = -8000 V/m and a = -1. The figure indicates that η_e and κ are nearly independent of T_w, and $\sigma_{eff}/\langle\sigma\rangle$, I_x, and i_z increase with T_w, for example the values of I_x and i_z for T_w = 1800 K are 1.50 and 1.58 times as large as those for T_w = 1300 K, respectively. This is because the current is prevented from flowing near the duct wall since a low value of T_w hinders the elevation of T_e there, and so it is apt to flow in the central region of generator duct. The values of η_e and $\sigma_{eff}/\langle\sigma\rangle$ are nearly equal to those in Fig.2.65 but the variations of I_x and i_z are larger than those in Fig.2.65.

6.3.4 Influence of inclination parameter

In Fig.2.67, we plot the relations of η_e, $\sigma_{eff}/\langle\sigma\rangle$, I_x, and i_z when $\kappa \fallingdotseq 0.5$ and T_w = 1600 K. It is shown that η_e increases

largely and $\sigma_{eff}/\langle\sigma\rangle$ does only a little when $|a|$ becomes large. Also I_x becomes negative and its variation due to a is small for $|a| > 0.4$, but I_x is positive for $|a| < 0.4$, and especially I_x becomes very large at $a = 0$, namely in the Hall type generator. Next, i_z is nearly constant in the range of $0 < |a| < 1$, but it increases fairly for $|a| > 1$.

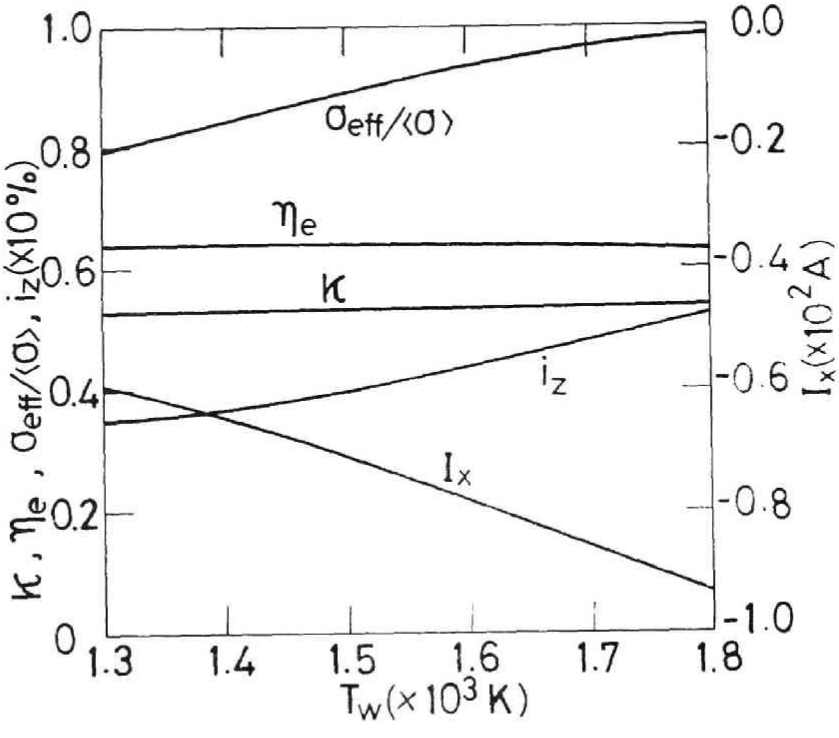

Fig. 2.66. Influence of T_w on I_x, i_z, η_e, κ, and $\sigma_{eff}/\langle\sigma\rangle$ when $E_x = -8000$ V/m and $a = -1$.

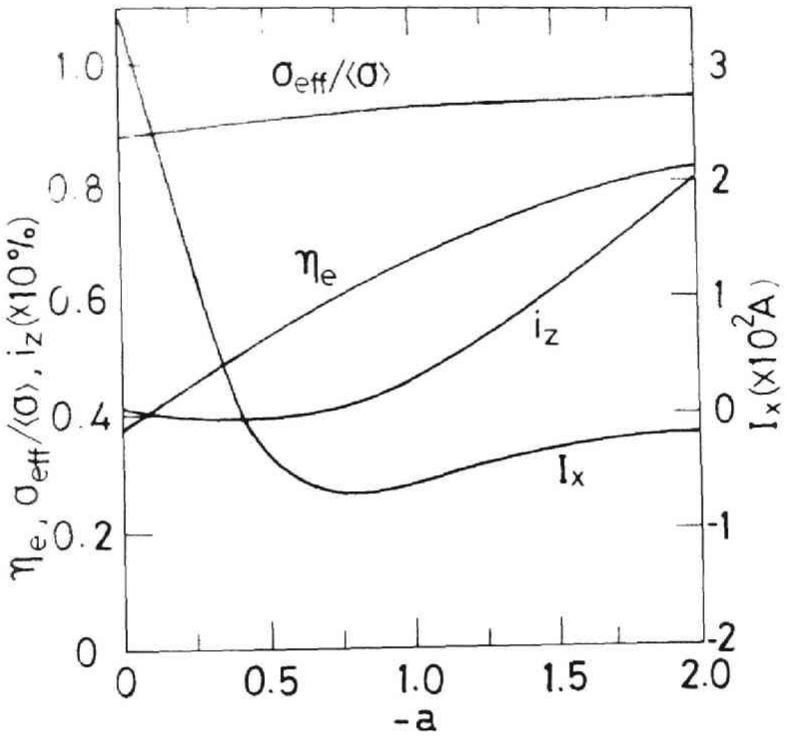

Fig. 2.67. Influence of a on I_x, i_z, η_e, and $\sigma_{eff}/\langle\sigma\rangle$ when $\kappa \doteq 0.5$ and T_w = 1600 K.

6.4 Concluding Remarks

The main conclusions, which have been derived from the above described two-dimensional analysis, are as follows.

(1) In the DCW, the current flowing into the electrodes on the sidewall increases with the load factor. In the GIS, it is difficult for the current to run near the sidewall and the most part of the current flows in the mid area of the generator duct. Also the electrode voltage drop becomes large with decreasing load factor.

(2) The generator characteristics such as the electrical efficiency and effective conductivity of the DCW are better than those of the GIS and this difference increases with the load factor and the wall temperature within the numerical conditions used in this chapter.

(3) The decreases of the duct wall temperature causes a reduction of the ratio i_x and a little degradation of generator performance of the DCW.

(4) The electrical characteristics of the generator improves as the magnitude of the inclination parameter increases.

Thus, it may be thought that the diagonal type MHD generator with nonequilibrium plasma should be equipped with the conducting sidewall within the assumptions in this chapter.

REFERENCES

PART I :

1. 1. Mori, Y., Homma, S. Korenaga, K. Onda, K. Takano, and S. Suemitsu, "Recent Experimental Results of ETL Mark VI," 6th Int. Conf. on MHD Elect. Power Gen., Vol. I, pp. 155-166, 1975.

1. 2. Wu, Y. C. L., B. Dicks, K. E. Tempelmeyer, L. W. Crawford, I. W. Muehlhauser, and G. Rajagopal, "Experimental and Theoretical Investigation on a Direct Coal Fired MHD generator," *ibid.*, Vol. I, pp. 199-214, 1975.

1. 3. Petty, S., R. Rosa, and G. Enos, "Developments with the Mark VI Long Duration MHD Generator," *ibid.*, Vol. I, pp. 231-250, 1975.

1. 4. Bitiurin, V. A., A. D. Iserov, V. I. Kovbasiuk, S. A. Medin, D. S. Pinkhasik, and B. Ya. Shuivatsky, "Some Results of Gas and Electrodynamic Studies of an MHD Generator on the V-25 Facility," *ibid.*, Vol. I, pp. 183-198, 1975.

1. 5. Hurwits, H., J. R. W. Kilb, and G. W. Sutton, "Influence of Tensor Conductivity of Current Distribution in an MHD Generator," *J. Appl. Phy.*, Vol. 32, No. 2, pp. 205-216, 1961.

1. 6. Dzung, L. S., "Favourable Configurations of Segmented Electrode for MHD Generators," *Brown Boveri Review*, Vol. 53, No. 3, pp. 238-250, 1966.

1. 7. Celinski, Z., "Electrical Equivalent Circuits of d. c. MHD Generators," Electricity from MHD, Vol. I, pp. 323-331, 1966.

1. 8. Oliver, D. A., "Inter-Electrode Breakdown on Electrode Walls Paralleled and Inclined to the Magnetic Field," 6th Int. Conf. on MHD Elect. Power Gen., Vol. I, pp. 329-343, 1975.

1. 9. Demetriades, S. T., and C. D. Maxwell, "Influence of Wall Roughness and Exit Pressure on the Performance of a Subsonic MHD Generator," *ibid.*, Vol. IV, pp. 237-246, 1975.

1.10. Marston, C. H., C. S. Cook, B. Zauderer, D. Hagford, and R. O. Hay, "Design of 50 MW Closed MHD Blowdown Experiment," Proc. of 15th Symp. on Eng. Aspects of MHD, VI. 2, 1976.

1.11. Velikhov, E. P., L. M. Regtyarev, and A. P. Favorskii, " Numerical Simulation of Ionization Instability," 5th Int. Conf. on MHD Elect. Power Gen., Vol. II, pp. 307-324, 1971.

1.12. Solbes A., "Quasi-Linear Plane Wave Study of Electrothermal Instabilities," Electricity from MHD, Vol. I, pp. 499-518, 1968.

1.13. Yoshikawa, K., and I. Michiyoshi, "Ionization Instability and Stable Region in Potassium Seeded Argon Gas Plasma MHD Generation," *Plasma Physics*, Vol. 16, No. 11, pp. 1085-1099, 1974.

1.14. Tanaka, D., "Performance Characteristics of Non-Equilibrium MHD Duct with Resistive Electrodes," *J. Nucl. Sci. Technol.*, Vol. 14, No. 4, pp. 257-266, 1977.

1.15. Bertolini, B., M. Gasparotto, P. Gay, L. Panaccione, and A. Tamburrano, "Closed Cycle MHD Subsonic Power Generation Experiments at Frascati," Proc. of 13th Symp. on Eng. Aspects of MHD, I.1, 1973.

1.16. Brederlow, G., and K. J. Witte, "Effective Electrical Conductivity and Electron Temperature Measurements in a Non-equilibrium MHD Generator Plasma at Atmospheric and Higher Pressures," *ibid.*, I.7, 1973.

1.17. Marston, C., E. Tate, and B. Zauderer, "Large Enthalpy Extraction Results in a Non-Equilibrium MHD Generator," 6th Int. Conf. on MHD Elect. Power Gen., Vol. III, pp. 89-104, 1975.

1.18. Nakamura, T., and W. Riedmüller, "Investigation of Non-Equilibrium MHD Plasma under the Conditions of Fully Ionized Seed," 5th Int. Conf. on MHD Elect. Power Gen., Vol. 2, pp. 291-306, 1971.

1.19. Blom, J., A. Veefking, J. Houben, and L. Rietijens, " High

Power Density Experiments in the Eindhoven Shocktunnel MHD Generator," 6th Int. Conf. on MHD Elect. Power Gen., Vol. III, pp. 73-88, 1975.

1.20 Shioda, S., and Y. Sato, "Performance of a Faraday MHD Generator with Supersonic Seeded Helium," *ibid.*, Vol. III, pp. 63-72, 1975.

1.21. Rosa, R. J., *Magnetohydrodynamic Energy Conversion*, McGraw-Hill, New York, Chap. 4, 1968.

1.22. Pishchikov, S. I., and M. S. Pinkhasik, "Some Results of Investigation on the V-25 Installation," 6th Int. Conf. on MHD Elect. Power Gen., Vol. I, pp. 167-182, 1975.

1.23. Takano, K., K. Onda, and Y. Mori, "Calculation of Performance of Large Scale Diagonal MHD-Steam Plants," Proc. of 13th Symp. on Eng. Aspects of MHD, V. 6, 1973.

1.24. Coney, M. W. E., and J. B. Heywood, "Some Design Considerations for a Single-Load MHD Generator," Electricity from MHD, Vol. IV, pp. 2687-2702, 1968.

1.25. Bobbio, S., F. Gasparini, O. Greco, and B. Niceletti, "Variational Optimization of Diagonally Cross-Connected Electrode MHD Generators," *ibid.*, Vol. IV, pp. 2703-2715, 1968.

1.26. Gorb, A. M., I. S. Gorobets, and N. I. Mazur, "Calculation of the Load Characteristics of an MHD Generator," *Magnitnaya Gidrodinamika*, Vol. 4, No. 2, pp. 97-102, 1968.

1.27. Yoshida, M. and J. Umoto, Convention Records at the Annual Meeting in Kansai District of I.E.E.J., No. G1-13, 1973.

1.28. Zauderer, B., C. Marston, and C. S. Cook, *Closed Cycle MHD for Central Station Power with Fossil or Nuclear Fuels*, General Electric Co., 1973.

1.29. Shioda, S., and M. Miyama, "Closed Cycle MHD with Combined Nuclear and Fossil Heat Sources," 6th Int. Conf. on MHD Elect. Power Gen., Vol. III, pp. 21-43, 1975.

1.30. Ishikawa, M., and J. Umoto, "Some Contributions to Optimiza-

tion Theory of Nonequilibrium Diagonal MHD Generator Duct," *Mem. Facul. Eng. Kyoto Univ.*, Vol. 36, Part 1, pp. 32-45, 1974.

1.31. Ishikawa, M., and J. Umoto, "Optimization of Diagonal Type Nonequilibrium Plasma MHD Generator," *Tech. Report, Inst. Atom. Energy, Kyoto Univ.*, No. 172, 1977.

1.32. Umoto, J., M. Yoshida, and M. Ishikawa, Convention Records at the Annual Meeting of I.E.E.J., No. 812, 1973.

1.33. Umoto, J., and M. Ishikawa, Convention Records at the Annual Meeting in Kansai District of I.E.E.J., No. G-12, 1973.

1.34. Ishikawa, M., and J. Umoto, Convention Records at the Annual Meeting of I.E.E.J., No. 695, 1974.

1.35 Ishikawa, M., and J. Umoto, *ibid.*, No. 837, 1975.

1.36 Koyama, K., " A Design Consideration of Superconducting Coils for MHD Generators," *Bull. Electrotech. Lab.*, Vol. 32, No. 5, pp. 469-482, 1968.

1.37. Hayashi, M., and G. Wakabayashi, *Technology of Electric Power Generation, I.E.E.J.*, Tokyo, 1976.

1.38. Tsu, T. C., W. E. Young, and S. Way, "Optimization Studies of MHD-Steam Plants," Electricity from MHD, Vol. III, pp. 899-911, 1966.

1.39. Nakamura, T., "Feasibility of Hydrogen-Oxygen Closed Cycle MHD Power Generation Based upon Thermochemical Decomposition of Water," 6th Int. Conf. on MHD Elect. Power Gen., Vol. IV, pp. 39-52, 1975.

1.40. Volkov, Y. M., "Investigation of Some Factors, Limiting Enthalpy Extraction of MHD-Generators," *Energy Conversion*, Vol. 15, pp. 45-49, 1975.

1.41 Schlichting, H., *Boundary-Layer Theory*, 6th ed., McGraw-Hill, New York, 1968.

1.42. Bobbio, S., L. De Menna, O. Greco, and E. Bertolini, "VARIATIONAL OPTIMIZATION OF SEGMENTED-ELECTRODE FARADAY TYPE CLOSED CYCLE MHD GENERATORS, 5th Int. Conf. on MHD

Elect. Power Gen., Vol. II, pp. 513-521, 1971.

PART II :

2. 1. Oliver, D. A., and M. Mitchner, "Nonuniform Electrical Conduction in MHD Channels," *AIAA J.*, Vol. 5, No. 8, pp. 1424-1432, 1967.

2. 2. Argyropoulos, G. S., and S. T. Demetriades, "Influence of Relaxation Effects in Nonequilibrium JxB Devices," *J. Appl. Phy.*, Vol. 40, No. 11, pp. 4400-4408, 1969.

2. 3. Lengyel, L. L., "Two-dimensional Current Distributions in Faraday Type MHD Energy Convertors Operating in the Non-Equilibrium Conduction Mode," *Energy Conversion*, Vol. 9, pp. 13-23, 1969.

2. 4. Denzel, D., "Raumliche Potential- und Stromverteilungen in Magnetohydrodynamishen Generatoren," *ETZ-A*, Vol. 91, pp. 254-257, 1970.

2. 5. Tanaka, D., Y. Hattori, and T. Noguchi, "Analysis of the Electric Current Distribution in a Hall Type Non-Equilibrium Plasma MHD Generator," *Trans. I.E.E.J.*, Vol. 94-A, No. 7, pp. 289-294, 1974.

2. 6. Kaidalov, V. A., E. I. Khanzhina, and E. I. Yantovskii, "Computation of MHD Flows in Ducts with Segmented Electrodes," *Magnitnaya Gidrodinamika*, Vol. 2, No. 4, pp. 55-61, 1966.

2. 7. Ishikawa, M., J. Umoto, and T. Hara, "Two Dimensional Analysis of a Diagonal Type Nonequilibrium Plasma MHD Generator," *Trans. I.E.E.J.*, Vol. 96-A, No. 12, pp. 559-566, 1976.

2. 8. Ishikawa, M., and J. Umoto, " Two Dimensional Analysis of Diagonal Type MHD Generator," Papers of Technical Meeting on Information Processing, I.E.E.J., IP-77-12, 1977.

2. 9. Hara, T., M. Ishikawa, and J. Umoto, Convention Records at the Annual Meeting of I.E.E.J., No. 691, 1974.

2.10. Ishikawa, M., and J. Umoto, Convention Records at the Annual

Meeting in Kansai District of I.E.E.J., No. G1-9, 1974.

2.11. Ishikawa, M., and J. Umoto, Convention Records at the Annual Meeting of I.E.E.J., No. 826, 1975.

2.12. Ishikawa, M., and J. Umoto, Convention Records at the Annual Meeting in Kansai District of I.E.E.J., No. G1-13, 1975.

2.13. Ishikawa, M., J. Umoto, and M. Saito, "Effects of Resistive Electrodes and Distribution of Applied Magnetic Flux Density on Electrical Characteristics of a Diagonal Type Nonequilibrium Plasma MHD Generator," *Trans. I.E.E.J.* Vol. 97-a, No. 10, pp. 489-496, 1977.

2.14. Ishikawa, M., M. Saito, and J. Umoto, Convention Records at the Annual Meeting of I.E.E.J., No. 174, 1976.

2.15. Ishikawa, M., and J. Umoto, Prep. 1976. Fall Meeting At. Energy Soc. Japan, A19, 1976.

2.16. Ishikawa, M., and J. Umoto, "Two-Dimensional Analysis of End Effects in Diagonal Type Nonequilibrium Plasma MHD Generator," *Mem. Facul. Eng. Kyoto Univ.*, Vol. 38, Part 4, pp. 182-197, 1976.

2.17. Ishikawa, M., J. Umoto, "Two-Dimensional Analysis of End Effects in Diagonal Type MHD Generator," *Energy Conversion*, Vol. 17, No.2, pp. 113-118, 1977.

2.18. Ishikawa, M., J. Umoto, "End Effects in Diagonal Type Nonequilibrium Plasma MHD Generator," to be published in *J. Nucl. Sci. Technol.*, Vol. 15, No. 3, 1978.

2.19. Ishikawa, M., J. Shimada, and J. Umoto, Convention Records at the Annual Meeting of I.E.E.J., No. 173, 1976.

2.20. Ishikawa, M., and J. Umoto, Convention Records at the Annual Meeting in Kansai District of I.E.E.J., No. G1-11, 1976.

2.21. Ishikawa, M., and J. Umoto, "Effects of Internal or External Connection of Electrodes in a Diagonal Type Nonequilibrium MHD Generator," *J. Nucl. Sci. Technol.*, Vol. 15, No. 2, pp. 91-99, 1978.

2.22. Ishikawa, M., and J. Umoto, Prep. 1977 Annu. Meeting At. Energy Soc. Japan, A32, 1977.

2.23. Owens, W. R., "A Theoretical Investigation of the Problem of Preionization in a Closed Cycle Magnetoplasma dynamic Generator," Thesis of Doctor of Philosophy, the University of Maryland, Maryland, USA, 1970.

2.24. Noguchi, T., "Study on Electrical Conductivity of Working Gas in Nonequilibrium Ionization MHD Generations," Doctral Thesis, Kyoto University, Kyoto, Japan, 1970.

2.25. Croitoru, Z., "Les Generateurs MHD a Electrodes Semi-Conductrices: Problemes et Perspectives," Electricity from MHD, Vol. II, pp.245-252, 1966.

2.26. Rosa, R. J., and S. Petty, "Status Report on the Mark VI Long-Duration Generator Facility," Proc. of 13th Symp. on Eng. Aspects of MHD, II. 7, 1973.

2.27. Tanaka, D., and Y. Hattori, "Characteristics of Resistive Electrode in MHD Generator Duct and a Minimizing Technique for Internal Power Loss," *J. Nucl. Sci., Technol.*, Vol. 12, No. 11, pp. 687-694, 1975.

2.28. Yoshikawa, K., and Y. Hattori, "Theoretical Study of the Performance Characteristics of a Resistive Electrode with a Connection at the Extreme Edge," *Plasma Physics*, Vol. 18, No. 4, pp. 301-315, 1976.

2.29. Ozawa, Y., and N. Kayukawa, "The Configuration of Applied Magnetic Induction for Equilibrium MHD Generation," 6th Int. Conf. on MHD Elect. Power Gen., Vol. I, pp. 399-418, 1975.

2.30. Mason, T. O., W. T. Petuskey, W. W. Liang, J. W. Halloran, F. Yen, T. M. Pollak, J. F. Elliott, and H. K. Bowen, "Properties and Thermochemical Stability of Ceramics and Metals in an Open-Cycle, Coal-Fired MHD System," *ibid*, Vol. II, pp. 77-104, 1975.

2.31. Frederikse, H. P. R., W. R. Hosler, A. J. Armstrong, and Negas, "Spinels for MHD-Electrodes," Proc. of 15th Symp. on Eng. Aspects of MHD, II. 2, 1976.

2.32. Sutton, G. W., "End Losses in Magnetohydrodynamic Channels with Tensor Electrical Conductivity and Segmented Electrodes," *J. Appl. Phys.*, Vol. 34, pp. 396-403, 1963.

2.33. Houben, J. W. M. A., J. H. Blom, and L. H. Rietjens, "End Effects in Faraday Type MHD Generators with Nonequilibrium Plasmas," *AIAA J.*, Vol. 10, No. 11, pp. 1513-1516, 1972.

2.34. Argyropoulos, G. S., M. A. Casteel, and S. T. Demetriades, "Two-Dimensional Distribution of Current along Magnetohydrodynamic Channels," Proc. of 10th Symp. on Eng. Aspects of MHD, pp. 29-32, 1969.

2.35. Dzung, L. s., "The Magnetohydrodynamic Generator with Hall Effect at the Duct Ends," *Brown Boveri Review*, Vol. 49, No. 6, pp. 211-225, 1962.

2.36. Norris, W. T., and J. B. Heywood, "End Region of a Single-Load Cross-Connected M.H.D. Generator," Proc. I.E.E., Vol. 115, No. 4, pp. 555-561, 1968.

2.37. Sonju, O. K., and J. Teno, "Further Analytical Investigations of MHD Generator Performance," Proc. of 12th Symp. on Eng. Aspects of MHD, II. 3, 1972.

2.38. Maxwell, C. D., E. D. Doss, D. A. Oliver, and B. P. Curry, "Consideration of Three-Dimensional Effects in MHD Power Generators," Proc. of 15th Symp. on Eng. Aspects of MHD, IX. 6, 1976.

2.39. Wu, Y. C. L., D. L. Denzel, R. E. Taylor, E. S. Jett, and J. B. Dicks, "Current Distribution in MHD Channels with Nonuniform Gas Properties," Proc. of 10th Symp. on Eng. Aspects of MHD, pp. 23-28, 1969.

2.40. Biturin, V. A., B. M. Burakhanov, V. A. Zhelnin, V. I. Koubasink, S. A. Medin, and I. M. Rutkevich, "Theoritical Analysis of the Two-Dimensional Electrical Effects and

Development of Engneering Method for Calculating Diagonal Type MHD Channels," 6th Int. Conf. on MHD Elect. Power Gen., Vol. I, pp. 501-516, 1975.

APPENDIX I

DERIVATION OF EQUATIONS (1.5) AND (1.7)

Equations (1.5) and (1.7) of the quasi one-dimensional basic equations are peculiar to a diagonal type MHD generator.

When the current continuity equation is applied to a hexahedron v which has the width of unit length in the z direction and an area (A'C'D'B') in the x-y plane in Fig.1.1, we obtain the following equation

$$\int_v div\boldsymbol{J} dv = 0, \tag{A.1}$$

where dv is an element of v. By Gauss' divergence theorem, the above equation is transformed to

$$\int_{S'} \boldsymbol{J} \cdot d\boldsymbol{S} = S_1 J_{n1} - S_2 J_{n2} = 0, \tag{A.2}$$

where $d\boldsymbol{S}$ is element vector of the surface S' of the hexahedron v, S_1 and S_2 the cross-sections $\overline{A'C'}$ x 1 and $\overline{B'D'}$ x 1, respectively, and J_{n1} and J_{n2} the current components perpendicular to the cross-sections S_1 and S_2, respectively.

$S_1 J_{n1} = S_2 J_{n2} = S J_n$ is equal to the load current I, namely

$$S_1 J_{n1} = S_2 J_{n2} = S J_n = I, \tag{A.3}$$

where S is a cross-section which intersects a normal cross-section A by the angle θ, J_n the current component perpendicular to S.

Using the x and y components J_{nx} and J_{ny} of J_n and A, J_n and S are written as

$$J_n = J_{nx} - J_{ny} = -(J_x cos\theta + J_y sin\theta), \tag{A.4}$$

$$S = -A/cos\theta. \tag{A.5}$$

From Eqs.(A.4) and (A.5), the following equations

$$(J_x + aJ_y)A = I, \quad a = tan\theta \tag{A.6}$$

are derived. These equations are nothing but Eqs.(1.5).

Next, since an electrode pair C and A is short-circuited, the potential difference between C and A becomes zero. Using this relation, as the component of E_x in the CA direction is $E_x sin\theta$ and that of E_y is $-E_y cos\theta$, the total electric field in the CA direction becomes

$$E_x sin\theta - E_y cos\theta = 0. \tag{A.7}$$

Accordingly,

$$E_y = aE_x. \tag{A.8}$$

This gives the relation in Eq.(1.7).

APPENDIX II

DERIVATION OF EQUATIONS (2.33) TO (2.35)

Neglection of the ion-slip and electron partial pressure terms in Ohm's law i.e. Eq.(2.4) for the diagonal type MHD generator yields

$$J_x = \sigma\{E_x + \beta(uB - E_y)\}/(1 + \beta^2), \tag{A.9}$$

$$J_y = \sigma\{\beta E_x - (uB - E_y)\}/(1 + \beta^2), \tag{A.10}$$

with respect to the x and y components J_x and J_y of $\boldsymbol{J}$.

If the quasi one-dimensional approximation can be assumed, the following equations

$$(J_x + aJ_y)A = I, \quad a = tan\theta, \tag{A.11}$$

$$E_y = aE_x \tag{A.12}$$

are formed as shown in the previous appendix.

From Eqs.(A.9) to (A.12), E_x is derived as

$$(E_x)_{I=0} = -(\beta - a)uB/(1 + a^2) \tag{A.13}$$

for no-load condition. Here, when the results of two-dimensional analysis are used, β must be replaced with $<\beta>$.

Let us define an ideal potential difference per one electrode pitch V_{ideal} by

$$V_{ideal} = -(E_x)_{I=0}\kappa s = (<\beta> - a)u_0 Bs\kappa/(1 + a^2), \tag{2.33}$$

where κ is the actual load factor [see Eqs.(A.14) and (A.15)]. This V_{ideal} becomes the potential difference per one electrode pitch when the ideal generator is opperated with κ.

Next, when J_x, J_y, E_x, and E_y are replaced with $<J_x>$, $<J_y>$, $<E_x>$, and $<E_y>$, respectively, σ and β are replaced by the effective electrical conductivity σ_{eff} and the effective Hall parameter β_{eff}, respectively, defined by

$$\langle J_x \rangle = \sigma_{eff}\{\langle E_x \rangle + \beta_{eff}(\langle u \rangle_B - \langle E_y \rangle)\}/(1 + \beta_{eff}^2), \quad (A.9)'$$

$$\langle J_y \rangle = \sigma_{eff}\{\beta_{eff}\langle E_x \rangle - (\langle u \rangle_B - \langle E_y \rangle)\}/(1 + \beta_{eff}^2), \quad (A.10)'$$

$$\langle E_y \rangle = a\langle E_x \rangle, \quad (A.11)'$$

$$(\langle J_x \rangle + a\langle J_y \rangle)A = I. \quad (A.12)'$$

with respect to the two-dimensional analysis.

When the load factor is defined by

$$\kappa = \langle E_x \rangle / (\langle E_x \rangle)_{I=0}, \quad (A.14)$$

from Eqs.(A.9)' to (A.12)' and (A.14) the following equation is derived

$$\kappa = 1 - I(1 + \beta_{eff}^2)/\{hw\sigma_{eff}\langle u \rangle_B(\beta_{eff} - a)\}. \quad (A.15)$$

This is nothing but Eq.(2.32).

Equation (2.33) can be derived from Eqs.(A.8)' to (A.10)'.

APPENDIX III

RELAXATION PARAMETER IN SOR METHOD

The convergence of the author's modified SOR method is explained as follows.

In general, simultaneous linear equations are written in the following matrix form

$$A\mathbf{x} = \mathbf{b}, \qquad A = D - E - F, \tag{A.16}$$

where A, D, E, and F are square, diagonal, lower triangular, and upper triangular matrices, respectively, and $\mathbf{b}$ and $\mathbf{x}$ known and unknown column vectors.

Now let us consider the following relaxation parameter matrix

$$\Omega = \begin{pmatrix} \omega_1 & 0 & \cdots & 0 \\ 0 & \omega_2 & & \vdots \\ \vdots & & \ddots & \vdots \\ 0 & \cdots & \cdots & \omega_m \end{pmatrix}, \tag{A.17}$$

where ω_i ($i = 1,2,\cdots,m$; m: total node number) is the relaxation parameter for the i-th node. Then, the $(k+1)$-th approximation $\mathbf{x}^{(k+1)}$ for $\mathbf{x}$ is given by

$$\begin{aligned} \mathbf{x}^{(k+1)} &= \mathbf{x}^{(k)} + \Omega\{D^{-1}(\mathbf{b} + E\mathbf{x}^{(k+1)} \\ &\quad + F\mathbf{x}^{(k)}) - \mathbf{x}^{(k)}\}. \end{aligned} \tag{A.18}$$

Further, this equation is rewritten as

$$\begin{aligned} \mathbf{x}^{(k+1)} &= M\mathbf{x}^{(k)} + \mathbf{g} \\ &= M^{k}\mathbf{x}^{(1)} + (M^{(k-1)} + \cdots + M + U)\mathbf{g}, \end{aligned} \tag{A.19}$$

where U is the unit matrix, and

$$\left.\begin{aligned} M &= (U - \Omega D^{-1}E)^{-1}\{U + \Omega(D^{-1}F - U)\}, \\ \mathbf{g} &= (U - \Omega D^{-1}E)^{-1}\Omega D^{-1}\mathbf{b}. \end{aligned}\right\}, \tag{A.20}$$

Next, if $\lim_{k\to\infty} \|M\| < 1$, where $\|M\|$ is the norm of M,

$$\lim_{k\to\infty} \mathbf{x}^{(k+1)} = (U - M)^{-1}\mathbf{g} = A^{-1}\mathbf{b}, \qquad (A.21)$$

Namely, when k tends to ∞, the value of $\mathbf{x}^{(k+1)}$ converges to the solution of Eq.(A.16).

Moreover, if A is a symmetric positive matrix, it can be proved that $\mathbf{x}$ converges for $0 < \omega_i$ $(i = 1,2,---,m) < 2$.